Geochemistry and Genesis of Late Paleoproterozoic Banded Iron Formations and Metamorphosed Chemical Precipitates Spatially Associated with Pb-Zn Broken Hill-type Mineralization near the Broken Hill Deposit, Curnamona Province, Australia

by

Erica Serna

December, 2014

Director of Thesis: Adriana Heimann

Major Department: Geological Sciences

Banded and massive iron formations (IFs) and garnet- and gahnite-quartz rocks are spatially associated with the giant, late Paleoproterozoic, Pb-Zn-Ag Broken Hill sulfide deposit and hundreds of minor Broken Hill-type deposits in the southern Curnamona Province, Australia. The sulfide deposits, host rocks, and a variety of chemical precipitates that include IFs and garnet- and gahnite-rich rocks were metamorphosed to the granulite facies. The IFs are found above, below, and along strike with the ore deposits and are among the youngest IFs that formed in the late Paleoproterozoic at ~ 1.69 Ga, after the Great Oxidation Event (GOE; ~2.35 Ga).

Here the petrology and geochemistry of banded and massive IFs and garnet- and gahnite-quartz rocks from near the Broken Hill, Little Broken Hill, Wild Dog, Pinnacles, and Nine Mile Pb-Zn-Ag sulfide deposits are investigated to determine the genesis of the rocks and the physicochemical conditions of the fluids in the intracontinental Broken Hill rift basin at ~1.69 Ga, and ultimately the redox state of the water in this basin at the time of deposition.

Banded and massive IFs mainly consist of magnetite-hematite, quartz, and ± garnet, while the rocks from Nine Mile consist of garnet and quartz, and gahnite and quartz. Bulk-rock major and trace element compositions show that the rocks are enriched in Si and Fe with moderate but variable amounts of Mn and Al, which reflect variations of hydrothermal (up to 80%) and detrital contribution in the precursor phases. The rocks formed as a mixture of Fe or Fe-Mn

oxyhydroxides and minor clays similar to sediments from the modern redox-stratified rift basin at the Red Sea. Post-Archean Australian Shale (PAAS) normalized rare-earth element (REE) patterns of banded and massive IFs and garnet-quartz rocks exhibit a variety of REE contents and signatures with absent, very small, and moderately strong positive Eu anomalies suggesting that the precursor minerals formed from source hydrothermal fluids of variable temperatures. Strong positive Eu anomalies reflect source fluids with T > 250 °C and are associated with Mn-rich compositions that favor the incorporation of Eu. Small Eu anomalies reflect dilution by the addition of detritus, whereas strong negative Eu anomalies in gahnite-quartz rocks from Nine Mile likely reflect the discrimination of Eu by Fe-rich minerals in the precursor phases.

Bulk-rock PAAS-normalized REE patterns range from flat, to light-REE (LREE) enriched, and slightly heavy-REE enriched, which reflect an oxygen-stratified water body. True negative Ce anomalies are only present in a few Mn-bearing banded IFs that have flat REE patterns and slightly higher Al contents than the rest, which reflects precipitation from relatively shallow and oxygenated water. Most rocks lack Ce anomalies, have variable LREE trends, some have LREE enrichment, and are Al-poor and Fe-rich, reflecting precipitation under suboxic conditions from deeper water than the other IFs, the existence of a redoxcline, and reductive dissolution of Fe-Mn oxyhydroxides that provided additional LREEs. Overall, the variety of REE patterns and LREE enrichment and the negative and absent Ce anomalies suggest that at ~ 1.7 Ga the water column in the intracontinental Broken Hill rift basin was stratified and supported the existence of an oxide shuttle that cycled LREEs, which is consistent with results from IFs of similar ages in other basins.

Geochemistry and Genesis of Late Paleoproterozoic Banded Iron Formations and Metamorphosed Chemical Precipitates Spatially Associated with Pb-Zn Broken Hill-type Mineralization near the Broken Hill Deposit, Curnamona Province, Australia

A Thesis

Presented to the Faculty of the Department of Geological Sciences
Thomas Harriot College of Arts and Sciences

East Carolina University

In Partial Fulfillment of the Requirements for the Degree

Masters of Science

Geology

by

Erica Serna

December, 2014

Geochemistry and Genesis of Late Paleoproterozoic Banded Iron Formations and Metamorphosed Chemical Precipitates Spatially Associated with Pb-Zn Broken Hill-type Mineralization near the Broken Hill Deposit, Curnamona Province, Australia

by

Erica Serna

APPROVED BY:

DIRECTOR OF THESIS: _____
Adriana Heimann, PhD

COMMITTEE MEMBER: _____
Terri L. Woods, PhD

COMMITTEE MEMBER: _____
Richard L. Mauger, PhD

COMMITTEE MEMBER: _____
Richard K. Spruill, PhD

CHAIR OF THE DEPARTMENT
OF GEOLOGICAL SCIENCES: _____
Stephen J. Culver, PhD

DEAN OF THE
GRADUATE SCHOOL: _____
Paul J. Gemperline, PhD

ACKNOWLEDGEMENTS

I owe my deepest gratitude to my advisor, Adriana Heimann Ríos, for her guidance and support in concluding my Master's thesis. I am grateful for the opportunity to work with you and all of your unconditional support you have provided me. I would also like to thank my committee members Drs. Eric Horsman, Richard Spruill, Richard Mauger, and Terri Woods. Special thanks go to Dr. Paul Spry from Iowa State University and Mr. Wolfgang Leyh (Eaglehawk Geological Consulting) for collecting and providing the rock samples for this research and for providing information about the local geology of the studied area and about iron formations from Broken Hill. Thanks to Josh O'Brien for the geologic map. I would also like to thank Mike Wise for doing electron microprobe analysis at the Smithsonian Institution in Washington, DC, and Nick Foster for helping with electron probe microanalysis at Fayetteville State University, NC. Also, thanks to Tom Fink for helping me with the scanning electron microscope, and Dr. Mauger for taking the time for helping me with XRD analysis. Last but not least, I thank Jim Watson and John Woods for helping with the equipment to prepare my rock samples.

This research was funded by the College of Arts and Sciences and the Division of Research and Graduate Studies at East Carolina University, and a North Carolina Space Grant New Investigator Grant (to Dr. Heimann), as well as a Sigma Xi (the Scientific Research Society) Grant-in-Aid of Research.

The inspiration to pursue a Master's thesis was given to me by Drs. David Bish and Robert Wintch, two of my professors at Indiana University. They taught me how to hit the ground running and to never give up. Thank you for caring, thanks for EVERYTHING; this thesis is dedicated to you both.

I am indebted to many of my ECU colleagues: Leatha Moretz, Heather Lancaster, Jason Yonts, Sarah Harrison, David Hawkins, David Young, Katie Cummings, and Jessica Strand, among many others. Thank you for always being there for me and for the unconditional support you extended over the past two years at East Carolina University.

Last but not least, I deeply thank my family. Mom I truly appreciate all of the sacrifices you have made. This accomplishment would not have been possible without you. Thanks to my sister, and all my family in Mexico for their kind words of encouragement.

TABLE OF CONTENTS

LIST OF TABLES

LIST OF FIGURES

1. INTRODUCTION

Iron formations (IFs), characterized by alternating Fe-rich and Fe-poor layers, were deposited during the Precambrian for more than three billion years (Ga). They provide most of the iron mined in the world and valuable information about the evolution of the early Earth, in particular, the evolution of the oxygen in the ocean-atmosphere system during the Precambrian (e.g., Bekker et al., 2010). Deposition of large IFs such as the low-metamorphic grade ~2.5 Ga Brockman IF from the Hamersley Basin, Western Australia (e.g., Webb et al., 2003) and the ~2.5 Ga Kuruman IF in the Transvaal Craton, South Africa (e.g., Beukes and Klein, 1990; Bau and Dulski, 1996; Planavsky et al., 2010) were deposited prior to the shift from reducing to oxidizing conditions in the ocean-atmosphere system. However, after the great oxidation event (GOE; 2.3 Ga; Bekker, 2004) only relatively small IF deposits formed and are particularly associated with volcanogenic massive sulfide (VMS) deposits. Such is the case for the 1.89 Ga Biwabik-Gunflint IF from the Animikie basin, north-central Minnesota and Ontario (e.g., Planavsky et al., 2010), the IFs spatially associated with the 1.72 Ga Jones Hill Zn-Cu-Pb-Ag-Au sulfide deposit, northern New Mexico (Slack et al., 2009), and the 1.7 Ga IFs spatially associated with the Jerome Cu-Zn-Au-Ag sulfide deposit in central Arizona (Slack et al., 2007).

The decrease in abundance of Precambrian IFs during the late Paleoproterozoic was used in in some studies as an argument for sulfidic conditions in the ocean similar to those present in the modern Black Sea (e.g., Canfield, 1998). However, several studies investigated Eu and Ce anomalies in REE + Y patterns of these young IFs and suggested that the redox state was mainly suboxic to oxic (Holland, 1984;Planavsky et al., 2009).

Banded and massive IFs from the southern Curnamona Province, Australia, are among the youngest IFs formed in the late Paleoproterozoic at ~1.69 Ga. These rocks are found closely

associated with the giant, Broken Hill, Pb-Zn-Ag deposit as well as hundreds of smaller Pb-Zn sulfide deposits (Richards, 1966; Stanton, 1972, 1976a, 1977b; Johnson and Klinger, 1975; Spry and Wonder, 1989; Spry, 2000; Heimann et al., 2009). These banded and massive IFs have been the subject of some studies (e.g., Richards, 1966; Stanton, 1976a, 1977b), but their major and trace element geochemistry has not been studied in detail and their origin is still unclear, in part due to the high degree of metamorphism and intense deformation they have undergone (Stevens et al., 1986; Stanton and Williams, 1978; Willis et al., 1983). Richards (1966) and Stanton (1972) investigated the mineralogy of the banded IFs and its relation to the Broken Hill ore and proposed that the sulfide deposit and the IFs were of exhalative hydrothermal origin and were deposited in Al-rich detrital sediments. Johnson and Klingner (1975) and Plimer (1986) suggested that the Broken Hill deposit and hundreds of other small deposits formed in an intracontinental rift basin. In addition, Parr et al. (1992) and Lottermoser (1989) studied REE patterns of a few banded and massive IFs and metamorphosed chemical precipitates from the southern Curnamona Province and suggested that those rocks formed from hydrothermal fluids proximal and distal to hydrothermal vents.

In this contribution, the mineralogy, mineral chemistry, and bulk-rock major and trace element (including REE) compositions of 1.69 Ga banded and massive IFs and garnet- and gahnite-quartz rocks from the Broken Hill domain are used to determine the origin of the rocks and reconstruct the physicochemical conditions of the fluids, including the redox state of the water in the depositional basin. In addition, the chemical compositions of IFs of similar age associated with stratiform sulfide deposits, as well as large banded IFs that formed before the GOE are used to understand the chemical signatures of the IFs near Broken Hill and the redox characteristics of the basin water.

1.1 Abstract

Amphibolite to granulite facies, banded and massive magnetite-hematite, quartz ± garnet iron formations (IFs) and garnet- and gahnite-rich rocks are spatially associated with the giant, late-Paleoproterozoic, Pb-Zn-Ag Broken Hill deposit and hundreds of minor Broken Hill-type deposits in the southern Curnamona Province, New South Wales, Australia. These IFs are among the youngest IFs that formed in the late-Paleoproterozoic (1.69 Ga) after the Great Oxidation Event (GOE; ~2.35 Ga). Here I investigated the petrology and geochemistry of the IFs and the garnet- and gahnite-rich rocks to determine the genesis of the rocks and the physicochemical conditions of the fluids in the intracontinental Broken Hill rift basin, and the redox state of the water in this basin at that time of deposition.

Bulk-rock major and trace element compositions show that the rocks are enriched in Si and Fe with moderate but variable amounts of Mn and Al that suggest that these rocks formed as a mixture of hydrothermal Fe- and Mn-oxyhydroxides and minor clays. Post-Archean Australian Shale (PAAS) normalized rare earth element (REE) patterns in banded and massive IFs, including garnet- and gahnite-rich rocks exhibit strong positive to strong negative Eu anomalies suggesting that the original sediments formed from reduced hydrothermal fluids at T ~ 250 °C, and T > 250 °C, and proximal and distal to hydrothermal vents. However, the size and character of the Eu anomalies are also related to the Fe-Mn content of the rock, and the Eu signatures also likely reflect the sorption characteristics of precursors upon incorporation of Eu.

Light REEs and Ce anomalies vary among all the rocks suggesting the redox state of the depositional fluid was at a transitional, suboxic state, where Mn-oxyhydroxides worked as transportation agents for the cycling of LREEs along an stablished suboxic-anoxic boundary.

2. REGIONAL GEOLOGIC SETTING

Banded and massive IFs are located near the large Broken Hill and Pinnacles deposits and the smaller Little Broken Hill and Wild Dog deposits, whereas the garnet- and gahnite-rich rocks are found close to the Nine Mile deposit (Fig. 1; Table 1). The Pinnacles deposit is the second largest Broken Hill-type (BHT) deposit in the area (Parr, 1992). Broken Hill-type deposits are metamorphosed, strata-bound, Proterozoic Pb-Zn-Ag deposits associated laterally with metamorphosed chemical precipitates (Johnson and Klingner, 1975; Parr and Plimer, 1993).

Massive and banded IFs and garnet- and gahnite-quartz rocks form part of the Willyama Supergroup, a late Paleoproterozoic sequence (~7-9 km thick) of metasedimentary and metavolcanic rocks that accumulated in an intracontinental rift basin that operated over a period of at least 80 m.y. between ~1.72 to 1.64 Ga (Plimer, 1986; Parr et al., 2004; Page et al., 2005; Huston et al., 2006; Conor and Preiss, 2008; Fig. 2). Changes in the evolving intracontinental rift basin are recorded in three domains in the Curnamona Province: the Olary, Mulyungarie, and Broken Hill (Conor and Preiss, 2008).

Uranium-lead zircon dating (Page et al., 2003; 2005) shows that the Olary domain, on the flank of the rift basin, contains the oldest rocks known in the Willyama Supergroup, ranging from 1.720 to 1.715 Ga. They consist of A-type granite sills interbedded in dominant pelitic schist. Overlying this unit is the Bimba Formation, which consists of albitic-calcsilicate-carbonate-pelite-sulfide (magnetite-pyrite and barite) rocks, which are followed by metamorphosed pelites (mudstones) and psammopelites (sandy mudstones) in the uppermost unit of the Olary domain (Cook and Ashley, 1992; Bierlein, 1995; Conor and Preiss, 2008). It is believed that the 1.7 Ga magma intrusions caused the thinning of the lithosphere and mantle upwelling and lead to a shallow water environment consistent with a sabkha environment (Cook

and Ashley, 1992). Evidence of the first mafic intrusions in the southern Curnamona Province is also recorded in the Olary domain, suggesting that crustal extension continued until ~1.71 Ga. Also at this time, the rift zone shifted eastwards from the Olary (horst) to the Broken Hill domain (graben), where mafic activity peaked at 1.69 Ga.

In the Broken Hill domain, magmatic activity started at ~1.71 Ga when A-type igneous sills and S-type sills intruded into magnetite-bearing, albitic-pelitic, psammopelitic and psammitic gneiss and were extruded as quartz-feldspathic rocks of the Thackaringa Group. It is in this group, within the Cues Formation, that the Pinnacles deposit is found. This deposit is ~10 m.y. older than the Broken Hill deposit and is located stratigraphically 700 m lower. It is accompanied by garnet-biotite-rich quartz-feldspathic gneiss, garnet-quartz, and garnet-gahnite-quartz horizons, and different types of IFs such as banded quartz-magnetite rocks, garnet-quartz±magnetite rocks, quartz-iron sulfide rocks, and quartz-iron oxide rocks (Parr et al., 1992). The uppermost part of the Thackaringa Group, the Himalaya Formation, consists of a sequence of laminated albite-rich metasediments interlayered with magnetite-rich bands (Parr et al., 1992).

Overlying the Thackaringa Group is the Broken Hill Group, which is the best-preserved succession in the Willyama Supergroup; thickness range from 300 to 2000 m. At the bottom part of the Broken Hill Group is the Ettlewood Calc-Silicate Member that grades from well-banded polymetallic, sulfidic calc-silicates to pyritic, carbonaceous shales followed by a high metamorphic-grade, pelitic-psammopelitic sequence of the Allendale Metasediments and the psammitic schist and amphibolite successions of the Parnell Formation (Johnson and Klingner, 1975). The uppermost unit of the Broken Hill Group is the Hores Gneiss. It is a volcaniclastic sequence intruded by tholeiitic sills and dikes and hosts the Pb-Zn-Ag Broken Hill sulfide

deposit, hundreds of minor Broken Hill-type deposits, and at least eight horizons of banded IFs (Johnson and Klingner, 1975), some of which were studied here (Fig. 2).

Minor Pb-Zn-Ag Broken Hill-type mineralization in the 1.686 Ga Hores Gneiss is enclosed by amphibolites derived from tholeiitic to subalkalic basalts, whereas the main Broken Hill deposit is enclosed by the Potossi gneiss, which consists of quartz-feldspar-garnet-biotite gneiss of rhyodacitic origin (Johnson and Klingner, 1975). The Broken Hill deposit is 8 km long and 2,000 m thick and consists of at least six stacked lenses of sphalerite and galena and minor rhodonite, apatite, fluorite, calcite, pyrrothite, and chalcophyrite. Zoning detected in the ore lenses shows that Pb increases upwards and that Zn decreases upwards (Plimer, 1986).

Eight IF horizons have been identified in the Broken Hill domain. They are a few centimeters to ~2 m thick and are found interlayered with the Hores Gneiss (Johnson and Klingner, 1975). Of the eight banded IF horizons four show continuity along strike but two of them show continuity along strike equivalent with the ore deposit (Johnson and Klingner, 1975). The banded IFs decrease in magnetite and increase in garnet content, becoming petrographically and chemically similar to garnet-quartz rocks (Richards, 1966). The uppermost part of the Broken Hill domain is dominated by a thick sequence of andalusite-bearing carbonaceous pelite interlayered with silty metapsammopelite of the Sundown Group that range in age from ~1.680 to 1.672 Ga. These are overlain by banded pyritic-carbonaceous metasiltstones and minor schist of the Paragon Group deposited ~1.655 Ga (Johnson and Klingner, 1975).

Recent studies suggest that the dominance of metasedimentary and tholeiitic metavolcanic rocks, and particularly the existence of Pb-Zn sulfide deposits are evidence that the Willyama Supergroup formed as part of an intracontinental rift system. The Broken Hill domain is considered to represent the main rift basin, whereas the Olary domain was interpreted to be the

rift shoulder, and the Mulyungarie domain was the transition zone between the two (Plimer, 1986; Huston et al., 2006; Conor and Preiss, 2008). Deposition of the Mulyungarie domain starts with a ~250 m thick tuff sequence of the Portia Formation that was deposited ~1.705 Ga, concurrent with the feldspathic extrusions of the Thakaringa Group in the Broken Hill domain. Mineralization at the southern Curnamona Province formed from seawater circulating through faults that leached metals from older rocks of the Willyama Supergroup and deposited them at the bottom of the rift basin (Plimer, 1986; Huston et al., 2006). However, because the area has undergone multiple deformation events and high-grade metamorphism, the original environment of deposition is a subject of debate (e.g., Stanton 1972, 1976a, 1977b; Johnson and Klingner, 1975; Plimer, 1986). During the late Paleoproterozoic-early Mesoproterozoic (~1.657 to 1.575 Ga), the southern Curnamona Province was affected by the Olarian orogeny, where metamorphic grade, especially in the Broken Hill domain, reached the granulite facies (700-800 °C and 5-6 kbars) followed by retrograde metamorphism (Stevens, 1986; Page and Laing, 1992; Phillips and Wall, 1981). Further deformation and metamorphism took place ~ 0.5 Ga during the Delamerian orogeny (Stevens, 1986).

3. SAMPLING AND ANALYTICAL METHODS

Samples of metamorphosed banded IFs were collected from surface locations near the main Broken Hill deposit (4 samples), the Wild Dog BHT deposit (4 samples), and the Little Broken Hill BHT deposit (2 samples). The Wild Dog and Little Broken Hill deposits are located ~15 km south to southeast and 14.4 km southeast, respectively, from the main Broken Hill deposit. Samples of metamorphosed massive IFs were also collected from surface locations near the Pinnacles BHT deposit (4 samples), 15 km southwest from the Broken Hill deposit, and near the Little Broken Hill deposit (5 samples). Gahnite-quartz and garnet-quartz rocks were collected near the Nine Mile BHT deposit (14 samples), 7 km northwest from the Broken Hill deposit (Fig. 1).

The samples were described in hand specimen, then marked, cut, and sent for polished thin-section preparation at Vancouver Petrographics. Petrographic analysis was conducted at East Carolina University (ECU) using Olympus BX51 and BX41 reflected/transmitted light microscopes. An FEI Quanta 200 Mark 1 scanning electron microscope (SEM) coupled with an Oxford Inca x-act, X-ray energy dispersive, spectroscopy (EDS) system housed in the Department of Biology at ECU was used for identification and qualitative analysis of unknown minerals. Analytical conditions of the SEM included an accelerating voltage of 20 kV and a beam current of 6 nA. Electron microprobe analysis (EMPA) of garnet, magnetite, hematite, and gahnite in rocks from near the Broken Hill, Little Broken Hill, Wild Dog, and Nine Mile deposits were obtained at Fayetteville State University using a JXA-8530F Jeol field emission, electron probe microanalyzer with standard JEOL software. Analytical conditions were an accelerating voltage of 15 kV, a current beam of 10 nA (garnet) and 20 nA (oxides), and a spot size of 3 microns. Natural and synthetic mineral standards were used, including almandine garnet (Si, Al,

Mg, Fe), apatite (P, Ca), rutile (Ti), albite (Al, Na), rhodonite (Mn), chromite (Cr), San Carlos olivine (Si, Mg), ilmenite (Ti), corundum (Al), pure cobalt (Co), and gahnite (Zn, Al). Electron microprobe analysis of garnet in garnet-quartz rocks from Nine Mile was also done at the Smithsonian Institution in Washington, DC, using a JEOL 8900 field-emission, electron superprobe microanalyzer with an accelerating voltage of 15 kV, a beam current of 20 nA, and a beam diameter of 6 microns. Mineral standards included Kakanui hornblende (Mg, K), apatite (Ca, P, F), ilmenite (Ti), gahnite (Zn), manganite (Mn), chromite (Cr), and grossular garnet (Si, Al). Mineral compositions are presented in Tables 2 and 3.

For bulk-rock major and trace element (including REEs) chemical analysis, 10 g slabs were cut and sent to ACME Analytical Laboratories, Vancouver, Canada. Major and trace element contents were obtained following a lithium metaborate/tetraborate dissolution technique. This technique involved mixing of the sample with lithium metaborate and lithium tetraborate and fusing in an induction furnace, then adding a solution of 5% nitric acid until complete dissolution occured. The samples were analyzed for major oxides and trace elements using a Thermo Jarrell-Ash ENVIRO II, inductively-coupled plasma (ICP)-emission spectrometry (ES) system and a Varian Vista 735 ICP- mass spectrometry (MS) system, respectively. Base metal (Cu, Pb, Zn) and Au contents were determined by dissolving 0.5 g of sample in aqua regia at 90°C and then analyzing using a Perkin Sciex ELAN 6000, 6100, or 9000 ICP-MS. Major and trace element compositions of the studied rocks are given in Table 4.

4. PETROGRAPHY

The rocks from near the Broken Hill, Little Broken Hill, Wild Dog, and Pinnacles deposits were grouped into banded magnetite-garnet-quartz rocks, massive hematite-quartz ± magnetite rocks, massive quartz-magnetite ± garnet rocks, and massive to poorly banded garnet-hematite-quartz ± magnetite rocks (Table 1; Fig. 3). Banded magnetite-garnet-quartz rocks are referred to as banded IF, whereas the massive rocks with magnetite, hematite, quartz ± garnet are referred to as massive IF. The rocks from the small Nine Mile deposit are simple massive garnet-quartz rocks and massive gahnite-quartz rocks (Table 1; Fig. 3).

Banded magnetite-garnet-quartz IFs from near the Broken Hill, Little Broken Hill, and Wild Dog deposits are moderately magnetic. They consist of interlayered iron-rich (dark reddish-brown color) and iron-poor (silica-rich, light reddish brown color) laminations ranging from millimeter scale (microbands) to almost 1cm thick (mesobands) (Fig. 3a). The bands have the same general mineralogy consisting of magnetite, garnet, and quartz, but the mineral proportions vary. The order of the mineral abundance in the iron-rich layers is magnetite, garnet, and quartz, whereas the iron-poor layers are primarily composed of quartz with minor garnet and magnetite. Accessory minerals include apatite and minor biotite, while hematite and minor chlorite are secondary minerals. Magnetite tends to occur as medium-grained, subhedral crystals, although some inclusions of magnetite in garnet and quartz have sub-rhombic habit (Fig. 4b). Small inclusions of garnet, apatite, and quartz are found in magnetite, and replacement of magnetite by hematite (i.e., martite) in trellis texture is also present (Fig. 4c). Garnet is more abundant in the iron-rich bands, it is medium-to fine-grained and contains small inclusions of magnetite, quartz, and apatite (Fig. 4a). In banded IFs from near the Broken Hill and Little Broken Hill deposits garnet has subhedral habit with granoblastic, interlobate textures and shows 120° triple-junctions

with quartz, whereas in the banded IFs from near Wild Dog garnet is moderately fractured and minor intergrowth texture with quartz is present at the garnet rims. In addition, the banded IFs from near Wild Dog have polycrystalline quartz that shows undulose extinction. Apatite is found in all banded IFs as inclusions in magnetite and garnet, and is commonly concentrated in the iron-poor laminations (Fig. 4a). It is very fine grained and exhibits the typical hexagonal prism and elongated needle like habit. Biotite is found in very small amounts (< 1%) as an accessory mineral and is brownish-green in plane light. The few biotite flakes usually coexist with magnetite and are only found in the banded IFs from near the Wild Dog deposit. Light-green chlorite also exists in very small amounts (< 1%), replacing biotite and altering some garnet rims, particularly in one sample (AD-10-012). Chlorite is also only seen in banded IFs from near Wild Dog.

The texture of all banded IF samples is very simple and consistent. Most exhibit granoblastic, interlobate textures, except for the banded IFs near the Wild Dog deposit that show porphyroclastic textures. These banded IFs are also more oxidized and show more iron stains than the banded IFs from near the Broken Hill and Little Broken Hill areas. In addition, one sample (AD-10-012) shows a micro-fault and another (AD-10-015) from Little Broken Hill is folded.

Massive hematite-quartz ± magnetite IFs from near the Pinnacles deposit show an advance state of oxidation where magnetite has been almost entirely replaced by hematite (Fig. 3b). These rocks consist of hematite and quartz, except for one sample (AD-10-007) in which most of its magnetiteis preserved. In addition, another sample (AD-10-009) has small amounts of accessory biotite (< 1%) and apatite (< 1%). In hand sample, the specimens have an even, dark-reddish-brown color (Fig. 3b). Quartz tends to occur as semi-rounded anhedral crystals and

varies from fine-to coarse-grained. Coarser grained quartz shows minor granoblastic, amoeboid texture, while fine-and medium-grained quartz has granoblastic, interlobate texture, including ~120° triple junctions (Fig. 4c). Inclusions of magnetite with sub-rhombic habit and inclusions of elongated apatite occur in quartz of only one sample (AD-10-009). This sample also has a few crystals of biotite. In plane light biotite is dark brown and is always present in mutual contact with hematite. Hematite tends to occur as coarse-grained crystals in a porous texture with vugs ~ 0.5 mm in diameter. It has subhedral habit, has experienced oxidation to goethite and limonite. Except for the one mentioned above (AD-10-007). None of the massive hematite-quartz ± magnetite IFs from Pinnacles are magnetic. Massive quartz-magnetite ± garnet IFs from Little Broken Hill are strongly magnetic. These rocks are coarser-grained than the other rock types. They consist primarily of milky quartz with minor magnetite and garnet (Fig. 3c). Trace minerals include coarse-grained sphalerite, pyrite (0.3%), and chalcopyrite (0.1%). Anhedral magnetite shows minor trellis texture along rims and fractures due to replacement by hematite (Fig. 4c). Polycrystalline quartz exhibits granoblastic amoeboid texture and undulose extinction. Quartz is also present as fine-grained inclusions in magnetite. Garnet is medium-grained, euhedral to subhedral, and is found only as inclusions in quartz. Anhedral sphalerite and anhedral chalcopyrite occur in mutual contact, and chalcopyrite shows concentric zoning and pyrite rims visible under the microscope.

Massive to poorly banded garnet-hematite-quartz ± magnetite IFs from Little Broken Hill have coarser garnet grains than other rock types. The mineral abundance and texture vary among these rocks. Two IFs are massive with a black-reddish color and consist of garnet, magnetite, and quartz (Fig. 3d). These samples are moderately fractured and extremely oxidized, where most of the oxidation has spread through and along fractures (Fig. 4d). Another IF is poorly

banded and richer in garnet (AD-10-020) compared with the two previously mentioned. It mainly consists of garnet and quartz with very minor amounts of magnetite. The layers are garnet-rich and garnet-poor. The garnet-rich layers contain most of the garnet and quartz with minor magnetite that gathers mainly at the boundary between layers. The garnet-poor layers mainly consist of quartz, lesser accessory apatite and very minor magnetite. Garnet in these massive to poorly banded IFs is coarse-grained, and exhibits subhedral to anhedral habit in an iron stained matrix. Accessory subhedral apatite is only found in the poorly banded IF (AD-10-020), and it is present as small inclusions in garnet but also as coarser-grained crystals in the garnet-poor layers. Magnetite is anhedral and exhibits a mesh-like texture (Fig. 4d). Most of the magnetite has been oxidized and is found filling spaces between garnet and quartz grains (Fig. 4d). Due to the oxidation of magnetite, the massive IFs are not magnetic while the poorly banded IF is slightly magnetic.

Massive garnet-quartz rocks from the Nine Mile deposit (Fig. 3e) are mostly pink in color, although one sample is dark pink and black (GA7). The pink rocks mainly consist of garnet and quartz with variable amounts of accessory apatite, very minor (< 1 %) ± biotite, ± muscovite, ± amphibole, disseminated magnetite and sphalerite, and chlorite. In addition, one sample (GA6) has a small vein of plagioclase. The dark pink and black rock (GA7) mainly consists of amphibole-biotite-quartz and minor but coarse garnet with disseminated magnetite and sphalerite. Overall, garnet is coarse-grained but moderately fractured. In some cases, chlorite is found along the fractures (Fig. 4e). Garnet has subhedral and anhedral habit, although, in the amphibole-biotite-quartz rock (GA7), garnet has idioblastic and poikiloblastic texture with large quartz inclusions. Disseminated, anhedral magnetite and sphalerite are present in small amounts in all of the samples, while tan to dark brown biotite frequently coexists with amphibole, when

this is present. Under plane light, amphibole has a light tannish-blue color. Polycrystalline quartz exhibits granoblastic amoeboid texture and undulose extinction.

The massive gahnite-quartz rocks from Nine Mile consist of euhedral and subhedral, dark green gahnite in a massive quartz matrix (Fig. 3f) with minor apatite and very minor muscovite and biotite (only in two samples; GH1 and GH7, respectively) and very minor disseminated magnetite and sphalerite. Gahnite is coarse-grained but highly fractured. Most gahnite crystals display poikiloblastic texture and have moderate to high amounts of quartz inclusions that, in some cases, concentrate at the core of the crystal (Fig 4f). Polycrystalline, coarse-grained quartz exhibits granoblastic amoeboid texture and undulose extinction. A few crystals of brown biotite (< 1%) are found in one sample while muscovite is found only surrounding some gahnite crystals. Minor disseminated magnetite and sphalerite (<1 %) are present as inclusions in gahnite and quartz.

5. MINERAL CHEMISTRY

5.1 Major element composition of garnet

Electron microprobe analyses of garnet in banded and massive IFs and garnet-quartz rocks from the study sites are presented in Table 2. Overall, the compositions of garnet from near the Broken Hill, Little Broken Hill, Wild Dog, and Nine Mile deposits are enriched in almandine (alm) and spessartine (sps) components with minor grossular (grs) + andradite (and) contents (Fig. 5, Table 2). The composition of garnet in the banded and massive IFs and garnet-rich rocks from Nine Mile can be represented by the following end-member ranges: $alm_{16.19\text{-}79.44}$ $sps_{34.26\text{-}76.1}$ grss + $adr_{0.6\text{-}25.16}$.

A ternary diagram of almandine-(grossular + andradite)-spessartine (Fig. 5) shows that garnet in massive to poorly banded garnet-hematite-quartz ± magnetite IF from near Little Broken Hill has the highest spessartine content (61 to 78 mol %), whereas garnet in the massive garnet-quartz rocks from Nine Mile has the highest almandine content (55 to 79 mol %). Both rock types, however, have two distinct populations of garnet (Fig. 5). One population in massive garnet-quartz rocks from Nine Mile has grossular + andradite contents of 7 to 10 mol % (samples GA1 and GA4), whereas the other has 20 to 25 mol % grossular + andradite. A similar subdivision is observed in garnet from the massive to poorly banded garnet-hematite-quartz ± magnetite rocks from Little Broken Hill, where one population of garnet (AD-10-019 and 20) has 4 to 7 mol % and the other (AD-10-021) has 12 to 13 mol % grossular + andradite content.

Garnet in banded magnetite-garnet-quartz IFs from near the Broken Hill deposit plots along the almandine-spessartine line (37 to 60 mol % spessartine and 29 to 55 mol % almandine) and has the lowest grossular + andradite content (1 to 7 mol %), although one sample (AD-10-001) has higher grossular + andradite contents (13 to 15 mol %; Fig. 5). Garnet in banded magnetite-

garnet-quartz banded IFs from Wild Dog and Little Broken Hill has roughly equal amounts of almandine and spessartine components. Garnet in Little Broken Hill has lower (7 to 11 mol %) grossular + andradite component, whereas that from Wild Dog has the highest grossular + andradite content (20 to 25 mol %).

5.2 Compositional zoning in garnet

Compositional zoning was identified in garnet and representative rim-core-rim chemical profiles are shown in Figure 6. Garnet in the majority of the IF from near the Broken Hill, Little Broken Hill, and Wild Dog deposits shows compositional zoning with respect to Fe and Mn. Major-element zoning in garnet in the massive garnet-quartz rocks from Nine Mile was not observed.

Overall, garnet in banded and massive IFs from near the Broken Hill, Little Broken Hill, and Wild Dog deposits has higher Mn and lower Fe contents at the core than at the rims (Fig. 6a). Chemical profiles of garnet in banded magnetite-garnet-quartz IF from near Broken Hill and Little Broken Hill show a gradational increase in Fe from core to rim (FeO ~ < 3 wt.%) and Mn decreases (MnO < 5 wt.%) from core to rim (Fig. 6a). In addition, garnet in banded magnetite-garnet-quartz IF from Wild Dog and garnet in massive to poorly banded garnet-hematite-quartz ± magnetite IF from Little Broken Hill also shows an increase in Fe and decrease in Mn contents from core to rim. These variations are up to ~ 2 wt.% oxides in garnet from banded IF near Wild Dog and up to ~ 5 wt.% oxides in that from Little Broken Hill (Fig. 6b). Garnet in banded IFs from Broken Hill and Little Broken Hill is richer in MnO than FeO (Fig. 6a). In contrast, garnet in banded and massive IFs from Wild Dog and Little Broken Hill is richer in FeO than MnO

(Fig. 6b) and thus compositional zoning profiles look different, but in fact, both show similar trands in core-rim variations (Fig. 6).

5.3 Major-element composition of magnetite, hematite, and gahnite

The composition of magnetite, hematite and gahnite from representative samples is presented in Table 3. As expected, magnetite and hematite in massive and banded IFs from near the Broken Hill, Little Broken Hill, Wild Dog, and Pinnacles deposits have small contents of Al (Al_2O_3 up to 0.4 wt.%), Mn (MnO up to 0.17 wt.%), Co (CoO up to 0.23 wt.%), and Ti (TiO_2 up to 0.6 wt.%). Gahnite in the gahnite-quartz rocks from Nine Mile is enriched in Zn (26-34 wt.% ZnO) with moderate Fe (7.68-14.61 wt.% FeO) and low Mg (1.27-1.66 wt.% MgO) contents.

6. WHOLE-ROCK GEOCHEMISTRY

6.1 Major-element compositions

Bulk-rock major and trace-element compositions appear in Table 4. Overall, banded and massive IFs from near the Broken Hill, Little Broken Hill, Wild Dog, and Pinnacles deposits are mostly composed of Fe (14.2 to 89.9 wt.% FeO), silica (6.4 to 68.2 wt.% SiO_2) and variable Mn, Ca, Al, and P (up to 16.6 wt.% MnO, 10.1 wt.% CaO, 8.9 wt.% Al_2O_3, and 7.1 wt.% P_2O_5). Garnet- and gahnite-quartz rocks from Nine Mile are rich in silica (30.5 to 87.5 wt. % SiO_2) and relatively low in Fe (2.5 to 24.2 wt.% FeO) and have much higher aluminum contents (6.1 to 38.5 wt.% Al_2O_3) compared with the IFs and banded IFs.

A Ca-Fe-Mn ternary diagram shows that most of the rocks are enriched in Fe with moderate Mn and low Ca contents (Fig. 7a). Massive hematite-quartz ± magnetite IFs from Pinnacles, one massive quartz-magnetite ± garnet IF from Little Broken Hill (AD-10-018), and most of the massive gahnite-quartz rocks from Nine Mile have > 93.4 mol % Fe. In contrast, massive to poorly banded garnet-hematite-quartz ± magnetite IFs from Little Broken Hill and one massive garnet-quartz rock (GA2) from Nine Mile plot along the Fe-Mn axis with up to 59.6 and 54.2 mol % Fe and Mn, respectively, and very low Ca content (< 4.1 mol % Ca). Banded magnetite-garnet-quartz IFs from near the Broken Hill, Little Broken Hill, and Wild Dog deposits, one massive quartz-magnetite ± garnet IF (AD-10-017) from Little Broken Hill, most garnet-quartz-rocks, and one massive gahnite-quartz (GH2) rock from Nine Mile cluster near the Fe corner (64 to 88 mol % Fe) with less than 20 mol % Ca and Mn content.

Proportions of detrital versus hydrothermal components are emphasized in an Al-Fe-Mn ternary diagram and in an Al/(Al+Fe+Mn) *vs.* Fe/Ti plot (Figs. 7b and 8a). Iron and Mn are considered to be of hydrothermal origin and Al and Ti are assumed to have been derived from a

detrital sediment source (Boström, 1973). In the Al-Fe-Mn ternary diagram, the garnet-free and garnet-poor rocks plot at the Fe corner and along the Fe-Al axis (Fig. 7b). Such is the case for massive hematite-quartz ± magnetite IF from Pinnacles and one massive quartz-magnetite ± garnet IF (AD-10-018) from Little Broken Hill. These rocks are rich in Fe (up to 97.7 mol %) and low in Al (up to 2.2 mol %) and Mn (up to 1.2 mol %). Banded magnetite-garnet-quartz IFs from near the Broken Hill, Little Broken Hill, and Wild Dog deposits plot together close to the Fe corner (78-87 mol % Fe) and display minor Al contents (5-12 mol %), while massive garnet-quartz rocks from Nine Mile have up to 35 mol % Al and 65 mol % Fe (Fig. 7b). Massive gahnite-quartz rocks from Nine Mile have the highest Al contents among the rock types analyzed and plot along the Fe-Al axis with up to 82 mol % Al.

The Al/(Al+Fe+Mn) *vs.* Fe/Ti diagram shows that the iron-rich, garnet-poor rocks have the highest Fe/Ti ratios and are similar in these components to East Pacific Rise (EPR) and Red Sea hydrothermal sediments (Boström, 1973; Marching et al., 1982; Fig. 8a). As the amount of garnet in the rocks increases, a gradational increase in Al/(Al+Fe+Mn) ratios is observed accompanied by a decrease in Fe/Ti ratios (Fig. 8a). Massive hematite-quartz ± magnetite IFs from Pinnacles and massive quartz-magnetite ± garnet IFs from Little Broken Hill plot along the Fe/Ti axis with the highest Fe/Ti ratios, similar to those of the EPR and Red Sea hydrothermal sediments. Banded magnetite-garnet-quartz IFs from near the Broken Hill, Little Broken Hill, and Wild Dog deposits, and the massive to poorly banded garnet-hematite-quartz ± magnetite IFs from Little Broken Hill plot along the mixing line between the EPR and the average continental crust with less than 20 % Al/(Al+Fe+Mn) (Fig. 8a). Massive garnet-quartz rocks from Nine Mile have low Fe/Ti ratios but ~ 50 % Al/(Al+Fe+Mn), similar to Fe-Mn metalliferous hydrothermal sediments from the EPR (Cronan and Hodkinson, 1997). In addition, both ratios in

the massive gahnite-quartz rocks from Nine Mile are high, and these rocks have the highest Al/(Al+Fe+Mn) values among those measured rocks and are similar to those in the average continental crust (Böstrom, 1976).

6.2 Minor and some trace element compositions

The trace-element contents of massive and banded IFs from near the Broken Hill, Little Broken Hill, Wild Dog, and Pinnacles deposits, and garnet- and gahnite-quartz rocks from the Nine Mile deposit are generally low (Table 4). Slight enrichment in Zn, Cu, Pb, Sr, Ba, and V is mainly present in the massive quartz-magnetite ± garnet IF and massive to poorly banded garnet-hematite-quartz ± magnetite IF from Little Broken Hill, and massive garnet- and gahnite-quartz rocks from Nine Mile. High Zn and Cu contents (up to 10,000 ppm and 280 ppm, respectively) occur in massive quartz-magnetite ± garnet IF from Little Broken Hill. Massive to poorly banded garnet-hematite-quartz ± magnetite IFs from Little Broken Hill and massive garnet-quartz rocks from Nine Mile also have high Zn (up to 1,873 and 757 ppm, respectively) and Cu contents (up to 1,352 and 180 ppm, respectively). Massive gahnite-quartz rocks from Nine Mile have very high Zn (up to 20%) and low Cu contents (up to 47 ppm). Magnetite-garnet-quartz banded IF near the Broken Hill deposit, massive to poorly banded garnet-hematite-quartz ± magnetite IF from Little Broken Hill, and massive garnet-quartz rocks and gahnite-quartz rocks from Nine Mile have the highest Pb contents (up to 2,492, 829, 1,409, and 3,787 ppm, respectively).

Strontium is present in banded magnetite-garnet-quartz IFs (32 to 351 ppm), while the highest Sr content was found in the massive to poorly banded garnet-hematite-quartz ± magnetite IFs (up to 989 ppm) from Little Broken Hill. Higher contents of Ba are only present in one

massive to poorly banded garnet-hematite-quartz-magnetite IF (AD-10-019; 1,901 ppm) from Little Broken Hill. Vanadium is particularly concentrated in all banded magnetite-garnet-quartz IFs (308 to 546 ppm) and massive garnet-quartz rocks (193 to 541 ppm) from Nine Mile. On an Fe-[(Co+Ni+Cu) x 10]-Mn ternary plot (Fig. 9) the various rocks plot close to the Fe-Mn line and have very minor Ni, Co, and Cu contents, with the exception of one massive hematite-quartz-magnetite IF from Little Broken Hill (AD-10-019) that plots at the center of the diagram due to its high Cu content (Fig. 9).

6.3 Rare earth element and yttrium compositions

Rare earth elements + yttrium contents are presented in Table 4, while PAAS-normalized REY patterns and chondrite-normalized REY patterns are shown in Figure 10. Both normalization schemes are used for comparison purposes because chondrite is commonly used in studies of the Broken Hill area whereas PASS normalization is used in most IF studied. The total REE contents in these rocks are relatively low, with values ranging from 7.8 to 249.7 ppm, although one massive gahnite-quartz rock from Nine Mile (GH2) has the highest total REE content of the studied rocks (886.8 ppm; Table 4). Banded magnetite-garnet-quartz IFs from near the Broken Hill, Little Broken Hill, and Wild Dog deposits have similar total REE contents ranging from 76.6 to 164.2 ppm. Massive hematite-quartz ± magnetite IFs from Pinnacles have low total REE contents (17.1 to 62.8 ppm). However, the only magnetite-rich rock (magnetic) from this location (AD-10-007) has a higher total REE content (249.7 ppm). Massive-quartz-magnetite ± garnet and massive to poorly banded garnet-hematite-quartz ± magnetite IFs from Little Broken Hill have variable total REE contents ranging from 9.3 to 93.9 ppm. Garnet-quartz rocks from Nine Mile have total REE contents ranging from 52.2 to 163.4 ppm, whereas gahnite-

quartz rocks from Nine Mile tend to have low but variable total REE contents (7.8 to 76.9 ppm), except for the sample mentioned previously (GH2; Table 4).

Based on PAAS-normalized REE patterns, enrichment in light REE (LREE = La to Gd) relative to heavy REEs (HREEs = Tb to Lu) is present in massive hematite-quartz ± magnetite IFs from Pinnacles and massive quartz-magnetite ± garnet IFs from Little Broken Hill (Fig. 10b, 10c). In contrast, massive garnet-quartz rocks from Nine Mile are characterized by LREE depletion and HREE enrichment (Fig. 10e). Banded magnetite-garnet-quartz IFs from Broken Hill, Little Broken Hill, and Wild Dog, massive to poorly banded garnet-hematite-quartz ± magnetite IFs from Little Broken Hill, and massive gahnite-quartz rocks from Nine Mile have somewhat flat REE patterns (Fig. 10a, d, f). Some rocks have a slight increase or decrease in HREEs from Y to Lu (Fig. 10b, c, f).

Bau and Dulski (1996) detected a slightly positive Gd anomaly in modern seawater. Therefore, the Eu anomaly (Eu/Eu*) is calculated using Tb, and it is defined quantitatively as $Eu/Eu^* = Eu_{SN}/(0.66Sm_{SN} + 0.33Tb_{SN})$, where SN = shale-normalized (Bau and Dulski, 1996, Planavsky et al., 2010). The majority of the rocks display a significant positive Eu anomaly (Eu/Eu* >1; Bau and Dulski, 1996) in PAAS-normalized plots. The strongest positive Eu anomalies occur in banded magnetite-garnet-quartz IFs from near the Broken Hill deposit (Eu/Eu* = 2.2 to 2.6; Fig. 10a) and massive quartz-magnetite ± garnet IF and massive to poorly banded garnet-hematite-quartz ± magnetite IF from Little Broken Hill (Eu/Eu* = 2.5 to 2.9; Fig. 10c-d). Moderately weak positive Eu anomalies are present in the banded magnetite-garnet-quartz IFs from Wild Dog and Little Broken Hill (Eu/Eu* =1.3 to 1.9 Fig. 10a). Slightly negative to slightly positive Eu anomalies are present in massive hematite-quartz ± magnetite IFs from Pinnacles (Eu/Eu* = 0.9 to 1.3; Fig. 10b) and massive garnet-quartz rocks from Nine Mile

(Eu/Eu* = 0.7 to 1.6; Fig 10e). Negative Eu anomalies are recorded in massive gahnite-quartz rocks from Nine Mile (Eu/Eu* = 0.5 to 0.7; Fig. 10f).

Intepretation of Ce anomalies in REE patterns can be a little complicated. This is because seawater may have anomalous La abundances and Ce anomalies in REE patterns may not necessarily be a consequence of Ce behavior. Therefore, true Ce anomalies were calculated using the relationship between Ce/Ce* (defined as $Ce_{SN}/(0.5Pr_{SN}+0.5La_{SN})$) and Pr/Pr* (defined as $Pr_{SN}/(0.5Ce_{SN}+0.5Nd_{SN})$) (Fig.12; Bau and Dulski, 1996; Planavksy et al., 2010). Only banded magnetite-garnet-quartz IFs from near the Little Broken Hill and Wild Dog deposits, one banded IF from near the Broken Hill deposit, and two massive to poorly banded garnet-hematite-quartz ± magnetite IFs from Little Broken Hill have true negative Ce anomalies (Fig. 12a). Banded IFs from Wild Dog have the strongest true negative Ce anomalies among all samples, whereas the rest have no Ce anomaly (Fig. 12a).

7. DISCUSSION

Given the observations mentioned in the previous section, the possible precursor phases and physicochemical conditions of the fluids involved in the formation of banded and massive IF from near the Broken Hill, Little Broken Hill, Wild Dog, and Pinnacles, deposits as well as garnet-quartz and gahnite-quartz rocks from near the Nine Mile deposit are evaluated.

The shape of the REE+Y patterns and Ce and Eu anomalies are utilized to interpret the hydrothermal, hydrogenetic and detrital contributions to the protolith of the rocks and the physicochemical characteristics of the water in the intracontinental Broken Hill rift basin and the nature of the original sediments.

7.1 Hydrothermal, hydrogenous, and detrital components

It is well known that the large, Pb-Zn-Ag, Broken Hill sulfide deposit formed in an intracontinental rift basin (Plimer, 1986; Johnson and Klingner, 1975; Parr and Plimer, 1993; Huston et al., 006; Connor and Preiss; 2008). The relationship of the Broken Hill ore deposit to banded and massive IFs and garnet-rich rocks have been the focus of several studies (e.g., Richards, 1966; Stanton, 1972, 1976a, 1977b; Lottermoser, 1989, 1991; Parr et al., 2004; Plimer, 2006; Spry and Wonder 1989; Spry and Heimann, 2007; Heimann et al., 2009, 2011). However, little attention has been given to the redox state of the water in the depositional basin.

The main chemical components in the massive and banded IFs from near the Broken Hill, Little Broken Hill, Wild Dog, and Pinnacles deposits are Fe (up to 89.9 wt.% FeO), Si (up to 68.2 wt.% SiO_2), Mn (up to 16.6 wt.% MnO) and Al (up to 8.9 wt.% Al_2O_3; Table 4). The garnet- and gahnite-quartz rocks from the Nine Mile deposit area are richer in silica (30.5 to 87.5

wt.% SiO_2), and lower in Fe (2.5 to 24.2 wt.% FeO), and have much higher Al contents (6.1 to 38.5 wt.% Al_2O_3) compared to the banded and massive IFs.

Hydrothermal fluids are characterized by high concentrations of Fe, Mn, Pb, Cd, Au, Ca, Sr, Ba, P, Eu, CO_2, and S, whereas detrital sediments, particularly aluminosilicate minerals, are rich in Si, Ti, Al, K, Zr, REEs (except Eu), Sc, V, Y, Yb, Co, Ni, and Cr (Boström, 1973). Therefore, the high Fe, Si, Mn, and Al contents suggest that both hydrothermal and detrital components contributed to the protolith of the banded and massive IFs and the garnet- and gahnite-quartz rocks from Nine Mile. The relative proportions of their hydrothermal and detrital inputs are indicated on the Al/(Al+Fe+Mn) *vs.* Fe/Ti diagram (Fig. 8a). In addition, metasedimentary rocks from Broken Hill and Nine Mile, other IFs of similar and different ages as those of the studied rocks, and Fe- and Al-rich metalliferous sediments from the Red Sea are presented for comparison purposes (Fig. 8b).

Banded magnetite-garnet-quartz IFs from near the Broken Hill, Little Broken Hill, and Wild Dog deposits and two massive to poorly banded garnet-hematite-quartz ± magnetite IFs from Little Broken Hill plot along the mixing line between East Pacific Rise hydrothermal sediments and average continental crust (Boström, 1973) and have high Fe/Ti ratios equivalent to ~ > 80 % hydrothermal component and minor detrital input (~ < 20 %; Fig. 8a). Heimann et al. (2009) studied the composition of two banded IFs from near the Broken Hill deposit and concluded that they had at least 80 % hydrothermal input. Similarly, Slack et al. (2009) studied quartz-magnetite IFs, garnet-quartz IFs, and one quartz-magnetite-garnet IF spatially associated with the 1.72 Ga Jones Hill (Zn-Cu-Pb-Ag-Au) sulfide deposit, northern New Mexico, and observed that the chemistry of the nearby quartz-magnetite-garnet IF had high hydrothermal input. Banded magnetite-garnet-quartz IFs from near the Broken Hill, Little Broken Hill, and Wild Dog

deposits and two massive to poorly banded garnet-hematite-quartz ± magnetite IFs from Little Broken Hill have similar Fe/Ti and Al/(Al+Fe+Mn) ratios to the banded IFs studied by Heimann et al. (2009) and Slack et al. (2009), and some Fe-rich metalliferous sediments from the Red Sea (Laurila et al., 2014). They have Al contents that are slightly higher (up to 8.95 % Al_2O_3) than the low-metamorphic grade, ~2.5 Ga magnetite-quartz-siderite Brockman IF from the Hamersley Basin, Western Australia (e.g., Webb et al., 2003), the slightly metamorphosed ~2.5 Ga siderite-hematite-magnetite Kuruman IF in the Transvaal Craton, South Africa (e.g., Beukes and Klein, 1990; Bau and Dulski, 1996; Planavsky et al., 2010), the 1.89 Ga chert-magnetite-hematite ± siderite ± ankerite Biwabik-Gunflint IFs from the Animikie basin, north-central Minnesota and Ontario, Canada (Planavsky et al., 2010) and most Fe-rich metalliferous sediments from the Red Sea (Laurila et al., 2014). They also have lower Al contents than metasedimentary rocks from the Broken Hill area and the Jones Hill deposit IF in New Mexico (Fig. 8b; Slack and Stevens, 1994; Slack et al., 2009).

A significant hydrothermal contribution and low detrital component are observed in massive hematite-quartz ± magnetite rocks from Pinnacles and massive quartz-magnetite ± garnet rocks and one massive to poorly banded garnet-hematite-quartz rock from Little Broken Hill (Fig. 8a). They plot along the Fe/Ti axis (Fe/Ti > 100) with the EPR hydrothermal sediments (Böstrom, 1973a, b) and Fe-rich metalliferous sediments from the Red Sea (Laurila et al., 2014), and have ~ > 90 % hydrothermal input. These rocks also plot similarly to the large Brockman (e.g., Webb et al., 2003) and Kuruman IFs (e.g., Beukes and Klein, 1990; Bau and Dulski, 1996; Planavsky et al., 2010), and the 1.7 Ga jasper and banded hematite-quartz IF spatially associated with the Jerome Cu-Zn-Au-Ag sulfide deposit in central Arizona (Slack et al., 2007). The massive hematite-quartz ± magnetite IFs from Pinnacles and the massive quartz-magnetite ± garnet IF

and one massive to poorly banded garnet-hematite-quartz IF from Little Broken Hill have low Al (< ~5 wt.% Al_2O_3) contents similar to those of the Brockman and Kuruman IFs (< 1.5 wt. % Al_2O_3), and reflect an Al-free or Al-poor precursor with > 90 % hydrothermal component (Fig. 8b).

Massive garnet-quartz rocks from the Nine Mile deposit have roughly equal amounts of hydrothermal and detrital input (Fig. 8a). They also have similar Fe/Ti and Al/(Al+Fe+Mn) ratios to the Al-rich metalliferous sediments from the Red Sea with the lowest Al contents (Laurila et al., 2014) and similar ratios to the garnet-bearing rocks near the Broken Hill deposit (Heimann et al., 2009) and garnet-quartz IFs from the Jones Hill deposit (Slack et al., 2009, Fig. 8b). The Al contents of the garnet-quartz rocks from Nine Mile (6 to 15 wt.% Al_2O_3) are higher than those of typical Archean-Proterozoic IFs but lower than most metasedimentary rocks from the Broken Hill area (Slack and Stevens, 1994). The gahnite-quartz rocks from Nine Mile have the highest Al/(Al+Fe+Mn) ratios (0.81) among all studied rocks, even higher than the average continental crust (0.6), argillite (0.61), and rhyolite (0.78) from Arizona (Slack et al., 2007), and metasediments from Broken Hill (0.56-0.68; Slack and Stevens, 1994; Fig. 8b). However, the gahnite-quartz rocks have high zinc content, which is of hydrothermal source. This is reflected in the high Fe/Ti ratios (up to 1000) suggesting a high hydrothermal component (Fig. 8). Previous studies have suggested that gahnite most likely formed by desulfication of sphalerite (Spry, 2000) during metamorphism.

An Fe-[(Co+Ni+Cu) x 10]-Mn ternary diagram displays the possible hydrogenous (adsorption or precipitation of certain elements from seawater) contribution into the protolith of the banded and massive IFs and garnet- and gahnite-quartz rocks from Nine Mile (Fig. 9). This diagram shows that the hydrogenous input in all of the rocks is minimal and that the rocks are

mainly hydrothermal, except for one sample (AD-10-019; Fig. 9) that, due to its high concentration of Cu (up to 1,353 ppm), plots in the hydrogenous field (Fig 9). However, Cu may have not been adsorbed from seawater, but instead could have originated with epigenetic mineralization during the Delamerian orogeny (Penhall, 2001). This is consistent with the observation that this sample also has high concentrations of Ba (1,901 ppm), Sr (539 ppm), Pb (829 ppm), and Zn (1,815 ppm), which are typical elements of hydrothermal origin. Thus, minimum hydrogenous input contributed to the precursor phases of all the banded and massive IFs from Broken Hill, Little Broken Hill, Pinnacles, and Rockwell as well as the garnet- and gahnite-quartz rocks from Nine Mile.

Overall, the geochemical data, suggest that most of the studied rocks were mixtures of hydrothermal and detrital components where hydrous Fe- and Mn-rich oxyhydroxides were most likely the initial precursors before being deposited with variable amounts of Al-rich detrital sediments (Fig. 8, 9). Banded IFs from Broken Hill, Little Broken Hill, and Wild Dog, and two massive to poorly banded garnet-hematite-quartz ± magnetite IFs have at least 80 % hydrothermal input with minor detrital components, while the massive IFs from Pinnacles and Little Broken Hill have > 90 % hydrothermal input, similar to the low Al late Archean-early Proterozoic Brockman and Kuruman IFs, younger IFs from Arizona, and present day Fe-rich metalliferous sediments from the Red Sea and East Pacific Rise. Massive garnet-quartz rocks from Nine Mile contain roughly equal amounts of hydrothermal and detrital inputs, and plot similarly to modern Al-rich metalliferous sediments from the Red Sea, whereas the gahnite-quartz rocks from Nine Mile have a highly detrital origin with a moderately high, hydrothermal-Fe component.

Richards (1966) noticed a gradual partial separation of Mn and Fe in banded IF horizons and Mn-rich, garnet-quartzite horizons near Broken Hill. He noticed that the IF horizons became more petrographically and chemically similar to the Mn-garnet rich rocks in the stratigraphic column. In other words, the magnetite content in the banded IFs decreases as the Mn-garnet content increases from the lowermost to the uppermost banded IF horizon, indicating a gradual change from a reduced to a more oxidized environment of deposition as the uppermost ore lode was approached. He concluded that the banded IFs and the garnet-rich rocks were in fact co-genetic. Later on, Stanton (1972) concluded that the IFs formed as the result of intensive submarine hydrothermal emissions deposited on Al-rich detrital sediments. Prior to the exhalative activity at the intracontinental Broken Hill rift basin, the water was somewhat oxygenated, but with the increase of hydrothermal activity, the local environment was overwhelmed and reduced hydrothermal fluids created slightly reducing conditions (Eh -0.2 to -0.6V) at a pH ~8 (Stanton, 1972, 1976a, 1977b). These conditions allowed for the transportation of dissolved iron until it reached a more oxygenated environment. A stratified water column is observed in modern oceans and restricted basins such as the Red Sea (e.g., Laurila et al., 2014). This is also envisioned for the environment of deposition of late Paleoproterozoic IFs of similar age to Broken Hill (e.g., Slack et al., 2007, 2009; Planavslky 2009, 2010) and in the intracontinental Broken Hill rift basin.

7.2 Significance of REE + Y patterns

It has been widely accepted that regional, high-grade metamorphism does not affect the REE patterns of rocks unless they go through partial melting and/or when fluid/rock ratios are higher than 100 (Muecke et al., 1979). At or near the Broken Hill deposit, metamorphic conditions

reached the granulite facies, but Lottermoser (1989), Parr (1992), Spry et al. (2007), and Heimann et al. (2009) showed that the REE composition of rocks from and near the Broken Hill deposit remained intact. Furthermore, Stanton (1972, 1976a, 1977b) stated that metamorphism at the Broken Hill area was that of a closed system where original meso- and micro-sediment bands in IFs were preserved.

Post-Archean Australian Shale-normalized REE + Y patterns of hydrothermal fluids, seawater, Fe- and Al-rich metalliferous sediments from the Red Sea, metasedimentary rocks from the Brocken Hill area, and other banded and massive IFs of various ages are illustrated in Figures 10 and 11 for comparison purposes. In PAAS-normalized REE patterns, hydrothermal fluids are characterized by quite flat patterns, strong positive Eu anomalies, and no Ce anomalies, whereas modern oxygenated seawater is characterized by low REE contents, slight enrichment in HREEs, and strong negative Ce anomalies (Fig. 11a; Mitra et al., 1994; Mills et al., 1995).

Banded magnetite-garnet-quartz IFs from Broken Hill, Little Broken Hill, Wild Dog, and massive to poorly banded garnet-hematite-quartz ± magnetite IFs from Little Broken Hill are characterized by flat REE patterns and weak to moderately strong positive Eu anomalies (Fig. 10a-d). Similarly flat REE patterns are seen in the Fe- and Al-rich metalliferous sediments from the Red Sea (Laurila et al., 2014), in metasediments from Broken Hill (Slack and Stevens, 1994), and in some of the Biwabik and Gunflint IFs (Planavsky et al., 2009), although, Eu anomalies vary among all of them (Fig. 10a-c). Iron- and Al-rich metalliferous sediments from the Red Sea have strong positive Eu anomalies similar to those of hydrothermal fluids, while metasediments from Broken Hill have strong negative Eu anomalies (Fig. 11a-b). Biwabik and Gunflint IFs have small to moderately strong positive Eu anomalies that are smaller than those of

hydrothermal fluids and similar to those of banded magnetite-garnet-quartz IFs from Broken Hill, Little Broken Hill, and Wild Dog, and massive to poorly banded garnet-hematite-quartz ± magnetite IFs from Little Broken Hill. In addition, the total REE contents in banded IFs from Broken Hill, Little Broken Hill, and Wild Dog are similar to some Al-rich metalliferous sediments from the Red Sea (Laurila et al., 2014), some metasediments from Broken Hill (Slack and Stevens, 1994) and some Biwabik and Gunflint IFs samples (Fig. 10, 11).

Slight enrichment in LREEs over HREEs is present in massive hematite-quartz ± magnetite IF from Pinnacles (except sample AD-10-009, Fig. 10b) and massive quartz-magnetite ± garnet IF from Little Broken Hill (Fig. 10b, c). However, massive IFs from Pinnacles do not have marked Eu anomalies, whereas massive IFs from Little Broken Hill have strong positive Eu anomalies similar to those of hydrothermal fluids and Fe- and Al-rich metalliferous sediments from the Red Sea (Laurila et al., 2014). Massive IFs from Pinnacles (Fig. 10b) and Little Broken Hill (Fig. 10c) and IFs from Brockman, Kuruman, and Arizona (Fig. 11d, e) have similar low Al contents. However, massive IFs from Pinnacles and Little Broken Hill are enriched in LREEs as opposed to the low Al IFs from Brockman, Kuruman, and Arizona that have smaller LREE/HREE ratios and positive Eu anomalies.

Massive garnet-quartz rocks from Nine Mile have somewhat similar REE patterns as the Brockman and Kuruman IFs and the younger IFs from Arizona and New Mexico. They are characterized by enrichment in HREEs with respect to LREEs (Figs. 10e, 11d, e, f). However, Eu anomalies in garnet-quartz rocks from Nine Mile are mostly small, negative, or absent (except for one sample, GA6, which has minor plagioclase, thus explaining the positive Eu anomaly) and are similar only to those of jasper and banded hematite-quartz IF from the Jerome District, Arizona, and to some garnet-quartz IF from Jones Hill, New Mexico (Slack et al., 2007,

2009; Figs. 10e, 11e, f). Massive gahnite-quartz rocks from Nine Mile have REE patterns characterized by strong negative Eu anomalies. These REE patterns, including the shape of the patterns, the negative Eu anomalies, and the total REE content, are very similar to the metasediments from Broken Hill (Slack and Stevens, 1994; Figs. 10f, 11a).

In an investigation of garnet-rich rocks, pelites, sulfide-rich and garnet-gahnite-bearing rocks from the Pinnacles deposit, Parr (1992) noticed that chondrite-normalized REE patterns and Eu anomalies of such rocks were related to their stratigraphic position with relation to the ore. She noticed that rocks on the footwall were characterized by LREE enrichment and had negative Eu anomalies, whereas less LREE enriched patterns and positive Eu anomalies characterized the rocks in the hanging wall. Banded and massive IFs from near the Broken Hill, Little Broken Hill, Wild Dog, and Pinnacles deposits and gahnite-quartz rocks from Nine Mile have chondrite-normalized REE patterns that are enriched in LREE and with Eu anomalies that vary according to their location. Garnet-quartz rocks from Nine Mile, however, are the only rocks that have flat chondrite-normalized REE patterns with negative or absent Eu anomalies. Spry et al. (2007) and Heimann et al. (2009, 2011) stated different conclusions from those of Parr (1992), emphasizing that mineralogy especially crystallography did in fact control the size and signatures of Eu anomalies in garnet-rich rocks.

Numerous studies have established that in order to have large accumulations of banded IFs on the seafloor, hydrothermal dissolved iron (Fe^{2+}) and manganese (Mn^{3+}) are transported into slightly oxygenated waters where Fe- and Mn-oxyhydroxides precipitate. Other elements in seawater or of hydrogenetic origin (Mg, Ni, Co, U, W, P, Cu, Y, Th and REEs, except Eu) can be scavenged by Fe- and Mn-oxyhydroxides and the initial hydrothermal REE patterns can be changed (e.g., Michard et al., 1989; German et al., 1990; Bau and Möller, 1993; Sholkovitz et al.,

1994; Bau et al., 1996; Bau and Dulski, 1996, 1999; Bau et al., 1997; Laurila et al., 2014). German et al. (1990) noticed that in oxygenated seawater, Fe- and Mn-oxyhydroxides favor the scavenging of LREEs over HREEs due to the differential REE particle reactivity. In addition, enrichment of LREEs has been recorded in Mn-oxyhydroxides from some modern, redox-stratified basins (e.g., Black Sea; German et al., 1990) and has been attributed to the presence of a suboxic-anoxic boundary (redoxcline; German et al., 1990). After precipitation, the Fe-oxyhydroxides settles to the bottom in the anoxic part of the basin, while Mn-oxyhydroxides dissolve below the redoxcline. When Mn-rich particles dissolve, the liberated LREEs are taken in by Fe-oxyhydroxides, which do not go through reductive dissolution at the boundary because requires more extreme reducing conditions (Bau and Dulski, 1996; Planavsky et al., 2010). Thus, Mn-oxyhydroxides fuction as a transportation agent of LREEs to Fe-oxyhydroxides in redox-stratified basins. This cycle is responsible for the enrichment of LREEs over HREEs in particles that precipitate or settle below the redox boundary.

During the Archean and early Proterozoic, a redoxcline was still absent and, IFs that formed at that time are LREE depleted (e.g., Planavsky et al., 2010). However, during the late Paleoproterozoic, after ~ 1.80 Ga and in particular at ~ 1.69 Ga, in the Broken Hill rift basin a suboxic-anoxic boundary was established and allowed for the cycling of Mn-Fe oxyhydroxides (e.g., Planavsky et al., 2010). This can explain the enrichment of LREEs relative to what is seen in some modern seawaters and Archean-Proterozoic IFs. Rare earth element patterns enriched in LREEs, either flat patterns or those with LREEs higher than HREEs, are consistent with the existence of a redox boundary and the shuttling of Fe-Mn particles from shallow to deep waters in the depositional basin. In massive hematite-quartz ± magnetite IFs from Pinnacles and massive quartz-magnetite ± garnet IFs from Little Broken Hill, LREE-enriched, HREE depleted

patterns suggest that the precursor minerals to these IFs were likely deposited below the redox boundary and inherited the LREEs from seawater that had excess LREEs from reductive dissolution of Mn oxyhydroxides. The LREE enrichment, the strong positive Eu anomalies, the low Al content, and the low Al/(Al+Fe+Mn) and high Fe/Ti ratios are consistent with these rocks reflecting a deeper origin and a higher hydrothermal component than those in the banded IFs.

Flat REE patterns in banded IFs from Broken Hill, Little Broken Hill, and Wild Dog, and massive to poorly banded garnet-hematite-quartz ± magnetite IFs from Little Broken Hill can also be explained by a shuttle of Fe-Mn particles along a redoxcline and likely reflect formation in somewhat shallower water relative to the massive IFs. Higher detrital and REE contents in banded IFs also imply that part of the REEs were derived from original sediments, and this is also consistent with these IFs having flat patterns similar to metasediments from the Broken Hill area and Al-rich metalliferous sediments from the Red Sea, except the difference in the nature of the Eu anomaly, and this will be discussed below.

The LREE depletion of the massive garnet-quartz rocks from Nine Mile can be linked to oxidized waters where LREE where already removed and transported by Mn- oxyhydroxides to the more anoxic part of the basin (German et al., 1990; Planavsky et al., 2010). It was noted that because the REEs in these rocks are mostly hosted in garnet, the LREE depleted patterns which are characterized by similar shapes, are also a reflection of the REE patterns of garnets (e.g., Heimann et al., 2011), and garnet thus reflects the composition of the protolith and the processes operating in seawater at the time of deposition. Finally, the variable Eu anomalies suggest lower temperatures of the source hydrothermal fluids or mixing with more seawater, which is also consistent with the idea that these rocks formed from more oxidized water in shallower parts of the basin.

7.3 Significance of Eu anomalies in REE patterns

Europium anomalies in REE patterns develop when Eu fractionates from the rest of the REEs due to a change in valence state (Eu^{2+} and Eu^{3+}). The rest of the REEs (except Ce) only have one oxidation state (+3). In hydrothermal fluids and seawater, the valence state of Eu is strongly dependent on the temperature and redox state of the fluids (e.g., Sverjensky, 1984; German et al., 1990; Möller and Dulski, 1992). Europium $^{2+}$ is more stable at high temperatures (> 250 °C) and under reduced conditions, whereas at lower temperatures and under oxidized conditions, Eu^{2+} rapidly oxidizes to Eu^{3+} (e.g., Sverjensky, 1984; Möller and Dulski, 1992). Thus, Sverjensky (1984) suggested that strong positive Eu anomalies in REE patterns were restricted hydrothermal rocks deposited by fluids with temperatures > 250 °C and that rocks associated with cooler fluids showed no Eu anomalies.

The massive and banded IFs and garnet- and gahnite-quartz rocks from Nine Mile have Eu anomalies that range from strongly negative to strongly positive (Fig 10e-f). Banded magnetite-garnet-quartz IFs from near the Broken Hill, Little Broken Hill, and Wild Dog deposits, and massive quartz-magnetite ± garnet IFs and massive to poorly banded garnet-hematite-quartz ± magnetite IFs from Little Broken Hill have small to moderately strong positive Eu anomalies similar to those IFs of various ages, black and white smoker fluids, and Fe- and Al-rich metalliferous sediments from the Red Sea (e.g., Planavsky et al., 2010; Figs. 10a, 11a, b). The positive Eu anomalies indicate that the temperature of the source hydrothermal fluids of these IFs was likely ≥ 250 °C.

Negative Eu anomalies in massive gahnite-quartz rocks from Nine Mile are similar to the metasediments from Broken Hill (Slack and Stevens, 1994), but total REE contents in the

gahnite-quartz rocks are lower (Figs. 10f, 11a). Massive hematite-quartz ± magnetite IFs from Pinnacles and massive garnet-quartz rocks from Nine Mile have negative, absent, or slightly positive Eu anomalies in PAAS normalized patterns. The absence of strong positive Eu anomalies in these rocks suggests that the temperature of the source hydrothermal fluids was cooler than 250 °C. Another possibility is that any strong positive Eu signature characteristic of hot hydrothermal fluids was weakened or lost as the fluids mixed with oxidized seawater at increasing distances from the hydrothermal vent. This was proposed by Lottermoser (1989) who studied chondrite-normalized REE compositions of tourmaline-, feldspar-, gahnite-, calcite-, magnetite-, amphibole- and garnet-rich rocks proximal and distal to the Broken Hill deposit. He found that the rocks were all enriched in LREEs, but those proximal to the ore deposit had positive Eu anomalies and rocks distal from the ore deposit had negative Eu signatures. However, Heimann et al. (2009, 2011) emphasized that the chemical and crystallographic characteristics of the precursor elements (Mn, Fe, Ca) could also control the size of the Eu anomalies in the garnet-rich rocks. Heimann et al. (2009) reported that rocks with abundant Fe-rich, Mn-poor, garnets were characterized by negative Eu anomalies while those with abundant Mn-rich, Fe-poor garnet-rich, rocks had positive Eu anomalies. Eu ($^{2+}$) easily substitutes for Mn and Ca, but can be discriminated against by Fe-rich minerals (Heimann et al., 2009, 2011). Therefore Mn-oxyhydroxides can incorporate more Eu whereas, Fe-oxyhydroxides discriminate against Eu.

At Broken Hill, most banded and massive IFs with positive Eu anomalies have garnet with at least 35 mol % spessartine, whereas the Mn-depleted rocks, such as the massive hematite-quartz ± magnetite IFs from Pinnacles and the massive gahnite-quartz rocks from Nine Mile have strong negative to very weak positive Eu anomalies supporting the findings of Heimann et

al. (2009). The absence of strong positive Eu anomalies can be explained by the high Fe and low Mn contents, which also support earlier findings (Heimann et al., 2009). However, massive quartz-magnetite ± garnet IFs from Little Broken Hill have very low Mn contents, are enriched in LREEs, and have moderately strong positive Eu anomalies similar to those in Al-rich metalliferous sediments and magnetite-rich IFs. The LREE enrichment, the positive Eu signatures, and the low inferred detrital components in these rocks reflect a deep, anoxic-suboxic environment where hot reduced hydrothermal fluids were the main contributors of REEs to the precursor phases. In addition, the LREE enrichment supports reductive dissolution of Mn oxyhydroxides along a redox-boundary. For these IFs the Mn and Fe contents do not seem to affect the nature of the Eu anomalies. Overall, the REE content and Eu anomalies in these rocks were determined by the temperature of the hydrothermal fluids, the Mn content of the precursor phases, and the mixing of reduced hydrothermal fluids with oxygenated waters away from the hydrothermal vent.

7.4 Ce anomalies and Y/Ho ratios and implications for the redox state of the local seawater at 1.69 Ga.

The existence of any true Ce anomalies were determined using the Ce/Ce* *vs*. Pr/Pr* diagram (Bau and Dulski, 1996). The studied rocks mainly plot in two fields: positive La anomaly but no Ce anomaly, and true negative Ce anomaly (Fig. 12a). True negative Ce anomalies are present in banded magnetite-garnet-quartz IFs from near the Little Broken Hill and Wild Dog deposits, one banded IF from near the Broken Hill deposit, and two massive to poorly banded garnet-hematite-quartz ± magnetite IFs from Little Broken Hill (Fig. 12a). Banded IFs from near the Wild Dog deposit have the strongest negative Ce anomalies. One metasedimentary rock from Nine Mile (MS1), metasediments from Broken Hill (Slack and

Stevens, 1994), modern Fe- and Al-rich metalliferous sediments from the Red Sea, as well as other IFs of various ages were plotted for comparison purposes. The majority of these rocks do not have true negative Ce anomalies (Fig. 12b).

Strong negative Ce anomalies are restricted to fully oxygenated open sea environments (Fig. 11a). This is due to the oxidation of Ce^{3+} to Ce^{4+} and the sorption of Ce^{4+} onto Fe-Mn oxyhydroxide particles, particularly Mn oxyhydroxides (Bau and Dulski, 1996). With the incorporation of Ce in Mn oxyhydroxides, seawater becomes depleted in Ce and develops a strong negative Ce anomaly, while particles that incorporate Ce^{4+} show positive Ce anomalies (German et al., 1990; Bau and Dulski, 1996). Modern redox stratified basins show evidence of REE cycling due to the presence of a redoxcline boundary where Fe- and Mn- oxyhydroxides work as to transport shuttle for REEs in oxic shallow waters to deeper anoxic environments (e.g., Planavsky et al., 2010). In the oxic shallow part of a stratified basin, water has a negative Ce anomaly because Ce^{4+} is incorporated into Fe and Mn oxyhydroxides and clay particles, while in deeper suboxic or anoxic waters, Ce anomalies are slightly positive due to release of Ce during the reductive dissolution of Mn oxyhydroxides (Planavsky et al., 2010). As a result, redox stratified waters can show slightly negative and or slightly positive Ce anomalies while strong negative Ce anomalies in water are mainly recorded above the redox boundary in more oxygenated parts of the basin (Planavsky et al., 2009, 2010). During the Archean and early Proterozoic, the oxygen content in the ocean-atmosphere system was very low and Ce stayed dissolved in its reduced state (Ce^{3+}). The seas did not have a redoxcline boundary or a transportation agent, resulting in the absence of Ce anomalies in the water and in the Mn-oxyhydroxides (Bau and Dulski, 1996; Planavsky et al., 2010). As a result, IFs that formed during the Archean and early-Proerozoic are also LREE depleted (e.g., Planavsky et al., 2010).

For example, older, ~2.5 Ga IFs such as the Brockman and Kuruman IFs have positive La anomalies but no Ce anomalies that are the result of anoxic condition of the seawater and the absence of a suboxic-anoxic boundary before the GOE (Bau and Dulski, 1996; Planavsky et al., 2010).

Iron formations such as the 1.7 Ga IFs from Arizona and New Mexico are spatially associated with ore deposits. They have been interpreted as chemical precipitates that formed under deep suboxic water conditions because they show moderately positive Ce anomalies (Slack et al., 2007, 2009). This also supports the presence of a suboxic-anoxic boundary and the existence of dissolved oxygen either persistently or periodically needed to oxidize Fe^{2+} and Ce^{3+} (Slack et al., 2007, 2009). However, these interpretations were based on the shape of PAAS-normalized REE patterns and not on the true Ce anomalies. In the Ce/Ce* *vs.* Pr/Pr* diagram, these rocks show mostly positive and negative La anomalies and positive Ce anomalies but no negative Ce anomalies (except for one sample). This is consistent with the idea that these rocks formed under suboxic conditions in a stratified basin (Fig. 12b). Similarly, the 1.89 Ga Biwabik and Gunflint IFs have positive La and Ce anomalies in shale-normalized REE patterns reflecting oxic to suboxic conditions (Planavsky et al., 2009, 2010).

Present day Fe- and Al-rich metalliferous sediments from the Red Sea also have positive La anomalies but no Ce anomalies and such are not reflecting the modern global oxygenated seawater but instead reflect their local environment. These anomalies are typical of sediments that are deposited in suboxic environments not too far below the redoxcline boundary. Recent studies have interpreted the lack of Ce anomalies in the Red Sea to be the result of the possible isolation of the basin from the open sea, and to the lack of mixing between the brines and oxygenated seawater (Laurila et al., 2014).

In the southern Curnamona Province, only banded magnetite-garnet-quartz IFs from Wild Dog and two massive to poorly banded garnet-hematite-quartz ± magnetite IFs from Little Broken Hill have true strong negative Ce anomalies, which suggest that these rocks formed under more oxygenated, shallower waters than the others. In contrast, the lack of Ce anomalies in massive quartz-magnetite ± garnet IFs from Little Broken Hill and massive hematite-quartz ± magnetite IFs from Pinnacles suggests that the precursor phases of these rocks precipitated below the redox boundary. In addition, the LREE enrichment in these rocks further supports the existence of a redoxcline boundary, the shuttle of Fe and Mn oxyhydroxides to deeper parts of the basin, the reductive dissolution of these oxides, and the liberation of LREEs to deeper water. Banded magnetite-garnet-quartz IFs from Broken Hill, Little Broken Hill, and massive gahnite-quartz rocks from Nine Mile also lack Ce anomalies, but they are characterized by flat PAAS-normalized REE patterns suggesting that the precursor phases precipitated at or near the redoxcline boundary.

Yttrium, in seawater has an affinity for Fe-oxyhydroxides and would likely compete with Ho in the Fe-rich particles because of their similar charges, and ionic radii. In addition, Y has lower particle reactivity compared with its geochemical twin Ho, which results in Y/Ho ratios in stratified seawater (44-74) that are higher than those in Cl chondrites, hydrothermal fluids, and most shales (28-38; e.g., Bau and Möller, 1993; Bau et al., 1996, 1997; Bau, 1999; Bau and Dulski, 1999; Laurila et al., 2014). A decrease in Y/Ho ratios in modern suboxic to anoxic seawater results from the dissolution of Mn-Fe particles near the redoxcline, which produces an increase in Ho relative to Y (Bau et al., 1997; Nozaki et al., 1997; Planavsky et al., 2010). Interestingly, Archean-Paleoproterozoic IFs have strong Y anomalies and high Y/Ho ratios,

which reflect the absence of an oxide shuttle across a Mn redoxcline and the correspondent lack of reductive dissolution and release of Ho (e.g., Planavsky et al., 2010).

Banded and massive IFs and garnet- and gahnite-quartz rocks from the southern Curnamona Province have quite variable Y/Ho ratios (25-60; Table 4). These wide compositional ranges in Y/Ho are consistent with precipitation of Fe-Mn oxyhydroxides from stratified waters at varying redox conditions and with a Mn redoxcline and shuttle of oxides to the deeper part of the basin. Banded magnetite-garnet-quartz IFs from near the Broken Hill, Little Broken Hill, and Wild Dog deposits and two massive to poorly banded garnet-hematite-quartz ± magnetite IFs from Little Broken Hill have Y/Ho ratios (28-39) similar to those of chondrites, hydrothermal fluids, and terrestrial materials. These ranges of Y/Ho values suggest that variable amounts of hydrothermal and detrital components were incorporated into the precursor phases of these banded IFs, which is consistent with Fe/Ti and Al/(Al+Fe+Mn) ratios and the shape of REE patterns. The Y/Ho ratios in these rocks are similar to those in the late Paleoproterozoic Biwabik and Gunflint IFs (avg. Y/Ho = 32), which have been interpreted to reflect formation from stratified water bodies and varying contributions of REEs and Y derived from dissolution and precipitation of Fe-Mn oxyhydroxides (Planavsky et al., 2010). The Y/Ho ratios in banded magnetite-garnet-quartz IFs from near the Broken Hill, Little Broken Hill, and Wild Dog deposits and two massive to poorly banded garnet-hematite-quartz ± magnetite IFs from Little Broken Hill also support the presence of a redoxcline boundary in the Broken Hill rift basin, the precipitation of these rocks close to the redoxcline boundary, and the incorporation of detrital input in the precursor phases of these rocks.

Somewhat lower Y/Ho ratios (25-30) are present in garnet- and gahnite-quartz rocks from Nine Mile (except one, Y/Ho = 40), one massive hematite-quartz ± magnetite IF from Pinnacles,

and one massive quartz-magnetite ± garnet IF from Little Broken Hill. The low Y/Ho ratios in the massive IFs from Pinnacles and Little Broken Hill and the enrichment of LREE in massive IFs from Pinnacles suggest that these rocks precipitated under more reduced conditions and below the redoxcline boundary, which is consistent with Fe/Ti and Al/(Al+Fe+Mn) ratios that reflect a dominant hydrothermal origin. Thus, these rocks originated at suboxic to anoxic water conditions under the influence of hydrothermal fluids and precipitated below the redoxcline boundary. The Y/Ho ratios and the absence of Y anomalies in the rocks from Nine Mile suggest precipitation of the Fe and Mn oxyhydroxides from relatively oxic water, which is consistent with Fe/Ti and Al/(Al+Fe+Mn) ratios and the flat shape of the REE patterns of the gahnite rocks, and all together suggest a shallow origin with detrital-hydrothermal contributions.

In contrast, some high Y/Ho ratios in two massive hematite-quartz ± magnetite IFs from Pinnacles (Y/Ho = 40 and 60), one massive to poorly banded garnet-hematite-quartz ± magnetite IF from Little Broken Hill (Y/Ho = 44), and one massive gahnite-quartz rock from Nine Mile (Y/Ho = 40), are similar to those of modern, oxygenated, shallow waters (e.g., Planavsky et al., 2010), and reflect some precipitation from seawater. However, the fact that rocks from the same site found in close proximity may show different Y/Ho ratios simply reflects small variations in the location and redox condition of the local water, as well as varying contributions of detrital and hydrothermal components in the precursor phases.

The effect of a small detrital component on the total REE contents, the shape of the REE patterns, and the Ce anomalies in the banded and massive IFs and garnet- and gahnite-quartz rocks from Nine Mile were investigated. The total REE content of the banded IFs has a positive correlation ($r^2 = 0.74$; Fig. 13) with the Al_2O_3 content of the rocks that reaches 8.94 wt.% Al_2O_3. This positive correlation suggests that detrital input contributed REEs to the precursor phases of

the rocks and that the REE patterns can be a mixture of REEs derived from hydrothermal fluids, detrital sediments, and seawater (Fig. 13), which is consistent with Fe/Ti and Al/(Al+Fe+Mn) ratios. However, a positive correlation is not seen in the rest of the rocks from this study, but it is present in the Al-rich metalliferous sediments from the Red Sea (up to 9.2 wt.% Al2O3; Laurila et al., 2014) and the metasediments from the Broken Hill area (up to 21.3 wt.% Al2O3; Slack and Stevens, 1994). Nonetheless, metasediments from Broken Hill have a much higher REE and Al content than the banded IFs from this study and the Al-rich metalliferous sediments from the Red Sea (Fig. 13; Laurila et al., 2014), while the latter has slightly higher detrital content (Al_2O_3) than the banded IFs (Fig. 13). Furthermore, there is no correlation between the size of the Ce anomaly and the Al_2O_3 content in the banded IFs (Fig. 14b). Similarly, some Archean and Proterozoic IFs have various Al that do not correspond with variability in REE+Y features, including Ce anomalies (Planavsky et al., 2010). In banded IFs, those with negative Ce anomalies have higher REE contents. This means that if the addition of REEs from a detrital component modified the original seawater/hydrothermal-derived REE patterns of the protolith it would have done so by generating a more negative Ce anomaly in the banded IFs. This could be consistent with the origin of the rocks from relatively shallow and oxygenated water based on the other geochemical indicators. However, modern metalliferous sediments and metasedimentary rocks from the Broken Hill areas do not have true negative Ce anomalies but instead lack Ce anomalies. Therefore, the negative Ce anomalies cannot have been derived from the addition of REEs with detritus, and most likely reflect the oxygenated character of the shallow zone of a stratified seawater body and precipitation at or near the redoxcline.

The absence of Ce anomalies in banded IFs from Broken Hill, massive IFs from Pinnacles, some massive IFs from Little Broken Hill, and massive garnet- and gahnite-quartz rocks from

Nine Mile, on the other hand, could possibly be explained by the addition of REEs with the detrital component of the rocks, but they have either lower total REE or Al contents than the other banded IFs. Banded IFs that lack Ce anomalies also have Fe/Ti and Al/(Al+Fe+Mn) ratios that reflect a higher hydrothermal content than those with negative Ce anomalies. Therefore, it is concluded that the absence of Ce anomalies in the rocks reflects an origin in a deeper, suboxic to anoxic part of a stratified water body compared with those that have negative Ce anomalies.

8. Conclusions

Bulk-rock major and trace element compositions, mineralogy, mineral chemistry, and texture of the banded and massive IFs near the Broken Hill, Little Broken Hill, Pinnacles, and Wild Dog Pb-Zn deposits and garnet- and gahnite-quartz rocks from the Nine Mile Pb-Zn deposit suggest that the protoliths of these rocks formed as a result of precipitation from intense submarine hydrothermal emissions mixed with seawater and deposition along with varying amounts of siliciclastic sediments. Ratios of Fe/Ti and Al/(Al+Fe+Mn) suggest that banded IFs from near the Broken Hill, Little Broken Hill, and Wild Dog deposits, including most massive to poorly banded garnet-hematite-quartz ± magnetite IF from Little Broken Hill, have at least 80% hydrothermal input with minor detrital contribution into their protoliths. Iron and Mn were derived from hydrothermal fluids, where dissolved Fe^{2+} precipitated as $Fe^{3+}(OH)_3$) when it mixed with oxygenated waters, whereas oxidation of Mn^{2+} to Mn^{4+} and precipitation occurred later on, in a more oxygenated environment of deposition. Therefore, the initial precursor phases in the banded and massive IFs and massive garnet-quartz rocks from Nine Mile were Fe- and/or Mn-oxyhydroxides and clays. Massive gahnite-quartz rocks from Nine Mile, on the other hand, have high detrital (Al) as well as a major hydrothermal Zn contribution.

Flat PAAS-normalized REE patterns of banded IFs from Broken Hill, Little Broken Hill, and Wild Dog are similar to those of Broken Hill metasedimentary rocks with low Al content and the positive correlation between total REE and Al_2O_3 contents suggests that part of the REEs were derived from a detrital source. However, the lack of correlation between Al and total REE contents and Ce and Eu anomalies indicates that the small amount of Al did not modify or define the anomalies. Small positive Eu anomalies in banded IFs suggest that the temperature of the source hydrothermal fluids that contributed in the formation of these rocks was > 250 °C.

Massive hematite-quartz ± magnetite IFs from Pinnacles and massive quartz-magnetite ± garnet IFs from Little Broken Hill have LREE enrichment over HREEs, relatively low REE contents, low Al contents, and high Fe/Ti and low Al/(Al+Fe+Mn) ratios that suggest they are mostly hydrothermal in origin. Massive IFs from Little Broken Hill have strong positive Eu anomalies similar to hydrothermal fluids and metalliferous sediments from the Red Sea, suggesting that the temperature of the hydrothermal fluids was > 250 °C. The lack of positive Eu anomalies in massive IFs from Pinnacles, on the other hand, could be the result of the loss of the Eu signature while the hydrothermal fluids traveled away from the vent, or the lack of Mn content and enrichment of Fe. Alternativily, the temperature of the hydrothermal fluids at Pinnacles could have been lower than 250 °C.

Based on Fe/Ti and Al/(Al+Fe+Mn) ratios and PAAS-normalized REE patterns, the massive garnet-quartz and gahnite-quartz rocks from Nine Mile have higher detrital contribution than the banded and massive IFs from the other study sites. Massive garnet-quartz rocks have roughly equal amounts of detrital and hydrothermal input, while gahnite-quartz rocks are mostly detrital in origin with high concentrations of hydrothermal Zn. These rocks also lack positive Eu anomalies and/or have strong negative Eu anomalies, which suggest they have a high detrital input, or that the Eu anomalies may have been lost while the fluids traveled away from the hydrothermal vent, and/or the enrichment of Fe content in these rocks may have discriminated against Eu, leading to a negative anomaly.

Based on the Ce sigantures along with the shape of the REE patterns in the rocks from the Broken Hill area, we propose that the redox structure of the Broken Hill rift basin at 1.69 Ga was characterized by a redoxcline and stratified, with an upper oxygenated part and a deep anoxic to suboxic zone dominated by hydrothermal fluids. Most of the rocks lack Ce anomalies and

formed under suboxic conditions just below the oxic-anoxic redox boundary, consistent with the existence of nearby hydrothermal discharge zones responsible for the deposition of spatially and temporally associated massive sulfide deposits. The negative Ce anomalies in IFs from Wild Dog, suggest that this area was relatively shallow and more oxygenated than the Broken Hill, Little Broken Hill, and Pinnacles areas.

Acknowledgements

This research was funded by the Division of Research and Graduate Studies and the Harriot College of Arts and Sciences at East Carolina University, a North Carolina Space Grant New Investigator Grant (to AH), and a Sigma Xi (the Scientific Research Society) Grant in Aid of Research (to ES). Appreciation is extended to Mike Wise from the Smithsonian Institution in Washington, DC, for performing electron microprobe analyses of garnet, and to Nick Foster for helping with electron probe microanalysis at Fayetteville State University, NC. Tom Fink is thanked for helping with SEM analysis, and Dr. Mauger for helping with XRD analysis.

References

Bau, M., 1999, Scavenging of dissolved yttrium and rare earths by precipitating iron oxyhydroxide: experimental evidence for Ce oxidation, Y-Ho fractionation, and lanthanide tetrad effect: Geochimica et Cosmochimica Acta, v. 63, p. 67-77.

Bau, M., Koschinsky, A., Dulski, P. and Hein, J.R., 1996, Comparison of the partitioning behaviours of yttrium, rare earth elements, and titanium between hydrogenetic marine ferromanganese crusts and seawater: Geochimica et Cosmochimica Acta, v. 60, p. 1709-1725.

Bau, M. and Dulski, P., 1999, Comparing yttrium and rare earths in hydrothermal fluids from the Mid-Atlantic Ridge: implications for Y and REE behaviour during near-vent mixing and for the Y/Ho ratio of Proterozoic seawater: Chemical Geology, v. 155, p. 77-90.

Bau, M. and Dulski, P., 1996, Distribution of yttrium and rare-earth elements in the Penge and Kuruman iron-formations, Transvaal Supergroup, South Africa: Precambrian Research, v. 79, p. 37-55.

Bau, M. and Möller, P., 1993, Rare earth element systematics of the chemically precipitated component in early Precambrian iron formations and the evolution of the terrestrial atmosphere-hydrosphere-lithosphere system: Geochimica et Cosmochimica Acta, v. 57, p. 2239-2249.

Bau, M., Möller, P. and Dulski, P., 1997, Yttrium and lanthanides in eastern Mediterranean seawater and their fractionation during redox-cycling: Marine Chemistry, v. 56, p. 123-131.

Bau, M., Koschinsky, A., Dulski, P. and Hein, J.R., 1996, Comparison of the partitioning behaviours of yttrium, rare earth elements, and titanium between hydrogenetic marine ferromanganese crusts and seawater: Geochimica et Cosmochimica Acta, v. 60, p. 1709-1725.

Bekker, A., Holland, H., Wang, P., Rumble, D., Stein, H., Hannah, J., Coetzee, L. and Beukes, N., 2004, Dating the rise of atmospheric oxygen: Nature, v. 427, p. 117-120.

Bekker, A., Slack, J.F., Planavsky, N., Krapež, B., Hofmann, A., Konhauser, K.O. and Rouxel, O.J., 2010, Iron formation: the sedimentary product of a complex interplay among mantle, tectonic, oceanic, and biospheric processes: Economic Geology, v. 105, p. 467-508.

Beukes, N.J. and Klein, C., 1990, Geochemistry and sedimentology of a facies transition — from microbanded to granular iron-formation — in the early Proterozoic Transvaal Supergroup, South Africa: Precambrian Research, v. 47, p. 99-139.

Bierlein, F., 1995, Rare-earth element geochemistry of clastic and chemical metasedimentary rocks associated with hydrothermal sulphide mineralisation in the Olary Block, South Australia: Chemical Geology, v. 122, p. 77-98.

Bonatti, E., 1975, Metallogenesis at oceanic spreading centers: Annual Review of Earth and Planetary Sciences, v. 3, p. 401-431.

Boström, K., 1973, The origin and fate of ferromanganoan active ridge sediments, Stockholm Contributions in Geology, v. 27, p. 147–243.

Canfield, D., 1998, A new model for Proterozoic ocean chemistry: Nature, v. 396, p. 450-453.

Conor, C. and Preiss, W., 2008, Understanding the 1720–1640Ma Palaeoproterozoic Willyama Supergroup, Curnamona Province, Southeastern Australia: implications for tectonics, basin evolution and ore genesis: Precambrian Research, v. 166, p. 297-317.

Cook, N. and Ashley, P., 1992, Meta-evaporite sequence, exhalative chemical sediments and associated rocks in the Proterozoic Willyama Supergroup, South Australia: implications for metallogenesis: Precambrian Research, v. 56, p. 211-226.

Cronan, D. and Hodkinson, R., 1997, Geochemistry of hydrothermal sediments from ODP Sites 834 and 835 in the Lau Basin, southwest Pacific: Marine Geology, v. 141, p. 237-268.

German, C., Klinkhammer, G., Edmond, J., Mura, A. and Elderfield, H., 1990, Hydrothermal scavenging of rare-earth elements in the ocean: Nature, v. 345, p. 516-518.

Heimann, A., Spry, P., Teale, G., Conor, C. and Pearson, N.J., 2011, The composition of garnet in garnet-rich rocks in the southern Proterozoic Curnamona Province, Australia: an indicator of the premetamorphic physicochemical conditions of formation: Mineralogy and Petrology, v. 101, p. 49-74.

Heimann, A., Spry, P., Teale, G., Conor, C. and Leyh, W.R., 2009, Geochemistry of garnet-rich rocks in the southern Curnamona Province, Australia, and their genetic relationship to Broken Hill-type Pb-Zn-Ag mineralization: Economic Geology, v. 104, p. 687-712.

Hein, J., Koschinsky, A. and McIntyre, B., 2005, Mercury-and silver-rich ferromanganese oxides, southern California borderland: Deposit model and environmental implications: Economic Geology, v. 100, p. 1151-1168.

Holland, H., 1984, The chemical evolution of the atmosphere and oceans, Princeton University Press.

Huston, D., Stevens, B., Southgate, P., Muhling, P. and Wyborn, L., 2006, Australian Zn-Pb-Ag ore-forming systems: a review and analysis: Economic Geology, v. 101, p. 1117-1157.

Johnson, I. and Klingner, G., 1975, The Broken Hill ore deposit and its environment: Economic Geology of Australia and Papua New Guinea, v. 1, p. 476-491.

Laurila, T., Hannington, M., Petersen, S. and Garbe-Schönberg, D., 2014, Early depositional history of metalliferous sediments in the Atlantis II Deep of the Red Sea: Evidence from rare earth element geochemistry: Geochimica et Cosmochimica Acta, v. 126, p. 146-168.

Lottermoser, B., 1991, Trace element composition of exhalites associated with the Broken Hill sulfide deposit, Australia: Economic Geology, v. 86, p. 870-877.

Lottermoser, B., 1989, Rare earth element study of exhalites within the Willyama Supergroup, Broken Hill Block, Australia: Mineralium Deposita, v. 24, p. 92-99.

Marchig, V., Gundlach, H., Möller, P. and Schley, F., 1982, Some geochemical indicators for discrimination between diagenetic and hydrothermal metalliferous sediments: Marine Geology, v. 50, p. 241-256.

McDonough, W. and Sun, S., 1995, The composition of the Earth: Chemical Geology, v. 120, p. 223-253.

McLennan, S., 1989, Rare earth elements in sedimentary rocks; influence of provenance and sedimentary processes: Reviews in Mineralogy and Geochemistry, v. 21, p. 169-200.

Michard, A., 1989, Rare earth element systematics in hydrothermal fluids: Geochimica et Cosmochimica Acta, v. 53, p. 745-750.

Mills, R. and Elderfield, H., 1995, Rare earth element geochemistry of hydrothermal deposits from the active TAG Mound, 26 N Mid-Atlantic Ridge: Geochimica et Cosmochimica Acta, v. 59, p. 3511-3524.

Mitra, A., Elderfield, H. and Greaves, M., 1994, Rare earth elements in submarine hydrothermal fluids and plumes from the Mid-Atlantic Ridge: Marine Chemistry, v. 46, p. 217-235.

Möller, P. and Dulski, P., 1992, The europium anomalies in banded iron formations and the thermal history of the oceanic crust: Chemical Geology, v. 97, p. 89-100.

Muecke, G., Pride, C. and Sarkar, P., 1979, Rare-earth element geochemistry of regional metamorphic rocks: Physics and Chemistry of the Earth, v. 11, p. 449-464.

Nozaki, Y., Zhang, J. and Amakawa, H., 1997, The fractionation between Y and Ho in the marine environment: Earth and Planetary Science Letters, v. 148, p. 329-340.

O'Brien, J.J., Spry, P.G., Nettleton, D., Xu, R. and Teale, G.S., 2014, Using Random Forests to distinguish gahnite compositions as an exploration guide to Broken Hill-type Pb-Zn-Ag deposits in the Broken Hill domain, Australia: Journal of Geochemical Exploration, in press.

Page, R., Stevens, B., Conor, C., Preiss, W., Crooks, A., Robertson, S., Gibson, G. and Foudoulis, C., 2003, SHRIMP U–Pb geochronology in the Curnamona Province: improving the framework for mineral exploration: Broken Hill Exploration Initiative, v. 2003, p. 122-125.

Page, R. and Laing, W., 1992, Felsic metavolcanic rocks related to the Broken Hill Pb-Zn-Ag orebody, Australia; geology, depositional age, and timing of high-grade metamorphism: Economic Geology, v. 87, p. 2138-2168.

Page, R., Stevens, B. and Gibson, G., 2005, Geochronology of the sequence hosting the broken hill Pb-Zn-Ag orebody, Australia: Economic Geology, v. 100, p. 633-661.

Parr, J. and Plimer, I., 1993, Models for Broken Hill-type lead-zinc-silver deposits: Mineral deposit modeling. Geol Assoc Can Spec Paper, v. 40, p. 253-288.

Parr, J., 1992, Rare-earth element distribution in exhalites associated with Broken Hill-type mineralisation at the Pinnacles deposit, New South Wales, Australia: Chemical Geology, v. 100, p. 73-91.

Parr, J.M., Stevens, B.P., Carr, G.R. and Page, R.W., 2004, Subseafloor origin for Broken Hill Pb-Zn-Ag mineralization, New South Wales, Australia: Geology, v. 32, p. 589-592.

Penhall, J.L., 2001: A Fluid Inclusion and Sulphur Isotope Study of Epigenetic Copper Mineralisation in the Bimbowrie Area, Olary Domain, South Australia.

Phillips, G.N., and Wall, V.J., 1981, Evaluation of prograde regional metamorphic conditions; their implication for the heat source and water activity during metamorphism in the Willyama Complex, Broken Hill, Australia. Bulletin Mineral, v. 104, p. 801–810.

Planavsky, N., Rouxel, O., Bekker, A., Shapiro, R., Fralick, P. and Knudsen, A., 2009, Iron-oxidizing microbial ecosystems thrived in late Paleoproterozoic redox-stratified oceans: Earth and Planetary Science Letters, v. 286, p. 230-242.

Planavsky, N., Bekker, A., Rouxel, O.J., Kamber, B., Hofmann, A., Knudsen, A. and Lyons, T.W., 2010, Rare earth element and yttrium compositions of Archean and Paleoproterozoic Fe formations revisited: new perspectives on the significance and mechanisms of deposition: Geochimica et Cosmochimica Acta, v. 74, p. 6387-6405.

Plimer, I., 2006, Manganoan garnet rocks associated with the Broken Hill Pb–Zn–Ag orebody, Australia: Mineralogy and Petrology, v. 88, p. 443-478.

Plimer, I., 1986, Sediment-hosted exhalative Pb-Zn deposits; products of contrasting ansialic rifting: South African Journal of Geology, v. 89, p. 57-73.

Richards, S., 1966, The banded iron formations at Broken Hill, Australia, and their relationship to the lead-zinc orebodies: Economic Geology, v. 61, p. 72-96.

Sholkovitz, E.R., Landing, W.M. and Lewis, B.L., 1994, Ocean particle chemistry: the fractionation of rare earth elements between suspended particles and seawater: Geochimica et Cosmochimica Acta, v. 58, p. 1567-1579.

Slack, J., Grenne, T., Bekker, A., Rouxel, O. and Lindberg, P., 2007, Suboxic deep seawater in the late Paleoproterozoic: evidence from hematitic chert and iron formation related to seafloor-hydrothermal sulfide deposits, central Arizona, USA: Earth and Planetary Science Letters, v. 255, p. 243-256.

Slack, J. and Stevens, B.P., 1994, Clastic metasediments of the Early Proterozoic Broken Hill Group, New South Wales, Australia: Geochemistry, provenance, and metallogenic significance: Geochimica et Cosmochimica Acta, v. 58, p. 3633-3652.

Slack, J.F., Grenne, T. and Bekker, A., 2009, Seafloor-hydrothermal Si-Fe-Mn exhalites in the Pecos greenstone belt, New Mexico, and the redox state of ca. 1720 Ma deep seawater: Geosphere, v. 5, p. 302-314.

Spry, P. and Wonder, J., 1989, Manganese-rich garnet rocks associated with the Broken Hill lead-zinc-silver deposit, New South Wales, Australia: Canadian Mineralogist, v. 27, p. 275-292.

Spry, P.G., Plimer, I.R. and Teale, G.S., 2008, Did the giant Broken Hill (Australia) Zn–Pb–Ag deposit melt?: Ore Geology Reviews, v. 34, p. 223-241.

Spry, P.G., Heimann, A., Messerly, J.D. and Houk, R., 2007, Discrimination of metamorphic and metasomatic processes at the Broken Hill Pb-Zn-Ag deposit, Australia: rare earth element signatures of garnet-rich rocks: Economic Geology, v. 102, p. 471-494.

Spry, P., 2000, Sulfidation and oxidation haloes as guides in the exploration for metamorphosed massive sulfide deposits: Review Econ.Geol, v. 11, p. 149-161.

Stanton, R., 1977b, Petrochemical studies of ore environment at broken hill, new south-wales: transactions of the institution of mining and metallurgy section b-Applied earth science, v. 86, p. B111-B117.

Stanton, R., 1976a, Speculations on the chemical metasediments of Broken Hill: New South Wales, Australia: Transactions of the Institution of Mining and Metallurgy, v. 85, p. B221-B233.

Stanton, R., 1972, A preliminary account of chemical relationships between sulfide lode and banded iron formation at Broken Hill, New South Wales: Economic Geology, v. 67, p. 1128-1145.

Stanton, R. and Williams, K., 1978, Garnet compositions at Broken Hill, New South Wales, as indicators of metamorphic processes: Journal of Petrology, v. 19, p. 514-529.

Stevens, B., 1986, Post- depositional history of the Willyama Supergroup in the Broken Hill Block, NSW: Australian Journal of Earth Sciences, v. 33, p. 73-98.

Sverjensky, D., 1984, Europium redox equilibria in aqueous solution: Earth and Planetary Science Letters, v. 67, p. 70-78.

Taylor, S., McLennan, S., Armstrong, R. and Tarney, J., 1981, The composition and evolution of the continental crust: rare earth element evidence from sedimentary rocks [and discussion]: Philosophical Transactions of the Royal Society of London, Series A, Mathematical and Physical Sciences, v. 301, p. 381-399.

Webb, A., Dickens, G. and Oliver, N., 2003, From banded iron-formation to iron ore: geochemical and mineralogical constraints from across the Hamersley Province, Western Australia: Chemical Geology, v. 197, p. 215-251.

Whitney, D. and Evans, B., 2010, Abbreviations for names of rock-forming minerals: American Mineralogist, v. 95, p. 185.

Willis, I., Brown, R., Stroud, W. and Stevens, B., 1983, The early Proterozoic Willyama supergroup: Stratigraphic subdivision and interpretation of high to low- grade metamorphic rocks in the Broken Hill Block, New South Wales: Journal of the Geological Society of Australia, v. 30, p. 195-224.

Appendix A

This manuscript will be submitted for publication

Geochemistry and Genesis of Late Paleoproterozoic Banded Iron Formations and Metamorphosed Chemical Precipitates Spatially Associated with Pb-Zn Broken Hill-type Mineralization near the Broken Hill Deposit, Curnamona Province, Australia

Erica Serna[a], Adriana Heimann[a], Paul G. Spry[b], and Wolfgang Leyh[c]

[a] *Department of Geological Sciences, East Carolina University, Greenville, North Carolina 27858-0861, U.S.A.*
[b] *Department of Geological and Atmospheric Sciences, 253 Science I, Iowa State University, Ames, Iowa 50011, U.S.A.*
[c] *Eaglehawk Geological Consulting Pty. Ltd., PO Box 965, Broken Hill, New South Wales, 2880, Australia*

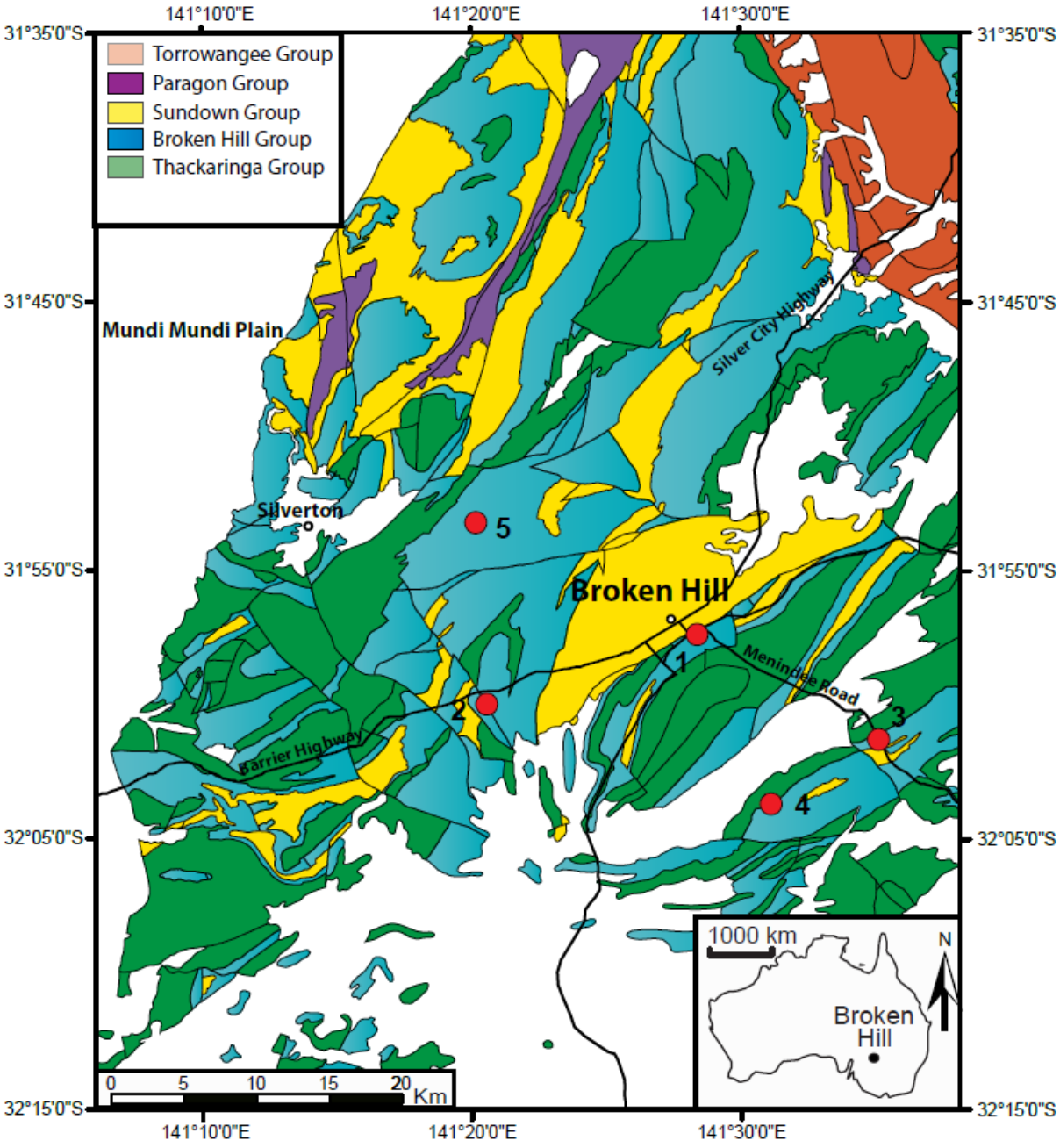

Figure 1. Geological map showing the location of the study sites in the Broken Hill domain of the southern Curnamona Province, Australia. 1. Banded IFs near the Broken Hill deposit. 2. Massive IFs near the Pinnacles deposit. 3. Banded IFs near the Wild Dog deposit. 4. Banded and massive IFs near the Little Broken Hill deposit. 5. Garnet-quartz and gahnite-quartz rocks near the Nine Mile deposit. Modified after O'Brien et al. (2015).

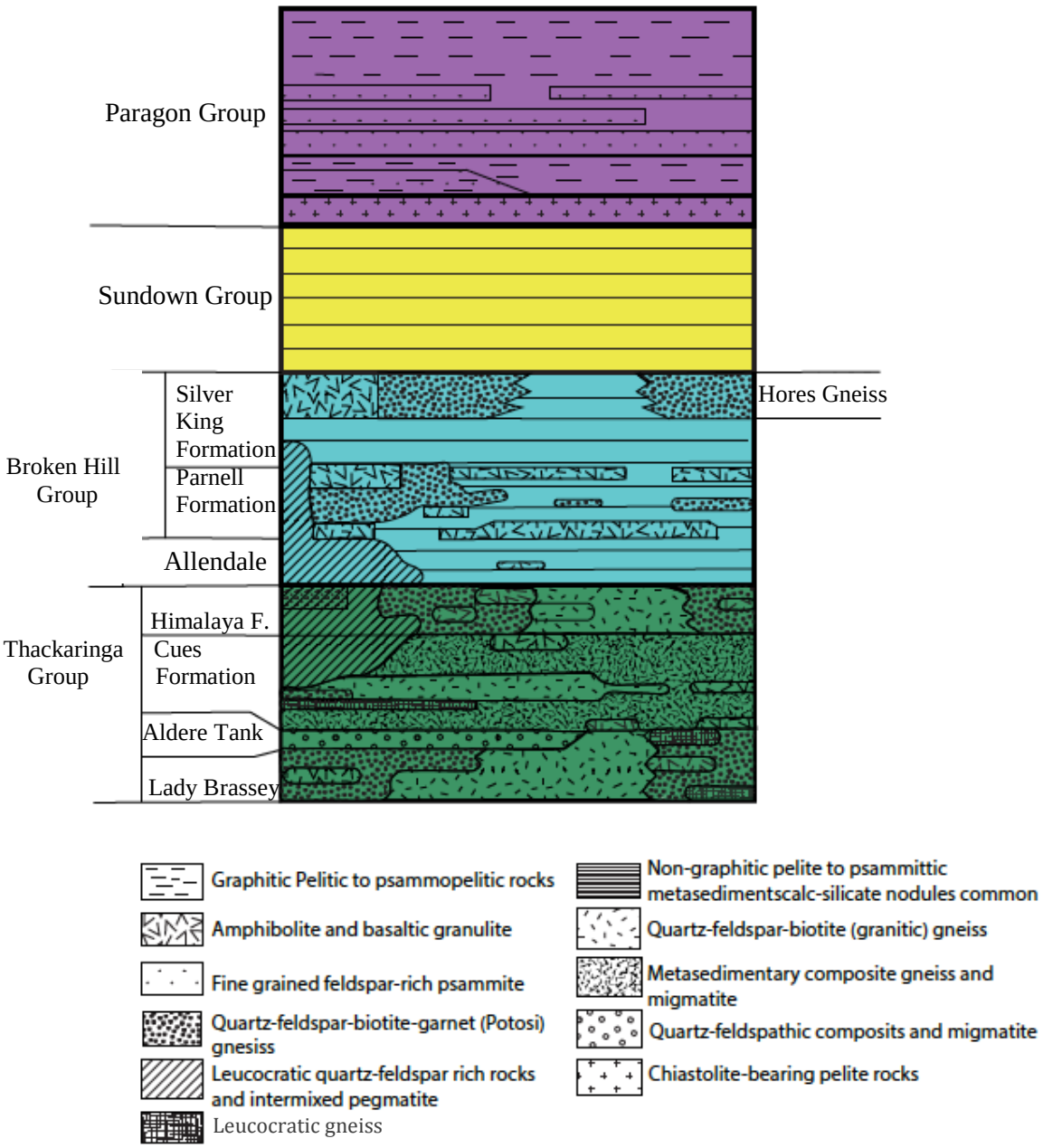

Figure 2. Stratigraphic column of the Broken Hill domain of the southern Curnamona Province. Banded IFs from near the Broken Hill deposit are located within the silver King Formation (Hores Gneiss) in the Broken Hill Group. Banded and massive IFs from near the Little Broken Hill and Wild Dog deposits are located from the Allendale metasediments to the Silver King Formation of the Broken Hill Group. Massive IFs from near the Pinnacles deposit are located in the Cues Formation of the Thackaringa Group, and massive garnet- and gahnite-quartz rocks from near the Nine Mile deposit are tentatively located between the upperpart of the Allendale Metasediments to the Freyers Metasediments of the Broken Hill Group. After Slack and Stevens (1994).

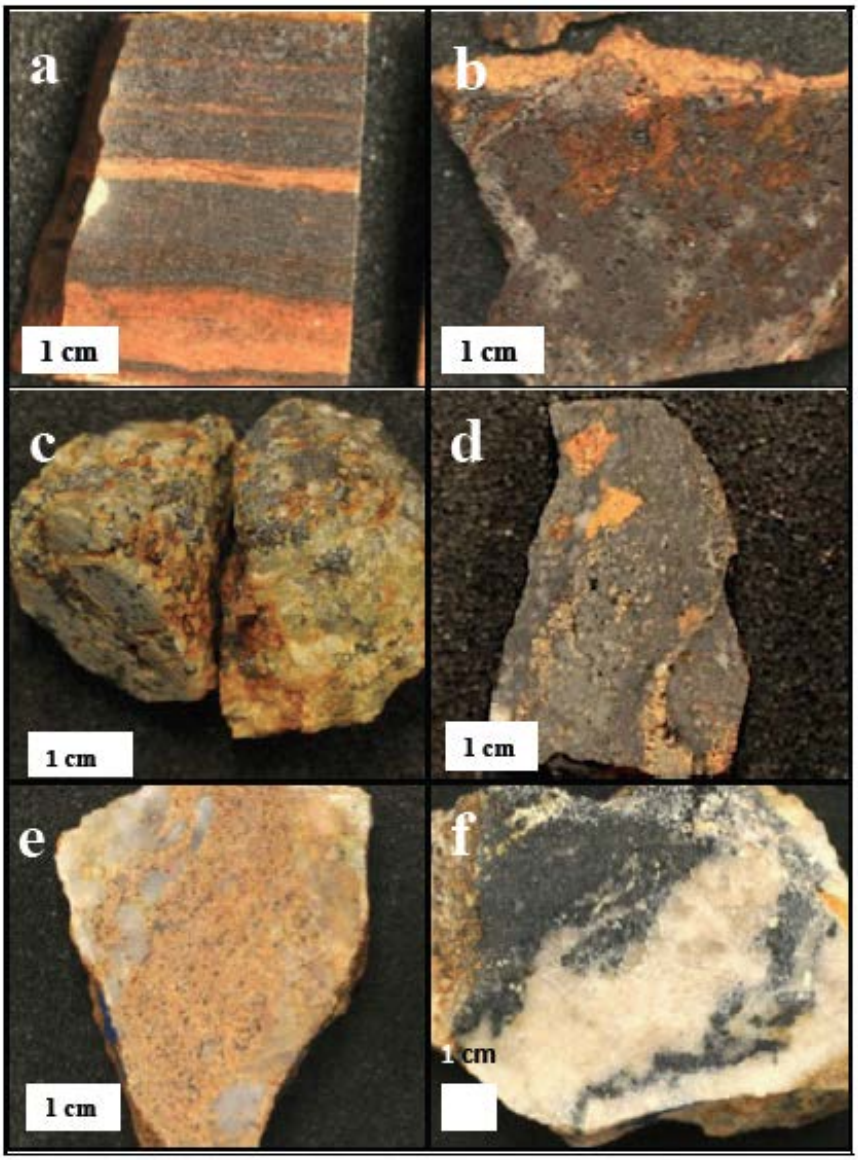

Figure 3. Photographs of representative hand samples from the study sites showing mineralogy and texture. **a.** Banded IF showing sharp iron-rich (black) and iron-poor (light reddish-brown) micro- and mesolaminations. Black layers are composed of magnetite, garnet and minor quartz and darker reddish-brown layers are mainly composed of quartz with minor garnet, apatite and magnetite. Sample AD-10-010, near the Little Broken Hill deposit. **b.** Massive hematite-quartz ± magnetite IF from near the Pinnacles deposit with dark reddish-brown color indicating oxidation. Sample AD-10-006. **c.** Massive quartz-magnetite ± garnet IF from near the Little Broken Hill deposit showing disseminated magnetite (grey) in a quartz-rich matrix (white). Sample AD-10-018. **d.** Massive to poorly banded garnet-hematite-quartz ± magnetite IF from near the Little Broken Hill deposit. The matrix consists of hematite and iron states from weathering (black color with orange patches) with white quartz and garnet. Sample AD-10-019. **e.** Massive garnet-quartz rock from the Nine Mile deposit showing light orange-pink garnet and white quartz. Sample GA1. **f.** Massive gahnite-quartz rock from the Nine Mile deposit showing dark green, subhedral gahnite in a white quartz matrix.

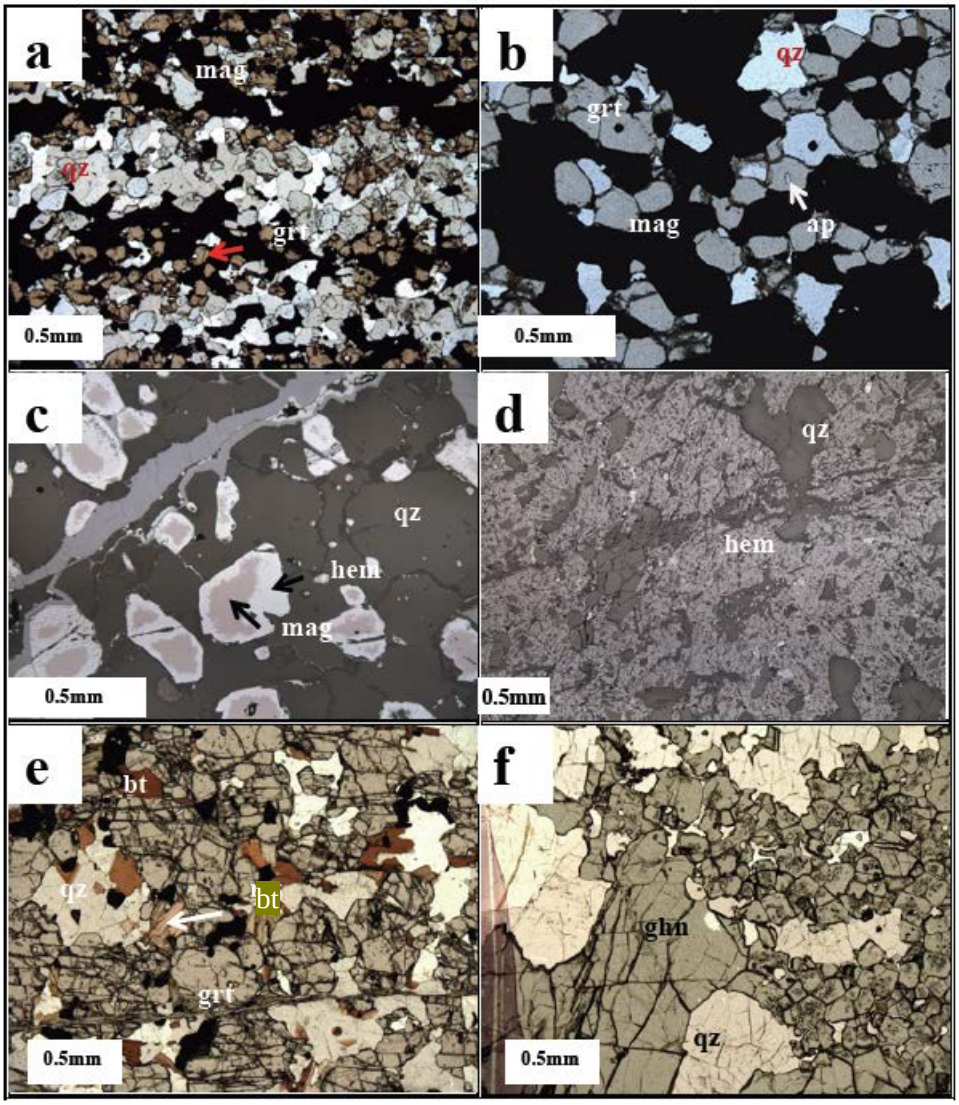

Figure 4. Photomicrographs of representative massive and banded IFs from the study sites showing: **a.** Banded IF with iron-rich and iron-poor bands composed of various amounts of garnet (grt), magnetite (mag), and quartz (qz). Sample AD-10-010, near the Wild Dog deposit. Plane polarized light, 4x. **b.** Banded IF composed of garnet, magnetite, and quartz, showing apatite (ap) inclusion in garnet and magnetite inclusions in garnet and quartz. Sample AD-10-003, near the Broken Hill deposit. Plane polarized light, 10x. **c.** Massive hematite (hem)-quartz ± magnetite IF from the Pinnacles deposit showing replacement of magnetite by hematite. Sample AD-10-006. Reflected light, 10x. **d.** Massive to poorly banded garnet-hematite-quartz ± magnetite IF from near the Little Broken Hill deposit showing the dominance of hematite (oxidation after magnetite) and quartz. Reflected light, 2x. **e.** Massive garnet-quartz rock from the Nine Mile deposit showing coarse grained garnet, quartz, and minor biotite (bt). Garnet is highly fractured. Sample GA4. Plane polarized light, 4x. **f.** Massive gahnite (ghn)-quartz rock from the Nine Mile deposit showing gahnite of various crystal sizes. Small gahnite crystals have tiny dusty inclusions whereas the large crystals are clean. Sample GH4. Plane polarized light, 4x. Mineral abbreviations as in Table 1.

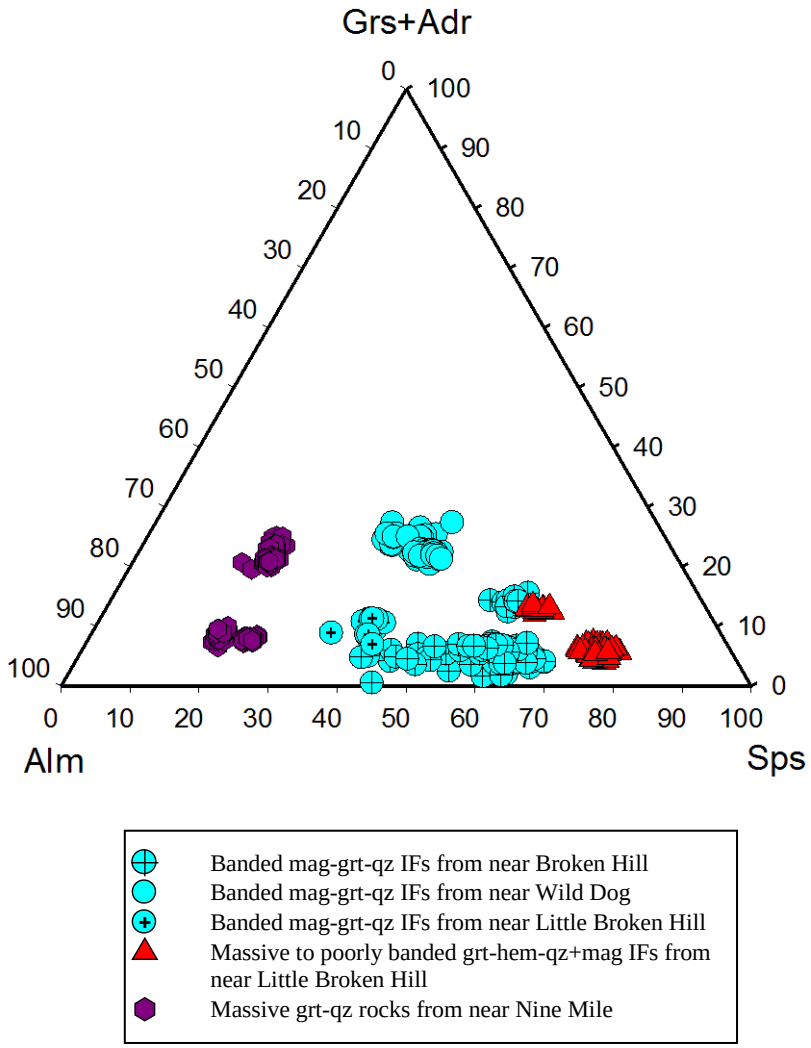

Figure 5. Diagram showing compositions of garnet in terms of almandine (Alm), spessartine (Sps), and grossular+andradite (Grs+Adr) (mol %). The diagram shows two populations of garnet with respect to the grossular + andradite contents.

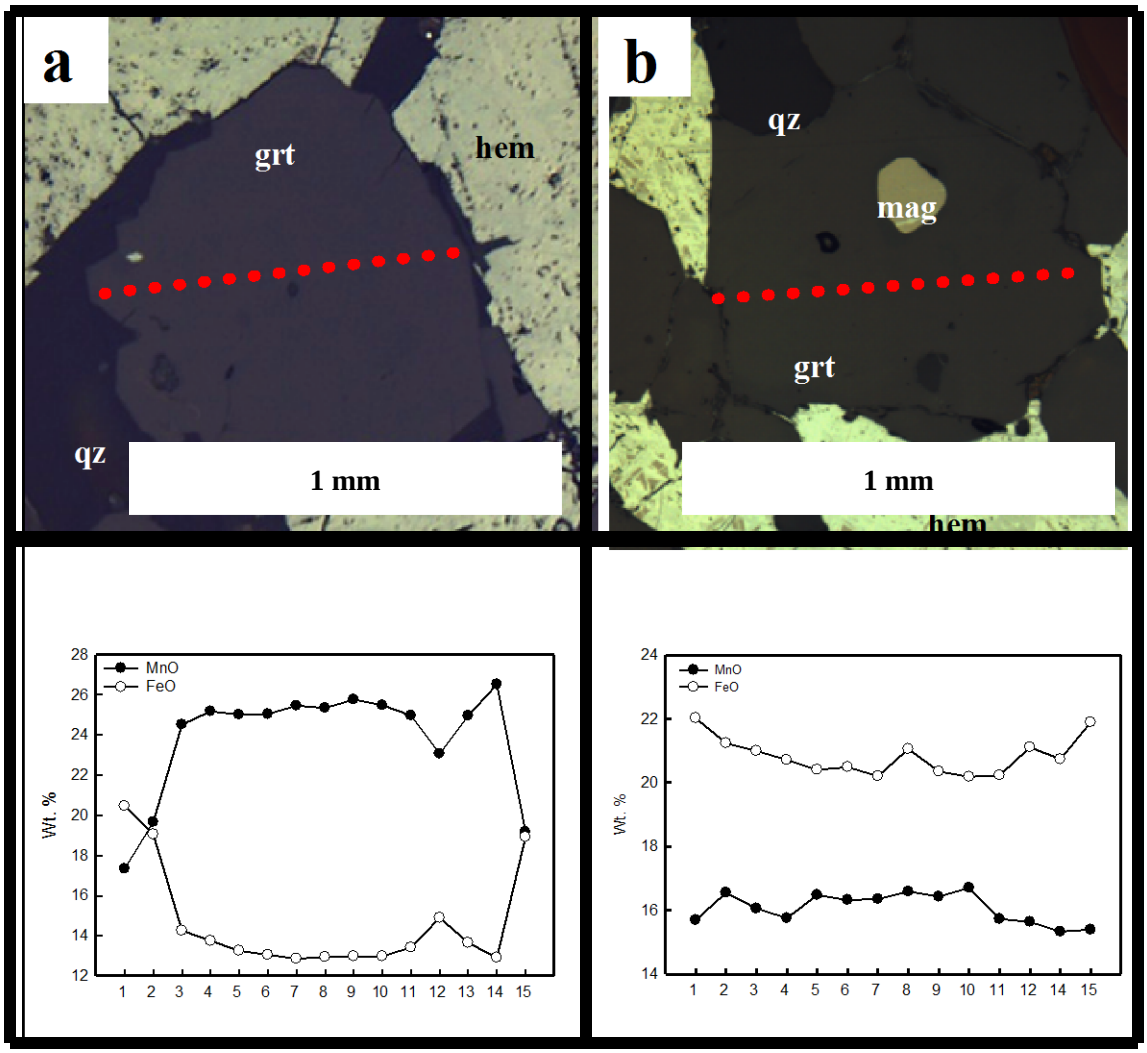

Figure 6. Representative compositional profiles showing Fe and Mn in garnet from banded and massive IFs near the Broken Hill and Little Broken Hill. Both profiles show an increase in Fe and decrease in Mn from rim-to-core-to-rim. **a.** Garnet in banded magnetite-garnet-quartz IF near the Broken Hill deposit. Sample AD-10-002. **b.** Garnet in magnetite-garnet-quartz IF from the Little Broken Hill deposit. Sample AD-10-015. Red dots are EMP analysis spots shown in the graphs.

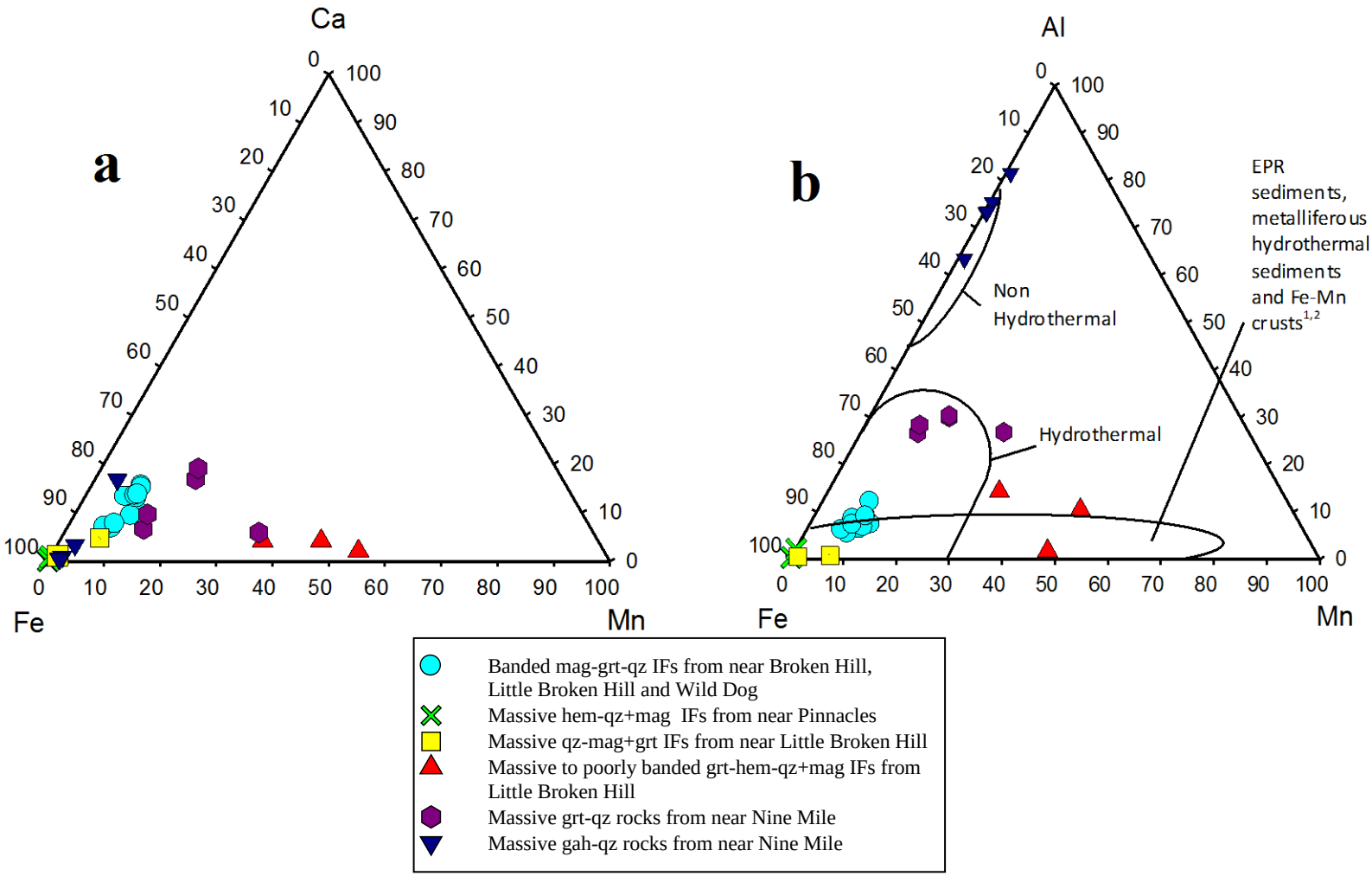

Figure 7. Diagrams showing the bulk-rock composition of banded and massive IFs from near the Broken Hill, Little Broken Hill, Wild Dog, and Pinnacles deposits, and massive garnet- and gahnite-quartz rocks from Nine Mile. **a.** Ca-Fe-Mn (mol %) ternary diagram. **b.** Al-Fe-Mn (mol %) ternary diagram showing the composition of the studied rocks and metalliferous sediments from the East Pacific Rise (EPR; Boström, 1973; Hein et al., 2005) and the hydrothermal and non-hydrothermal fields for comparison purposes. Modified after Boström (1973). [1] Boström (1973), [2] Hein et al. (2005).

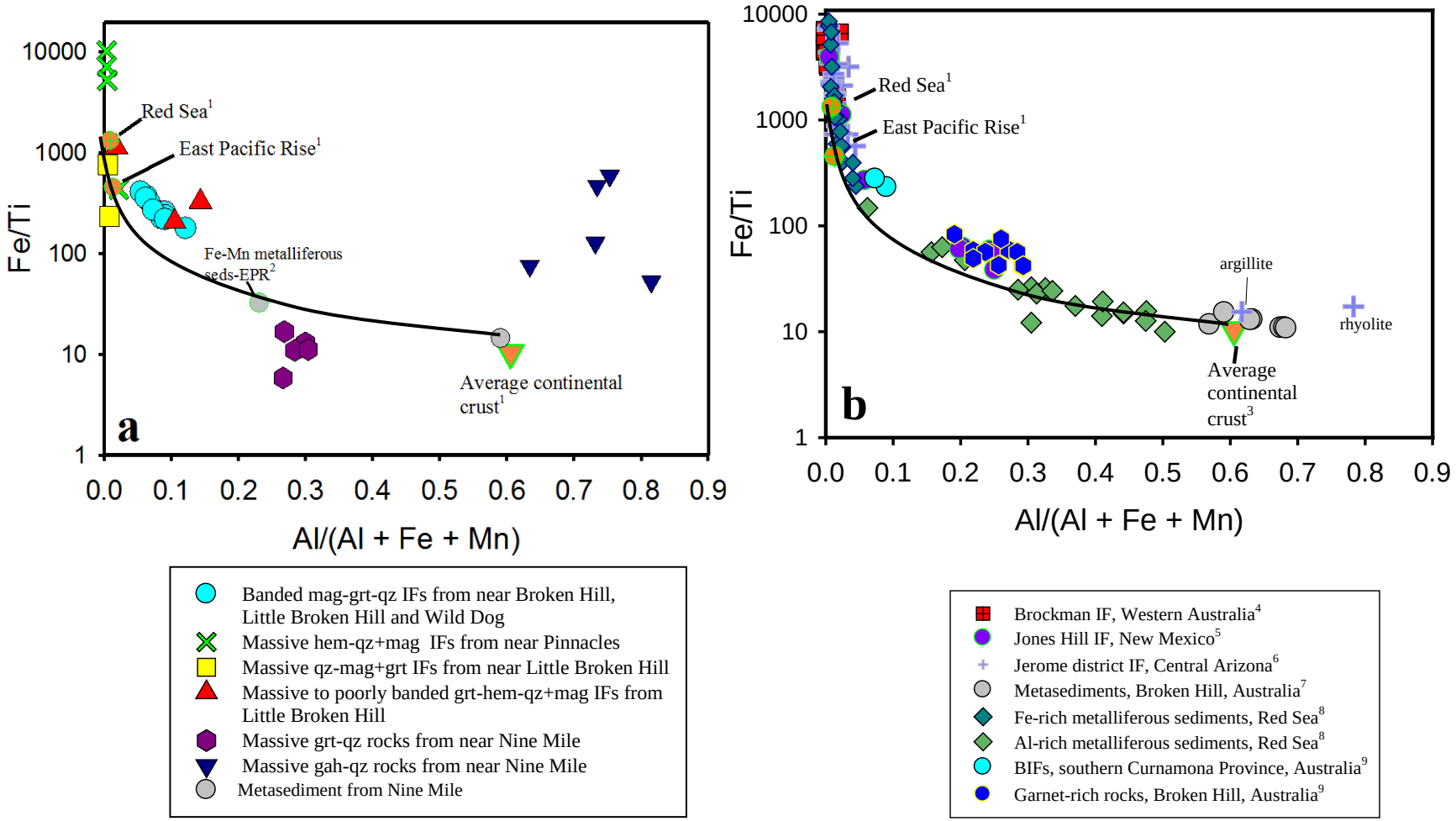

Figure 8. Diagrams of Al/(Al + Fe + Mn) *vs*. Fe/Ti (mol.) showing the bulk-rock compositions. **a.** Banded and massive IFs and massive garnet-quartz and gahnite-quartz rocks from the study sites. Also shown are modern hydrothermal sediments from the EPR and the Red Sea and the average continental crust. [1] Marchig et al. (1982), [2] Cronan and Hodkinson (1997), [3] Boström (1973). **b.** Older and younger banded IFs and Fe- and Al-rich metalliferous sediments from the Red Sea. [4] Webb et al. (2003), [5] Slack et al. (2009), [6] Slack et al. (2007), [7] Slack and Stevens (1994), [8] Laurila et al. (2014), [9] Heimann et al. (2009). Curved line in both diagrams represents the mixing line between Al-free hydrothermal sediments from the EPR and the Red Sea and the average continental crust. Modified after Boström (1973).

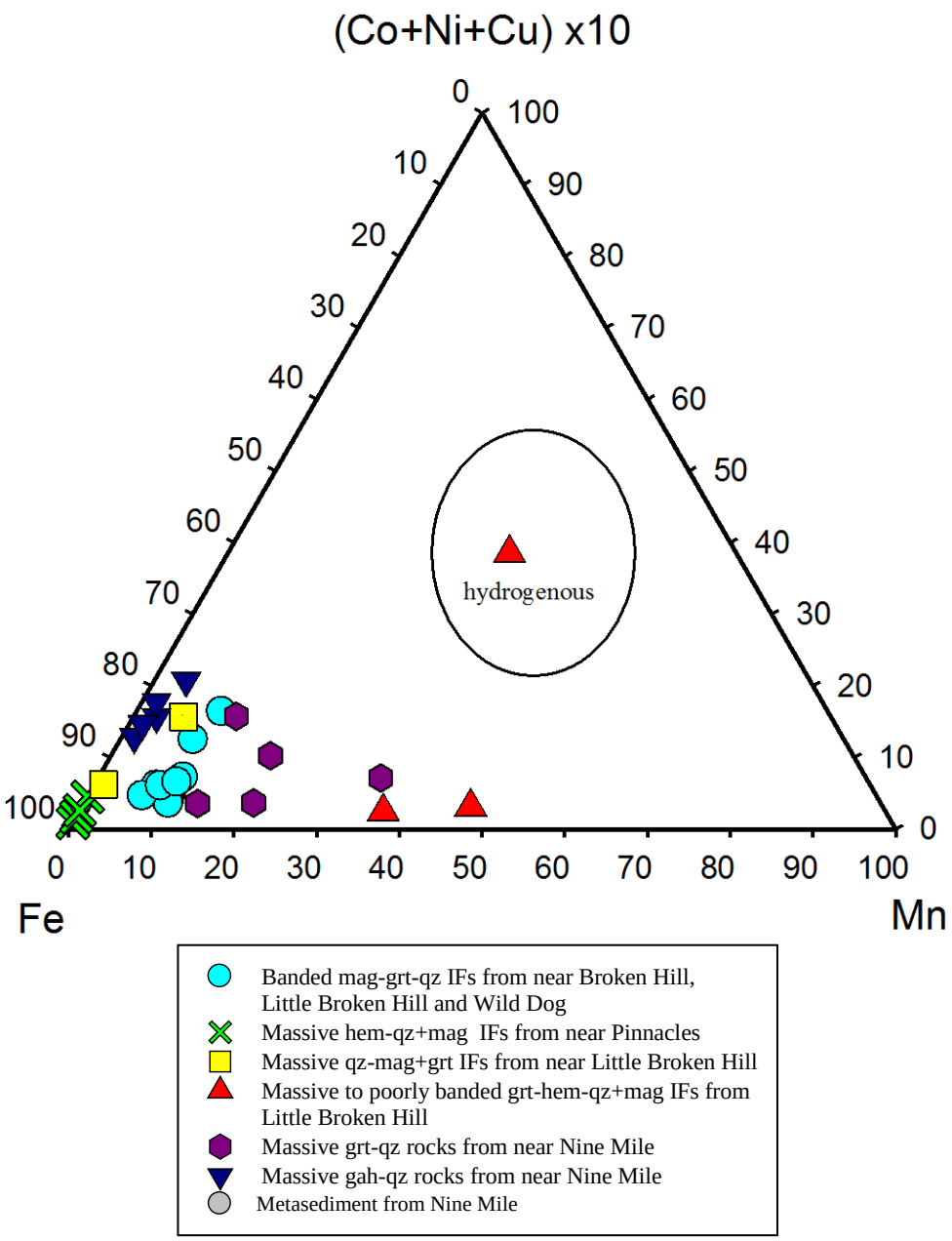

Figure 9. Fe-[(Co+Ni+Cu) x 10]-Mn diagram showing the general field for hydrogenous Fe-Mn nodules (Bonnatti et al., 1972), and the possible hydrogenous contribution to the protolith of the studied banded and massive IFs and garnet- and gahnite-quartz rocks from Nine Mile. After Bonatti et al. (1975).

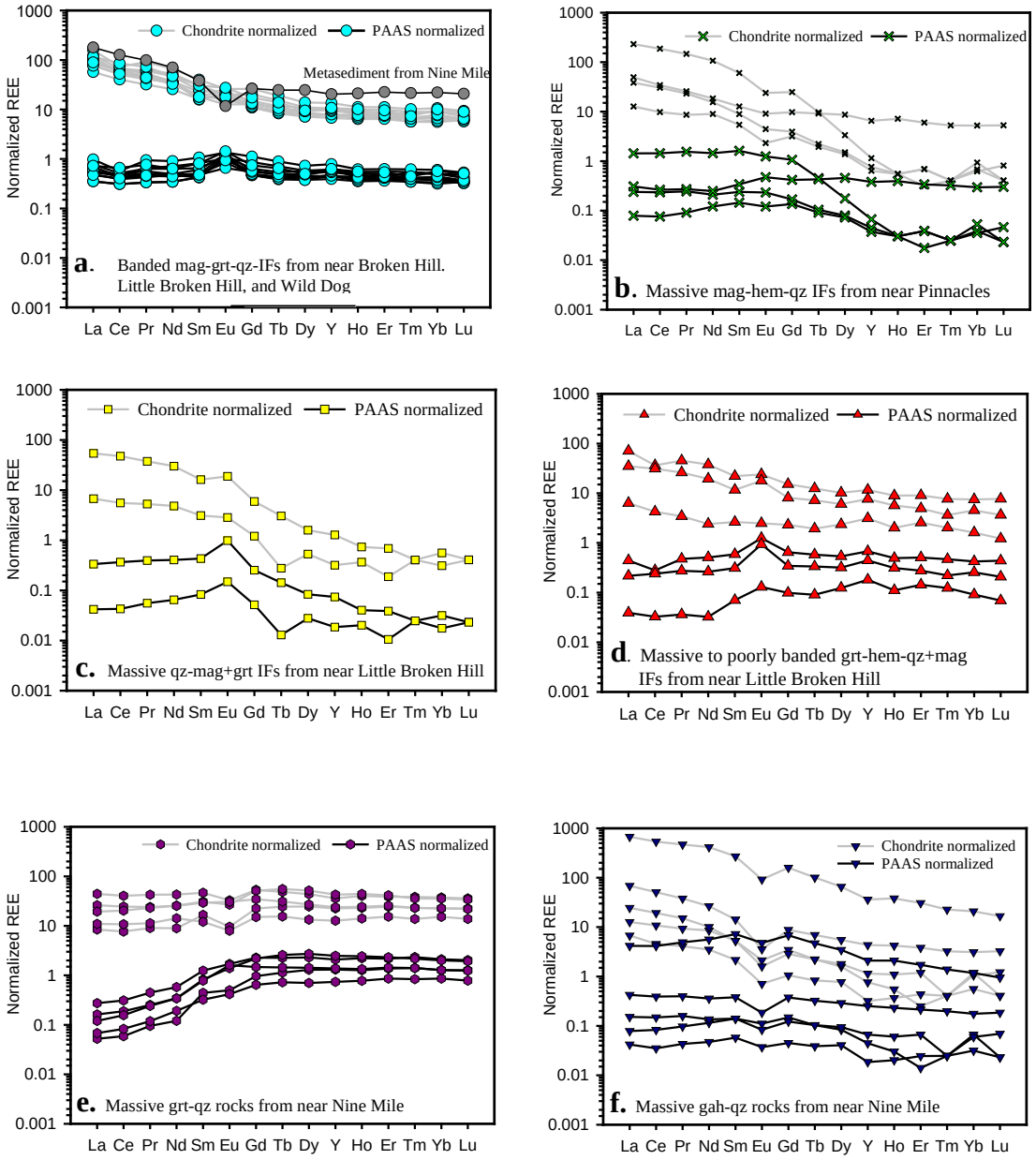

Figure 10. Chondrite- and PAAS-normalized rare earth element patterns of banded and massive IFs and massive garnet- and gahnite (ghn)-quartz rocks from the study sites, southern Curnamona Province, Australia. **a.** Banded mag-grt-qz IFs near the Broken Hill, Little Broken Hill, and Wild Dog deposits. **b.** Massive hemematite (hem)-qz ± mag IFs near the Pinnacles deposit. **c.** Massive qz-mag ± grt IFs from near the Little Broken Hill deposit. **d.** Massive to poorly banded grt-hem-qz ± mag IFs from Little Broken Hill deposit. **e.** Massive grt-qz rocks near the Nine Mile deposit. **f.** Massive ghn-qz rocks nearthe Nine Mile deposit. Mineral abbreviations as in previous Figures. Chondrite normalizing values from McDonough and Sun (1995) and PAAS normalizing values from McLennan (1989).

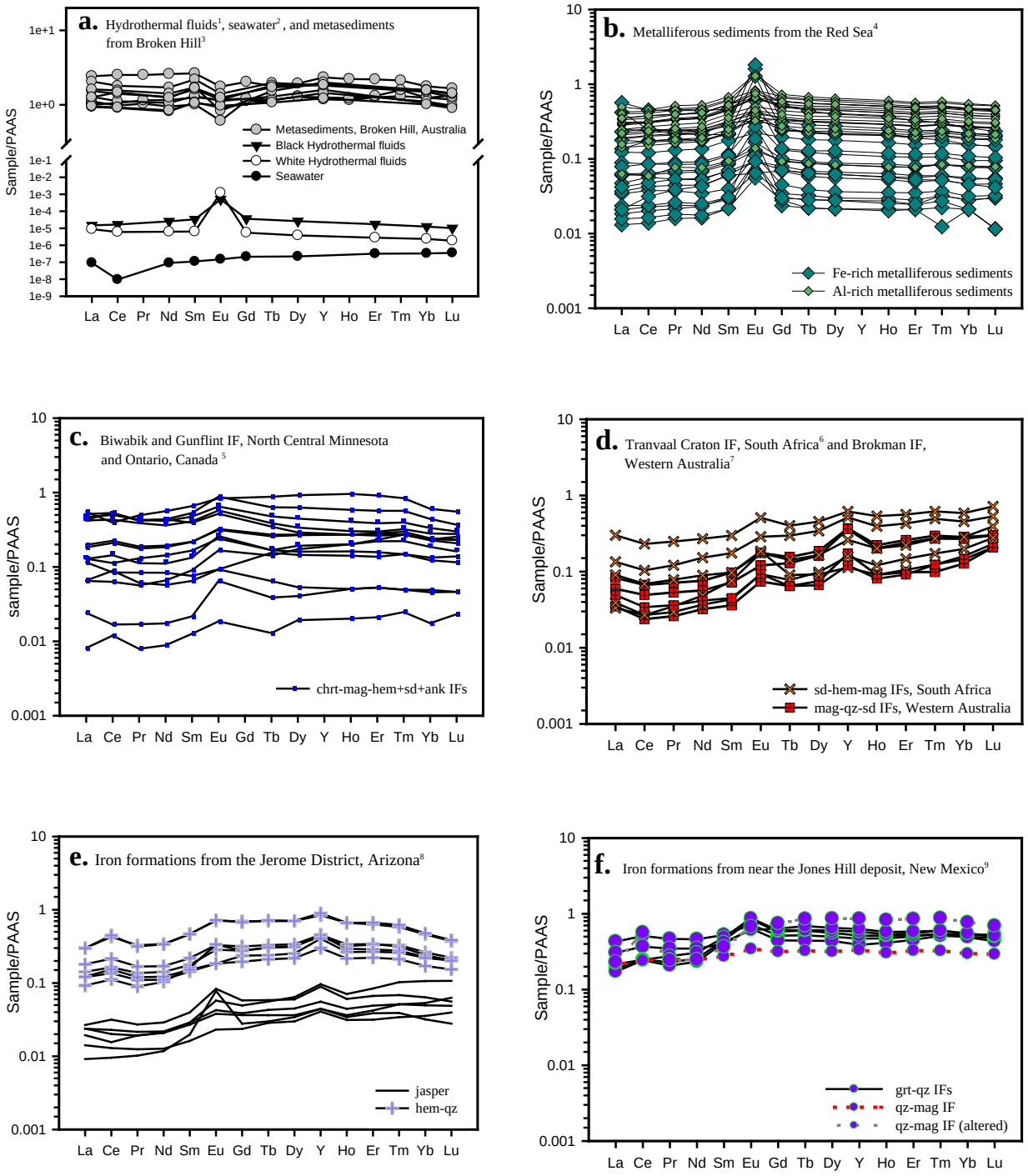

Figure 11. Rare earth element patterns of: **a**. Hydrothermal fluids, seawater, and metasedimentary rocks from near Broken Hill, **b.** Metalliferous sediments, and **c-f**. Banded IFs of various ages and garnet-quartz rocks analyzed in previous studies. [1, 2] Mitra et al., 1994, [3] Slack and Stevens (1994), [4] Laurila et al. (2014), [5] Planavsky et al. (2009), [6] Bau and Dulski (1996), [7] Planavsky et al., 2010, [8] Slack et al. (2007), [9] Slack et al. (2009). Chrt = chert, sd = siderite, ank = ankerite. Post Archean Australian Shale normalizing values from McLennan (1989).

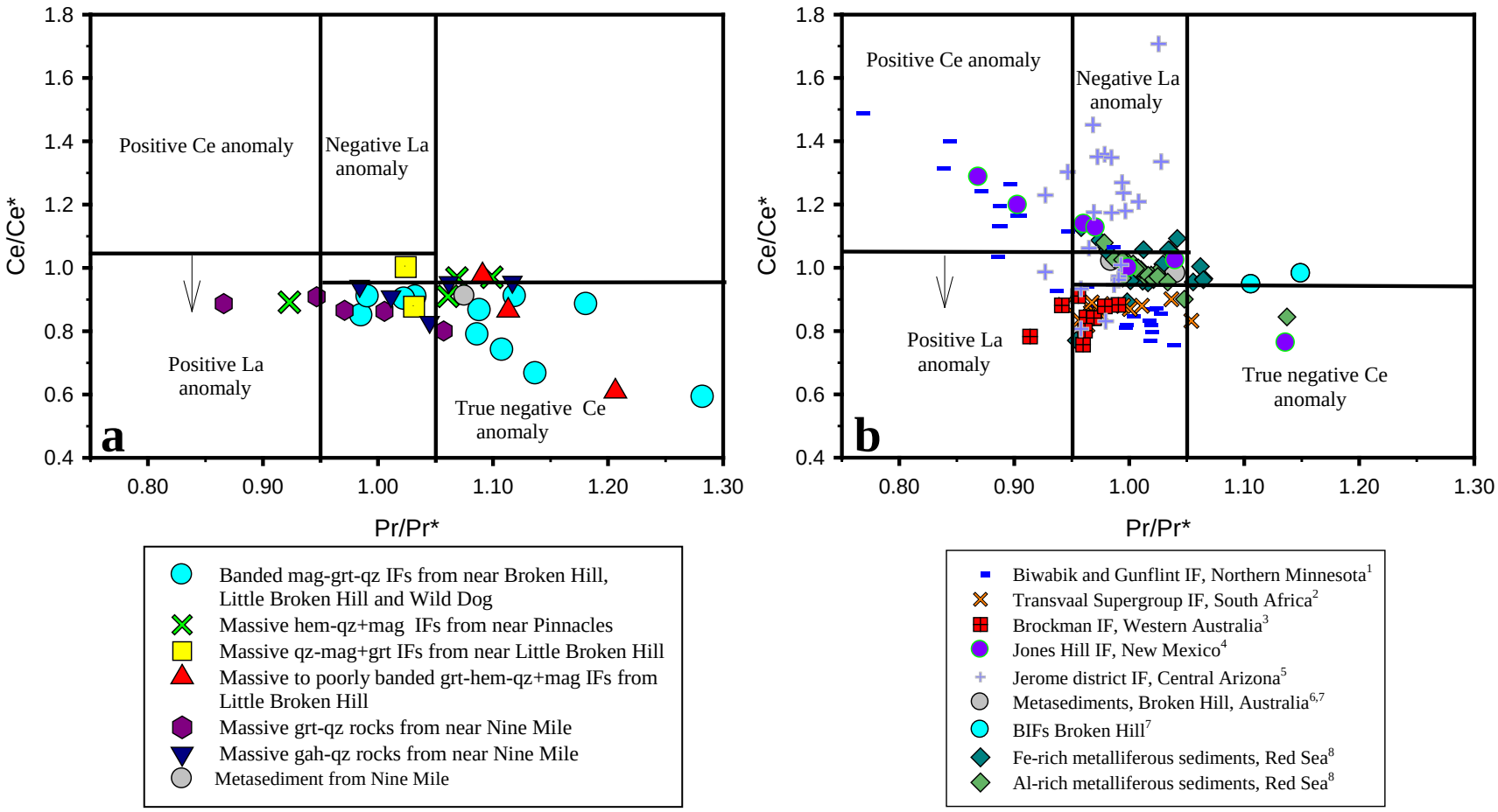

Figure 12. Diagram of Ce/Ce* *vs* Pr/Pr* showing the fields defined for true negative Ce anomalies, positive Ce anomalies, and positive and negative La anomalies. **a.** Banded and massive IFs and massive garnet-quartz and gahnite-quartz rocks from the study sites. Only banded IFs from the Little Broken Hill and Wild Dog deposits have true negative Ce anomalies. The rest have positive La anomalies and no Ce anomalies. **b.** Banded IFs, garnet-quartz rocks, metalliferous sediments from the Red Sea, and metasedimentary rocks from the Broken Hill area. [1] Planavsky et al. (2009), [2] Planavsky et al. (2010), [3] Webb et al. (2003), [4] Slack et al. (2009), [5] Slack et al. (2007), [6] Slack and Stevens (1994), [7] Heimann et al. (2009), [8] Laurila et al. (2014). Modified after Bau and Dulski, (1996). $Ce/Ce^* = Ce_{SN}/(0.5Pr_{SN} + 0.5La_{SN})$, $Pr/Pr^* = Pr_{SN}/(0.5Ce_{SN} + 0.5Nd_{SN})$.

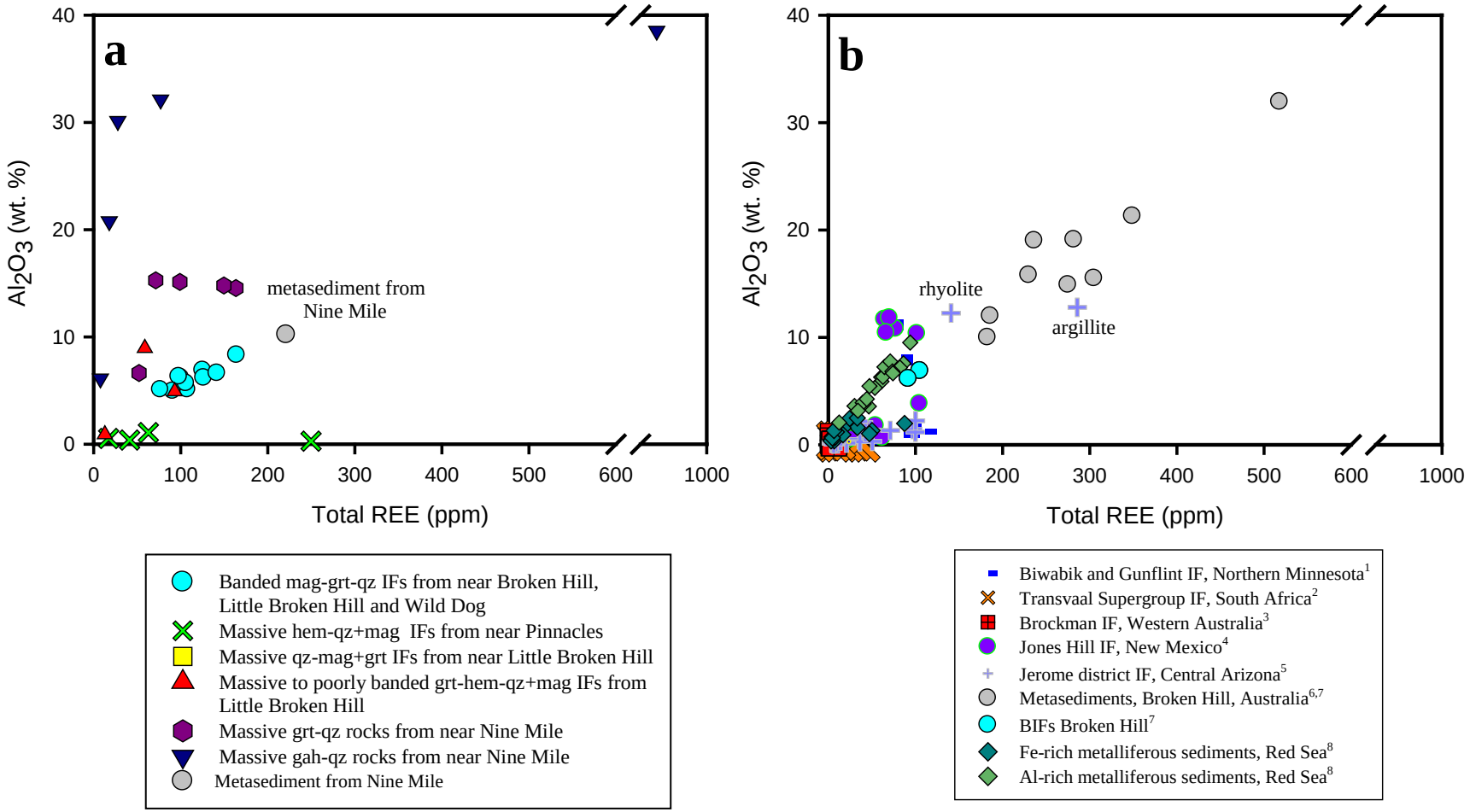

Figure 13. Al_2O_3 (wt.%) *vs.* total REE (ppm) plot showing the correlations in: **a.** Banded and massive IFs and massive garnet-quartz and gahnite-quartz rocks from the study sites. **b.** Banded IFs of various ages, garnet-quartz rocks, metalliferous sediments from the Red Sea, and metasedimentary rocks from the Broken Hill area. Positive correlation ($r^2 = 0.74$) between aluminum and total REE contents is seen in banded IFs from the Broken Hill, Little Broken Hill, and Wild Dog deposits, Al-rich metalliferous sediments from the Red Sea, and metasediments from the Broken Hill area. [1] Planavsky et al. (2009), [2] Planavsky et al. (2010), [3] Webb et al. (2003), [4] Slack et al. (2009), [5] Slack et al. (2007), [6] Slack and Stevens (1994), [7] Heimann et al. (2009), [8] Laurila et al. (2014).

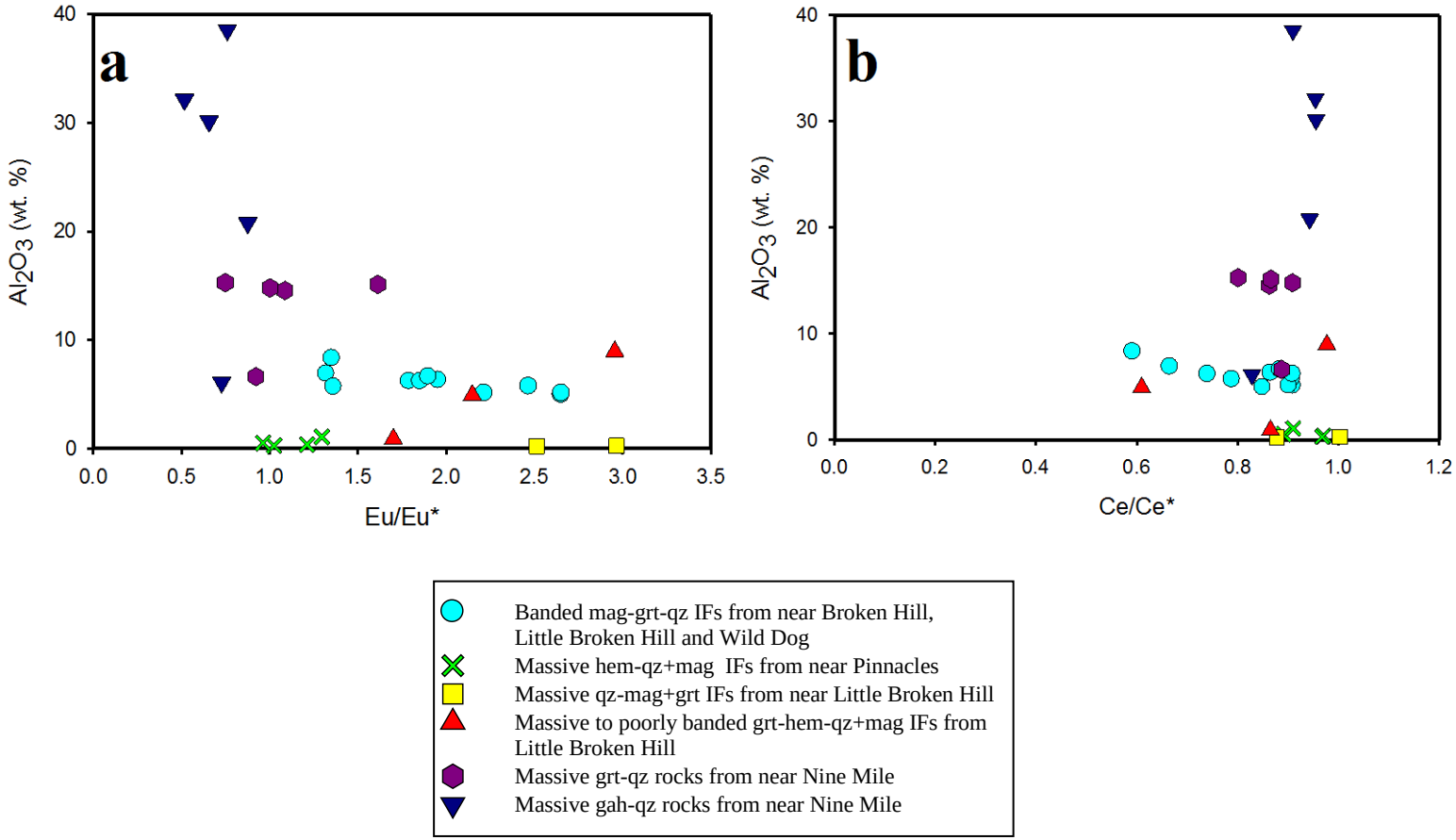

Figure 14. Al_2O_3 (wt.%) *vs.* Eu/Eu* (a) and Ce/Ce* (b) plots showing possible correlations among Al_2O_3 content and Eu and Ce anomalies in the studied rocks. **a.** No correlation exists between the Al_2O_3 content and the Eu anomalies in the rocks. **b.** A very weak negative to absent correlation between the Al_2O_3 content and negative Ce anomaly is only present in a few banded IFs from the study sites. Eu/Eu* = $Eu_{SN}/(0.66Sm_{SN} + 0.33Tb_{SN})$.

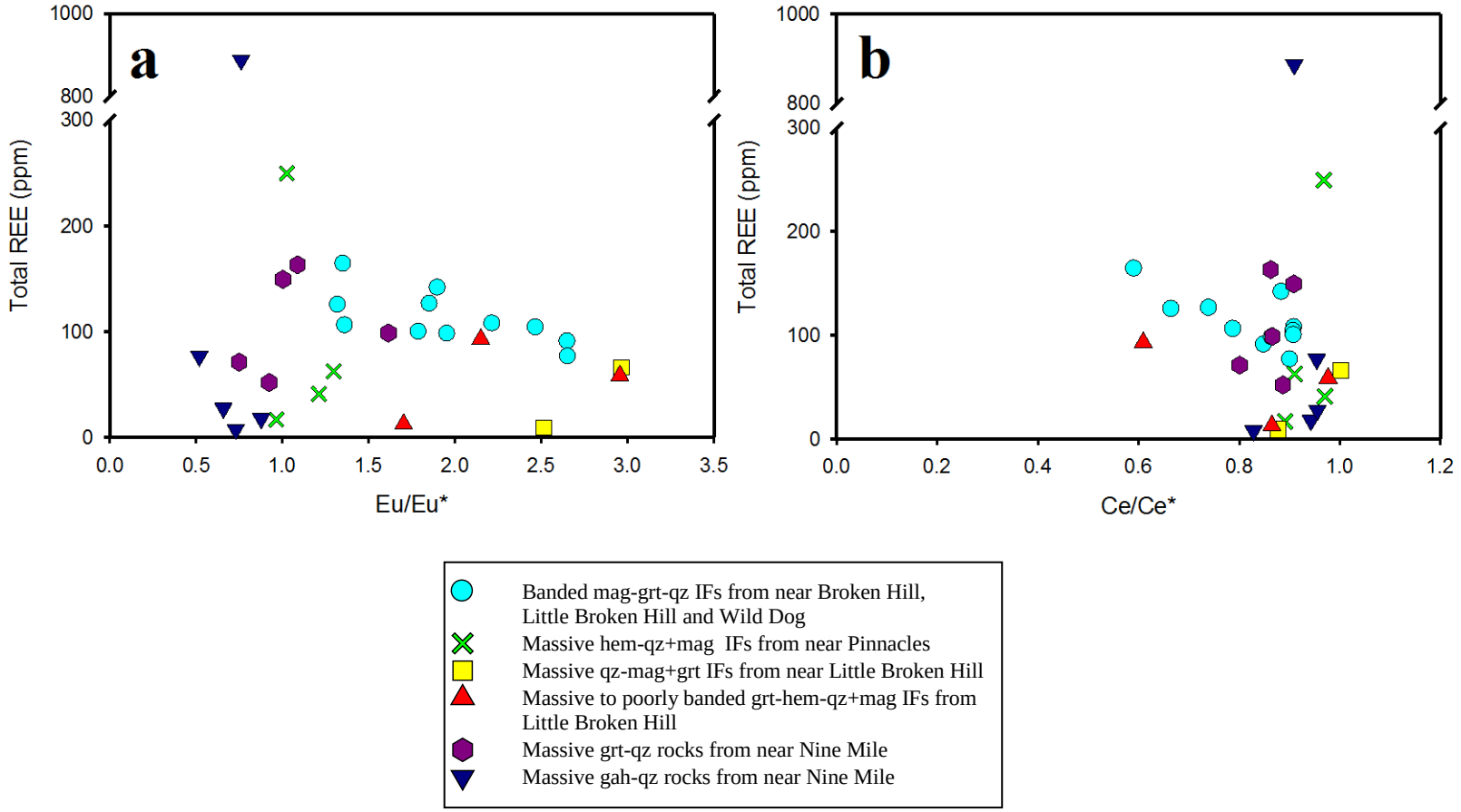

Figure 15. Total REE (ppm) *vs.* Eu/Eu* and Ce/Ce* anomalies showing possible correlations between the size of the anomalies and the total REE content in the studied rocks. **a.** A very weak negative correlation between the total REE content and the Eu anomaly exists only for banded IFs from the Broken Hill, Litlle Broken Hill, and Wild Dog deposits. **b.** A negative correlation between Ce anomalies and the total REE content is only observed in some banded IFs.

Table 1. Mineralogy of banded IFs, massive IFs, and gahnite- and garnet-quartz rocks from the study sites in the Broken Hill domain, southern Curnamona Province, Australia.

Sample	Type	Mag	Grt	Qz	Ap	Hem	*Bt	Ms	Py	Ccp	Sp	*Chl	Ghn	Amp	Location	Coordinates
AD-10-001	BIF	xxx	xxx	xxx	x	•									Near the Broken Hill deposit	S31°57.805' E141°29.442'
AD-01-002	BIF	xxx	xx	xxx	•	•										
AD-10-003	BIF	xx	xxx	xxx	•	•										
AD-10-004	BIF	xxxx	xx	xxx	•	•										
AD-10-006	IF	x		xxx		xxxx									Near the Pinnacles deposit	S 32°01.408' E141°20.847'
AD-10-007	IF	xxx		xxxx		x										
AD-01-008	IF	x		x		xxxx										
AD-10-009	IF	x		xxxx	•	xxx	•									
AD-10-010	BIF	xxxx	xxxx	xx	x	•	•					•			Near the Wild Dog deposit	S 32°01.600' E141°35.434'
AD-10-011	BIF	xx	xxx	xxx	x	x	•					•				
AD-10-012	BIF	xxx	xx	xxx	x	x	•					•				
AD-10-013	BIF	xxxx	xxx	x	•	x	•					•				
AD-10-014	BIF	xxx	xxxx	x	•	x	•					•				
AD-10-015	BIF	xxx	xxxx	x	•	x									Near the Little Broken Hill deposit	S 32°4.007 E141°31.523'
AD-10-016	BIF	xx	xxxx	xxx	x	•										
AD-10-017	IF	xx	•	xxxx		•			•	•	•					S 32°04.560' E141°31.846'
AD-10-018	IF	xxx		xxxx		•			•	•	•					
AD-10-019	IF	•	xx	xxx		xxxx										
AD-10-020	IF	xx	xxxx	xxx	x											
AD-10-021	IF	xx	x	xx		xxxx										
GA 1	Grt-qz rock		xx	xxx							•				Near the Nine Mile deposit	
GA 2	Grt-qz rock		xxxx	xxx			•	•			•					
GA 3	Grt-qz rock		xxxx	xx			•	•			•			•		
GA 4	Grt-qz rock		xxx	xx			x	•			•			x		
GA 5	Grt-qz rock		xxxx	x			x				•			x		
GA 6	Grt-qz rock		xxxx	x			x				•			x		
GA 7	Grt-qz rock		xx	x			xx				•			xxx		
GH 1	Ghn-qz rock			xxxx							•		x			
GH 2	Ghn-qz rock			xxx							•		x			
GH 3	Ghn-qz rock			x							•		xxx			
GH 4	Ghn-qz rock			xxx							•		x			
GH 5	Ghn-qz rock			xxx			•	•			•		xx			
GH 6	Ghn-qz rock			xxx							•		xx			
GH 7	Ghn-qz rock			xxxx			•				•		xx			

Mineral abundance as follows: xxxx = very abundant, xxx = moderate, xx = medium-low, x = low, • = minor and accessory, * = secondary minerals. BIF = banded iron formation. IF = massive iron formation. Mineral abbreviations after Whitney and Evans (2010).

Table 2. Major element composition of garnet from banded and massive IFs from the Broken Hill, Little Broken Hill and Wild Dog deposits.

Sample	AD-10-001 C1	AD-10-001 C1	AD-10-001 C1	AD-10-001 C2	AD-10-001 C2	AD-10-001 C4	AD-10-001 C4	AD-10-001 C5	AD-10-001 C5	AD-10-001 C5	AD-10-001 C7	AD-10-001 C7	AD-10-001 C7	AD-10-001 C8
Wt. %	P2	P3	P4	P1	P4	P1	P4	P2	P3	P4	P1	P2	P4	P1
SiO_2	36.812	37.049	36.400	36.409	36.753	36.282	36.334	36.624	36.566	36.734	36.416	36.580	36.533	36.512
P_2O_5	0.000	0.000	0.000	0.000	0.000	0.000	0.000	0.000	0.006	0.000	0.000	0.000	0.000	0.000
TiO_2	0.000	0.033	0.000	0.020	0.033	0.028	0.043	0.000	0.000	0.016	0.000	0.018	0.012	0.065
CaO	4.587	4.523	4.522	3.932	4.681	1.314	4.297	4.167	4.202	4.262	4.434	4.503	4.465	4.826
MgO	1.810	1.954	1.823	1.990	1.837	1.400	1.959	1.960	1.968	1.968	1.843	1.966	1.810	1.847
Al_2O_3	19.197	19.343	19.073	19.176	19.272	19.901	19.266	19.393	19.464	19.086	19.241	19.222	19.277	18.832
MnO	22.122	22.959	22.865	23.061	23.556	27.323	24.035	23.508	24.164	23.062	23.547	23.280	23.589	23.143
FeO	15.890	14.485	14.467	14.533	13.764	13.321	14.291	14.281	14.163	14.189	13.848	13.856	14.008	14.526
Cr_2O_3	0.000	0.008	0.000	0.000	0.000	0.000	0.000	0.000	0.073	0.027	0.075	0.000	0.008	0.033
ZnO	0.000	0.000	0.000	0.065	0.102	0.000	0.000	0.000	0.082	0.025	0.132	0.042	0.000	0.000
Total	100.418	100.354	99.150	99.186	99.998	99.569	100.225	99.933	100.688	99.369	99.536	99.467	99.702	99.784
Apfu based on 12 oxygen atoms														
Si	3.001	3.011	3.001	2.999	3.002	2.991	2.974	2.994	2.976	3.015	2.992	3.001	2.995	2.998
P	0.000	0.000	0.000	0.000	0.000	0.000	0.000	0.000	0.000	0.000	0.000	0.000	0.000	0.000
Ti	0.000	0.002	0.000	0.001	0.002	0.002	0.003	0.000	0.000	0.001	0.000	0.001	0.001	0.004
Ca	0.401	0.394	0.399	0.347	0.410	0.116	0.377	0.365	0.366	0.375	0.390	0.396	0.392	0.425
Mg	0.220	0.237	0.224	0.244	0.224	0.172	0.239	0.239	0.239	0.241	0.226	0.240	0.221	0.226
Al	1.845	1.853	1.854	1.862	1.855	1.934	1.859	1.869	1.867	1.847	1.863	1.859	1.863	1.823
Mn	1.528	1.580	1.597	1.609	1.630	1.908	1.666	1.628	1.666	1.604	1.639	1.618	1.638	1.610
Fe	1.083	0.984	0.998	1.001	0.940	0.918	0.978	0.976	0.964	0.974	0.952	0.951	0.961	0.998
Cr	0.000	0.001	0.000	0.000	0.000	0.000	0.000	0.000	0.005	0.002	0.005	0.000	0.001	0.002
Zn	0.000	0.000	0.000	0.004	0.006	0.000	0.000	0.000	0.005	0.002	0.008	0.003	0.000	0.000
Total	8.077	8.061	8.072	8.069	8.069	8.041	8.095	8.071	8.088	8.060	8.074	8.068	8.072	8.085
Spessartine	50.43	52.28	52.75	53.21	53.9	63.27	54.89	53.78	54.96	53.06	54.17	53.49	54.12	53.09
Pyrope	7.26	7.83	7.40	8.08	7.4	5.71	7.87	7.89	7.88	7.97	7.46	7.95	7.31	7.46
Almandine	28.16	26.53	25.79	26.46	24.51	26.00	22.87	25.19	23.26	26.38	24.37	24.74	24.6	24.47
Grossular	4.11	4.69	4.60	3.38	5.17	0.00	3.14	4.13	3.58	3.93	4.75	4.84	4.73	3.49
Andradite	9.12	8.22	8.59	8.04	8.28	3.76	9.15	7.93	8.28	8.34	7.91	8.19	8.17	10.21

Cont. Table 2

Sample Wt.%	AD-10-001 C8 P2	AD-10-001 C8 P3	AD-10-001 C14 P1	AD-10-001 C14 P3	AD-10-001 C14 P4	AD-10-002-C2-P1	AD-10-002-C2-P2	AD-10-002-C2-P3	AD-10-002-C2-P4	AD-10-002-C2-T1 L3	AD-10-002-C2-T1 L14	AD-10-002-C2-T1 L15	AD-10-002-C2-T1 L23	AD-10-002-C2-T1 L28
SiO_2	36.621	36.411	36.404	36.596	36.670	36.895	36.980	36.645	36.638	36.819	37.490	37.012	37.180	36.929
P_2O_5	0.000	0.000	0.000	0.000	0.000	0.000	0.000	0.000	0.000	0.000	0.000	0.000	0.000	0.000
TiO_2	0.000	0.000	0.022	0.000	0.024	0.000	0.000	0.000	0.000	0.006	0.024	0.000	0.018	0.000
CaO	4.506	4.481	4.904	4.491	4.526	1.882	1.621	1.785	1.737	1.809	1.985	1.687	1.635	1.851
MgO	1.824	1.903	1.950	1.900	1.851	1.682	1.800	1.740	2.071	1.727	2.187	2.213	2.315	1.754
Al_2O_3	18.995	19.137	18.879	19.101	18.855	19.485	19.887	19.886	19.581	19.959	19.705	20.116	19.559	19.405
MnO	23.503	23.420	23.663	23.549	23.193	24.220	25.050	26.024	20.855	25.165	18.069	19.496	16.574	25.619
FeO	13.603	14.320	14.105	13.889	14.429	14.900	14.475	14.652	18.458	14.250	21.050	19.766	22.978	15.068
Cr_2O_3	0.000	0.025	0.000	0.019	0.031	0.044	0.000	0.000	0.031	0.069	0.002	0.000	0.014	0.044
ZnO	0.092	0.139	0.077	0.057	0.000	0.032	0.000	0.190	0.000	0.136	0.042	0.079	0.000	0.000
Total	99.144	99.836	100.04	99.602	99.579	99.140	99.813	100.92	99.371	99.940	100.54	100.39	100.23	100.67
Apfu based on 12 oxygen atoms														
Si	3.016	2.988	2.986	3.003	3.013	3.036	3.022	2.983	3.012	3.008	3.036	3.005	3.026	3.012
P	0.000	0.000	0.000	0.000	0.000	0.000	0.000	0.000	0.000	0.000	0.000	0.000	0.000	0.000
Ti	0.000	0.000	0.001	0.000	0.002	0.000	0.000	0.000	0.000	0.000	0.002	0.000	0.001	0.000
Ca	0.398	0.394	0.431	0.395	0.398	0.166	0.142	0.156	0.153	0.158	0.172	0.147	0.143	0.162
Mg	0.224	0.233	0.238	0.232	0.227	0.206	0.219	0.211	0.254	0.210	0.264	0.268	0.281	0.213
Al	1.844	1.851	1.826	1.848	1.826	1.890	1.915	1.908	1.897	1.922	1.881	1.925	1.876	1.866
Mn	1.639	1.628	1.644	1.637	1.614	1.688	1.734	1.795	1.452	1.742	1.239	1.341	1.143	1.770
Fe	0.937	0.983	0.968	0.953	0.991	1.026	0.989	0.998	1.269	0.974	1.426	1.342	1.564	1.028
Cr	0.000	0.002	0.000	0.001	0.002	0.003	0.000	0.000	0.002	0.005	0.000	0.000	0.001	0.003
Zn	0.006	0.008	0.005	0.004	0.000	0.002	0.000	0.011	0.000	0.008	0.003	0.005	0.000	0.000
Total	8.063	8.086	8.100	8.073	8.072	8.017	8.021	8.062	8.039	8.028	8.022	8.032	8.034	8.054
Spessartine	54.26	53.74	54.17	54.09	53.32	56.17	57.64	59.44	48.17	57.91	41.21	44.54	37.92	58.61
Pyrope	7.41	7.69	7.86	7.68	7.49	2.79	5.45	7.00	8.42	6.84	4.97	8.90	7.57	7.06
Almandine	24.98	24.21	22.21	24.42	25.61	32.46	30.81	26.6	37.67	29.86	45.23	41.51	47.91	26.6
Grossular	4.59	3.98	3.55	4.25	3.34	2.90	1.61	0.00	0.00	1.25	2.39	0.70	0.00	0.00
Andradite	8.57	8.95	10.59	8.74	9.65	2.48	3.11	5.16	4.97	3.76	3.18	4.17	4.58	5.22

Cont. Table 2

Sample Wt.%	AD-10-002-C2-T1 L31	AD-10-002-C2-T1 L38	AD-10-002-C2-T1 L41	AD-10-002-C2-T1 L47	AD-10-002-C2-T1 L54	AD-10-002-C2-T1 L61	AD-10-002-C2-T1 L62	AD-10-002-C2-T1 L67	AD-10-002-C2-T1 L80	AD-10-002-C6-P1	AD-10-002-C6-P2	AD-10-002-C6-P3	AD-10-002-C6-P4	AD-10-002-C7-P2
SiO_2	36.975	37.079	37.103	37.815	34.071	37.145	36.837	37.068	37.110	37.293	36.854	36.902	36.958	37.029
P_2O_5	0.000	0.164	0.000	0.000	0.184	0.000	0.000	0.000	0.000	0.000	0.000	0.000	0.000	0.000
TiO_2	0.000	0.032	0.000	0.000	0.109	0.026	0.083	0.044	0.000	0.060	0.010	0.026	0.018	0.048
CaO	1.332	1.248	1.418	0.974	1.480	2.140	1.222	1.472	1.611	1.090	1.910	1.951	0.880	1.847
MgO	1.871	1.772	2.118	2.288	1.954	1.726	1.878	2.041	1.866	1.839	1.801	1.799	2.058	2.074
Al_2O_3	19.644	19.751	20.145	20.358	19.241	19.257	20.234	19.952	20.182	20.361	19.958	20.074	20.158	19.920
MnO	26.591	25.402	20.377	17.195	17.473	24.609	23.111	20.535	24.564	23.657	24.879	25.919	21.784	21.289
FeO	14.116	14.464	19.835	21.309	24.523	15.396	16.723	19.005	15.580	15.150	13.928	13.766	18.184	18.106
Cr_2O_3	0.032	0.017	0.000	0.054	0.037	0.000	0.000	0.000	0.000	0.031	0.027	0.000	0.029	0.000
ZnO	0.000	0.000	0.000	0.000	0.057	0.131	0.000	0.027	0.012	0.079	0.002	0.030	0.067	0.015
Total	100.561	99.929	101.00	99.993	99.129	100.43	100.088	100.14	100.925	99.560	99.369	100.47	100.14	100.33
Apfu based on 12 oxygen atoms														
Si	3.013	3.025	3.001	3.055	2.867	3.031	3.002	3.018	3.004	3.036	3.019	3.000	3.010	3.010
P	0.000	0.011	0.000	0.000	0.013	0.000	0.000	0.000	0.000	0.000	0.000	0.000	0.000	0.000
Ti	0.000	0.002	0.000	0.000	0.007	0.002	0.005	0.003	0.000	0.004	0.001	0.002	0.001	0.003
Ca	0.116	0.109	0.123	0.084	0.134	0.187	0.107	0.128	0.140	0.095	0.168	0.170	0.077	0.161
Mg	0.227	0.216	0.255	0.276	0.245	0.210	0.228	0.248	0.225	0.223	0.220	0.218	0.250	0.251
Al	1.887	1.899	1.921	1.939	1.908	1.852	1.944	1.915	1.926	1.954	1.927	1.924	1.935	1.909
Mn	1.835	1.755	1.396	1.177	1.245	1.701	1.595	1.416	1.684	1.632	1.726	1.785	1.503	1.466
Fe	0.962	0.987	1.342	1.440	1.726	1.051	1.140	1.294	1.055	1.032	0.954	0.936	1.239	1.231
Cr	0.002	0.001	0.000	0.003	0.003	0.000	0.000	0.000	0.000	0.002	0.002	0.000	0.002	0.000
Zn	0.000	0.000	0.000	0.000	0.004	0.008	0.000	0.002	0.001	0.005	0.000	0.002	0.004	0.001
Total	8.043	8.006	8.038	7.974	8.151	8.042	8.021	8.022	8.033	7.982	8.016	8.036	8.020	8.032
Spessartine	60.85	58.55	46.32	39.35	40.83	56.46	53.04	47.08	55.91	54.54	57.42	59.24	49.99	48.68
Pyrope	7.54	3.55	8.47	9.22	8.04	4.50	7.59	6.92	7.47	7.46	5.60	7.24	7.77	8.35
Almandine	25.29	31.53	40.13	48.15	35.96	30.97	35.81	40.75	31.7	34.48	30.11	27.51	38.79	37.64
Grossular	0.00	1.40	0.00	0.52	0.00	0.28	0.21	0.73	0.37	1.49	3.01	1.15	0.00	0.34
Andradite	3.75	1.99	4.08	0.00	3.91	5.77	3.09	3.27	4.27	0.00	2.41	4.42	2.35	4.78

Cont. Table 2

Sample Wt. %	AD-10-002-C7-P3	AD-10-002-C7-P4	AD-10-002-C8-P1	AD-10-002-C8-P4	AD-10-002-C9-P1	AD-10-002-C9-P2	AD-10-002-C11-P1	AD-10-002-C11-P2	AD-10-002-C11-P3	AD-10-002-C11-P4	AD-10-002-C12-P1	AD-10-002-C12-P2	AD-10-002-C12-P3	AD-10-003 C1 P1
SiO_2	37.036	37.077	37.393	37.225	37.440	36.965	36.672	37.193	37.156	37.033	37.153	36.944	36.854	36.189
P_2O_5	0.000	0.000	0.000	0.000	0.000	0.000	0.000	0.000	0.000	0.000	0.000	0.000	0.000	0.000
TiO_2	0.000	0.000	0.068	0.030	0.018	0.000	0.000	0.000	0.024	0.000	0.038	0.010	0.066	0.026
CaO	1.971	2.145	0.797	1.423	2.190	1.220	1.279	1.705	1.767	1.870	1.391	2.254	1.380	0.651
MgO	1.720	1.804	1.898	2.205	1.745	1.865	1.744	1.772	1.804	1.807	1.708	1.990	1.846	1.812
Al_2O_3	19.829	19.597	20.247	20.191	19.586	19.916	19.909	19.756	19.561	19.478	19.733	19.455	20.045	19.979
MnO	25.510	23.145	25.787	18.177	25.115	25.151	26.373	26.063	26.233	25.229	25.509	19.304	24.331	24.284
FeO	13.894	16.750	14.277	20.375	14.701	14.147	13.633	14.106	14.037	14.496	14.586	19.970	15.219	16.254
Cr_2O_3	0.000	0.013	0.000	0.025	0.000	0.021	0.000	0.019	0.015	0.000	0.004	0.000	0.000	0.062
ZnO	0.000	0.000	0.040	0.077	0.002	0.000	0.076	0.005	0.064	0.000	0.000	0.000	0.099	0.128
Total	99.960	100.531	100.51	99.728	100.80	99.285	99.686	100.62	100.661	99.913	100.12	99.927	99.840	99.385
Apfu based on 12 oxygen atoms														
Si	3.023	3.018	3.028	3.028	3.035	3.030	3.008	3.022	3.022	3.029	3.031	3.021	3.011	2.985
P	0.000	0.000	0.000	0.000	0.000	0.000	0.000	0.000	0.000	0.000	0.000	0.000	0.000	0.000
Ti	0.000	0.000	0.004	0.002	0.001	0.000	0.000	0.000	0.002	0.000	0.002	0.001	0.004	0.002
Ca	0.172	0.187	0.069	0.124	0.190	0.107	0.112	0.149	0.154	0.164	0.122	0.198	0.121	0.058
Mg	0.209	0.219	0.229	0.267	0.211	0.228	0.213	0.215	0.219	0.220	0.208	0.243	0.225	0.223
Al	1.908	1.880	1.933	1.936	1.871	1.924	1.925	1.892	1.875	1.878	1.897	1.875	1.930	1.943
Mn	1.764	1.596	1.769	1.252	1.724	1.746	1.832	1.794	1.807	1.748	1.763	1.337	1.684	1.697
Fe	0.948	1.140	0.967	1.386	0.997	0.970	0.935	0.959	0.955	0.992	0.995	1.366	1.040	1.121
Cr	0.000	0.001	0.000	0.002	0.000	0.001	0.000	0.001	0.001	0.000	0.000	0.000	0.000	0.004
Zn	0.000	0.000	0.002	0.005	0.000	0.000	0.005	0.000	0.004	0.000	0.000	0.000	0.006	0.008
Total	8.024	8.041	8.002	8.002	8.029	8.007	8.030	8.031	8.038	8.032	8.018	8.040	8.020	8.040
Spessartine	58.61	52.92	58.97	41.76	57.27	58.16	60.88	59.56	59.98	58.04	58.62	44.35	56.02	56.33
Pyrope	5.11	6.90	3.82	5.03	3.82	3.91	7.09	5.72	6.04	4.97	3.69	7.22	6.74	7.40
Almandine	29.17	33.7	32.04	46.16	30.21	31.6	27.88	28.73	27.33	29.79	31.23	41.26	32.66	31.68
Grossular	2.20	0.00	1.81	3.87	1.92	2.45	0.00	0.22	0.00	0.73	1.11	0.46	0.91	0.00
Andradite	3.53	6.16	0.08	0.00	4.29	1.05	3.73	4.65	4.92	4.71	2.68	6.03	2.70	1.63

Cont. Table 2

Sample Wt. %	AD-10-003 C1 P2	AD-10-003 C1 P3	AD-10-003 C1 P4	AD-10-003 C1 P5	AD-10-003 C2 P2	AD-10-003 C2 P3	AD-10-003 C2 P4	AD-10-003 C3 P1	AD-10-003 C3 P3	AD-10-003 C4 P1	AD-10-003 C4 P4	AD-10-003 C5 P1	AD-10-003 C5 P2	AD-10-003 C5 P3
SiO_2	36.258	36.760	36.409	36.682	36.434	36.494	36.649	36.463	36.671	36.365	36.509	36.711	36.249	36.809
P_2O_5	0.000	0.000	0.000	0.000	0.000	0.000	0.000	0.000	0.000	0.000	0.000	0.000	0.000	0.000
TiO_2	0.048	0.000	0.016	0.026	0.094	0.000	0.032	0.000	0.040	0.000	0.000	0.030	0.000	0.006
CaO	1.635	1.875	1.951	1.518	1.372	1.615	1.543	1.539	1.941	2.102	1.312	1.432	1.963	1.874
MgO	1.714	1.915	1.884	1.844	1.733	1.817	1.695	1.741	1.898	1.725	1.776	1.863	1.647	1.637
Al_2O_3	19.365	19.372	19.220	19.446	19.632	19.602	19.557	19.889	19.628	19.605	19.709	19.756	19.764	19.480
MnO	25.423	24.234	24.044	15.956	25.505	25.096	24.005	25.697	25.273	20.145	26.441	25.948	23.127	25.794
FeO	15.341	16.124	15.539	24.889	15.820	15.335	17.172	15.157	14.884	20.202	14.583	14.932	16.871	14.599
Cr_2O_3	0.002	0.000	0.014	0.000	0.021	0.072	0.006	0.000	0.000	0.020	0.035	0.000	0.053	0.027
ZnO	0.000	0.091	0.079	0.000	0.000	0.084	0.044	0.000	0.025	0.094	0.035	0.076	0.151	0.000
Total	99.786	100.371	99.156	100.361	100.61	100.12	100.703	100.49	100.360	100.26	100.40	100.75	99.825	100.23
Apfu based on 12 oxygen atoms														
Si	2.990	3.007	3.010	3.005	2.982	2.993	2.995	2.981	2.996	2.983	2.989	2.992	2.982	3.013
P	0.000	0.000	0.000	0.000	0.000	0.000	0.000	0.000	0.000	0.000	0.000	0.000	0.000	0.000
Ti	0.003	0.000	0.001	0.002	0.006	0.000	0.002	0.000	0.003	0.000	0.000	0.002	0.000	0.000
Ca	0.145	0.164	0.173	0.133	0.120	0.142	0.135	0.135	0.170	0.185	0.115	0.125	0.173	0.164
Mg	0.211	0.234	0.232	0.225	0.211	0.222	0.207	0.212	0.231	0.211	0.217	0.226	0.202	0.200
Al	1.883	1.868	1.873	1.878	1.894	1.895	1.884	1.917	1.890	1.896	1.902	1.898	1.916	1.879
Mn	1.776	1.679	1.684	1.107	1.768	1.743	1.662	1.780	1.749	1.400	1.834	1.791	1.612	1.788
Fe	1.058	1.103	1.074	1.705	1.083	1.052	1.174	1.036	1.017	1.386	0.999	1.018	1.161	0.999
Cr	0.000	0.000	0.001	0.000	0.001	0.005	0.000	0.000	0.000	0.001	0.002	0.000	0.004	0.002
Zn	0.000	0.006	0.005	0.000	0.000	0.005	0.003	0.000	0.002	0.006	0.002	0.005	0.009	0.000
Total	8.065	8.060	8.052	8.055	8.065	8.057	8.061	8.061	8.057	8.068	8.059	8.057	8.058	8.046
Spessartine	58.72	55.59	55.79	36.65	58.46	57.74	54.99	58.87	57.9	46.3	60.69	59.32	53.39	59.27
Pyrope	6.97	7.73	7.69	7.46	6.99	7.36	6.83	7.02	7.65	6.98	7.17	7.50	6.69	6.62
Almandine	25.98	28.76	29.21	48.35	26.35	27.72	30.36	27.15	27.07	38.79	24.95	26.09	32.98	27.32
Grossular	0.00	0.00	0.00	0.00	0.00	0.00	0.00	0.00	0.00	0.00	0.00	0.00	0.36	0.00
Andradite	4.62	5.44	5.63	4.33	3.62	4.47	4.35	4.46	5.50	6.05	3.70	4.05	5.20	5.34

Cont. Table 2

Sample Wt. %	AD-10-003 C8 P1	AD-10-003 C8 P2	AD-10-003 C8 P3	AD-10-003 C8 P4	AD-10-003 C9 P1	AD-10-003 C9 P2	AD-10-003 C12 P1	AD-10-003 C12 P2	AD-10-003 C13 P1	AD-10-003 C13 P2	AD-10-003 C13 P3	AD-10-003 C13 P4	AD-10-003 C14 P2	AD-10-003 C14 P3
SiO_2	36.511	36.293	36.403	36.711	36.744	36.855	36.779	36.461	36.035	36.865	36.596	36.427	36.494	36.145
P_2O_5	0.000	0.000	0.000	0.000	0.000	0.000	0.000	0.000	0.000	0.000	0.000	0.000	0.000	0.000
TiO_2	0.000	0.000	0.000	0.000	0.000	0.000	0.046	0.020	0.072	0.044	0.000	0.075	0.000	0.020
CaO	1.223	1.918	2.247	1.867	2.018	1.913	1.292	1.783	1.021	1.748	2.079	1.667	1.917	1.989
MgO	1.820	1.692	1.770	1.661	1.601	1.722	1.894	1.863	1.845	1.698	1.830	1.770	1.635	1.752
Al_2O_3	19.829	19.680	19.198	19.293	19.597	19.958	19.761	19.378	20.148	19.410	19.164	19.559	19.270	19.344
MnO	25.774	25.087	24.929	24.925	25.068	25.696	25.179	24.198	25.425	22.807	24.495	24.462	23.662	24.664
FeO	14.451	15.091	15.568	14.918	15.256	14.704	15.550	15.308	16.026	18.220	15.712	15.654	17.518	15.450
Cr_2O_3	0.000	0.000	0.019	0.045	0.000	0.000	0.008	0.000	0.004	0.000	0.000	0.027	0.000	0.000
ZnO	0.015	0.180	0.000	0.012	0.049	0.062	0.007	0.057	0.047	0.000	0.134	0.057	0.012	0.138
Total	99.623	99.941	100.13	99.432	100.33	100.91	100.516	99.068	100.623	100.80	100.01	99.698	100.51	99.502
Apfu based on 12 oxygen atoms														
Si	3.000	2.984	2.993	3.024	3.005	2.994	3.000	3.012	2.949	3.008	3.008	2.997	2.994	2.988
P	0.000	0.000	0.000	0.000	0.000	0.000	0.000	0.000	0.000	0.000	0.000	0.000	0.000	0.000
Ti	0.000	0.000	0.000	0.000	0.000	0.000	0.003	0.001	0.004	0.003	0.000	0.005	0.000	0.001
Ca	0.108	0.169	0.198	0.165	0.177	0.167	0.113	0.158	0.090	0.153	0.183	0.147	0.169	0.176
Mg	0.223	0.207	0.217	0.204	0.195	0.209	0.230	0.230	0.225	0.207	0.224	0.217	0.200	0.216
Al	1.921	1.907	1.861	1.873	1.889	1.911	1.900	1.887	1.944	1.867	1.856	1.897	1.864	1.885
Mn	1.794	1.747	1.736	1.739	1.737	1.768	1.740	1.693	1.763	1.576	1.705	1.705	1.645	1.727
Fe	0.993	1.038	1.071	1.028	1.044	0.999	1.061	1.058	1.097	1.243	1.080	1.077	1.202	1.068
Cr	0.000	0.000	0.001	0.003	0.000	0.000	0.001	0.000	0.000	0.000	0.000	0.002	0.000	0.000
Zn	0.001	0.011	0.000	0.001	0.003	0.004	0.000	0.004	0.003	0.000	0.008	0.004	0.001	0.008
Total	8.040	8.063	8.076	8.038	8.050	8.051	8.047	8.043	8.074	8.056	8.064	8.049	8.074	8.069
Spessartine	59.51	57.86	57.32	57.71	57.55	58.59	57.65	56.17	58.23	52.17	56.44	56.5	54.32	57.13
Pyrope	7.40	6.87	7.16	5.35	6.47	6.91	7.63	7.61	7.44	6.84	7.42	7.20	6.61	7.14
Almandine	27.95	28.24	25.90	30.18	29.28	28.20	28.28	30.00	26.80	33.02	27.64	29.59	29.77	27.52
Grossular	0.00	0.00	0.00	0.00	0.00	0.11	0.00	0.00	0.00	0.00	0.00	0.00	0.00	0.00
Andradite	3.57	5.60	6.47	5.32	5.86	5.41	3.58	5.17	2.73	4.92	6.06	4.55	5.57	5.77

Cont. Table 2

Sample Wt. %	AD-10-003 C14 P4	AD-10-004 C2 P1	AD-10-004 C2 P3	AD-10-004 C2 P4	AD-10-004 C6 P2	AD-10-004 C6 P3	AD-10-004 C6 P4	AD-10-004 C7 P1	AD-10-004 C7 P2	AD-10-004 C7 P3	AD-10-004 C7 P4	AD-10-004 C8 P1	AD-10-004 C8 P2	AD-10-004 C8 P4
SiO_2	36.909	36.922	36.543	36.453	36.960	37.023	36.909	36.812	36.642	36.610	36.952	36.666	36.556	36.703
P_2O_5	0.000	0.000	0.000	0.000	0.000	0.000	0.000	0.000	0.000	0.000	0.000	0.000	0.000	0.000
TiO_2	0.032	0.000	0.006	0.000	0.006	0.000	0.000	0.051	0.000	0.000	0.091	0.000	0.000	0.000
CaO	1.608	2.121	1.993	2.100	2.229	2.227	1.202	1.197	2.119	2.161	1.496	1.920	2.152	2.190
MgO	1.782	1.952	1.993	2.052	2.013	2.018	2.191	2.407	1.929	1.904	2.710	2.106	2.000	2.155
Al_2O_3	19.466	19.989	19.769	19.735	20.015	19.881	20.193	19.824	19.903	19.561	20.671	20.099	19.962	19.901
MnO	18.006	22.346	23.117	22.252	23.830	23.555	24.654	18.787	23.296	23.524	18.571	21.654	23.966	21.389
FeO	23.068	16.998	16.773	16.811	15.724	15.703	15.174	21.448	15.711	16.705	20.248	18.135	16.056	17.587
Cr_2O_3	0.045	0.000	0.002	0.000	0.000	0.000	0.000	0.047	0.027	0.002	0.000	0.039	0.008	0.000
ZnO	0.032	0.000	0.000	0.139	0.050	0.069	0.022	0.035	0.176	0.097	0.000	0.000	0.000	0.052
Total	100.948	100.328	100.20	99.542	100.83	100.48	100.345	100.61	99.803	100.56	100.74	100.62	100.70	99.977
Apfu based on 12 oxygen atoms														
Si	3.007	3.004	2.988	2.994	2.995	3.007	2.999	2.994	2.998	2.990	2.978	2.981	2.975	2.996
P	0.000	0.000	0.000	0.000	0.000	0.000	0.000	0.000	0.000	0.000	0.000	0.000	0.000	0.000
Ti	0.002	0.000	0.000	0.000	0.000	0.000	0.000	0.003	0.000	0.000	0.006	0.000	0.000	0.000
Ca	0.140	0.185	0.175	0.185	0.194	0.194	0.105	0.104	0.186	0.189	0.129	0.167	0.188	0.192
Mg	0.216	0.237	0.243	0.251	0.243	0.244	0.265	0.292	0.235	0.232	0.326	0.255	0.243	0.262
Al	1.869	1.917	1.905	1.910	1.912	1.904	1.934	1.900	1.920	1.883	1.964	1.926	1.915	1.915
Mn	1.243	1.540	1.601	1.548	1.636	1.621	1.697	1.294	1.615	1.627	1.268	1.491	1.652	1.479
Fe	1.572	1.156	1.147	1.155	1.066	1.067	1.031	1.459	1.075	1.141	1.365	1.233	1.093	1.201
Cr	0.003	0.000	0.000	0.000	0.000	0.000	0.000	0.003	0.002	0.000	0.000	0.003	0.001	0.000
Zn	0.002	0.000	0.000	0.008	0.003	0.004	0.001	0.002	0.011	0.006	0.000	0.000	0.000	0.003
Total	8.055	8.038	8.059	8.051	8.049	8.041	8.033	8.052	8.041	8.068	8.035	8.055	8.067	8.047
Spessartine	41.15	51.08	52.98	51.32	54.22	53.78	56.34	42.87	53.62	53.82	42.08	49.36	54.62	49.03
Pyrope	7.17	7.85	8.04	8.33	8.06	8.11	8.81	9.67	7.81	7.67	10.81	8.45	8.02	8.69
Almandine	43.91	34.58	31.85	33.48	30.6	31.48	30.54	40.66	31.97	30.27	41.86	35.33	29.52	35.25
Grossular	0.00	1.33	0.00	0.76	1.09	1.06	0.00	0.00	1.56	0.00	1.28	0.50	0.34	1.22
Andradite	4.41	4.80	5.75	5.36	5.31	5.37	3.47	3.15	4.52	6.25	2.73	4.91	5.83	5.13

Cont. Table 2

Sample Wt. %	AD-10-004 C10 P1	AD-10-004 C10 P3	AD-10-010 C1 P1	AD-10-010 C1 P2	AD-10-010 C1 P3	AD-10-010 C1 P4	AD-10-010 C2 P1	AD-10-010 C2 P2	AD-10-010 C2 P3	AD-10-010 C2 P4	AD-10-010 C3 P1	AD-10-010 C3 P3	AD-10-010 C3 P4	AD-10-010 C4 P1
SiO_2	37.076	36.487	36.725	36.626	36.533	37.015	36.481	36.488	36.725	37.001	36.519	36.553	36.513	36.797
P_2O_5	0.000	0.000	0.000	0.000	0.000	0.000	0.000	0.000	0.000	0.000	0.000	0.000	0.000	0.000
TiO_2	0.000	0.016	0.000	0.025	0.047	0.064	0.076	0.000	0.072	0.025	0.058	0.062	0.019	0.037
CaO	1.211	2.346	7.610	7.602	7.828	7.652	8.315	8.277	8.299	8.172	8.037	8.257	8.205	7.912
MgO	2.109	2.001	1.118	1.136	1.164	1.094	1.000	1.154	1.078	0.951	1.074	1.074	1.072	1.080
Al_2O_3	20.217	19.520	19.106	18.484	18.637	18.717	18.487	19.347	18.727	18.659	18.664	18.634	18.764	18.972
MnO	24.525	23.212	16.586	16.999	16.489	17.014	17.094	16.277	16.484	17.043	16.735	15.556	16.419	16.907
FeO	15.734	15.905	18.829	18.775	18.740	18.522	18.826	17.652	19.012	18.475	18.178	18.952	18.487	18.460
Cr_2O_3	0.000	0.000	0.008	0.017	0.050	0.023	0.015	0.000	0.019	0.000	0.000	0.000	0.000	0.000
ZnO	0.067	0.000	0.000	0.047	0.129	0.012	0.002	0.000	0.065	0.055	0.151	0.077	0.089	0.174
Total	100.939	99.487	99.982	99.711	99.617	100.11	100.296	99.195	100.481	100.38	99.416	99.165	99.568	100.34
Apfu based on 12 oxygen atoms														
Si	3.000	3.000	3.001	3.011	3.003	3.022	2.990	2.992	2.996	3.018	3.005	3.011	3.000	3.000
P	0.000	0.000	0.000	0.000	0.000	0.000	0.000	0.000	0.000	0.000	0.000	0.000	0.000	0.000
Ti	0.000	0.001	0.000	0.002	0.003	0.004	0.005	0.000	0.004	0.002	0.004	0.004	0.001	0.002
Ca	0.105	0.207	0.666	0.670	0.689	0.669	0.730	0.727	0.725	0.714	0.709	0.729	0.722	0.691
Mg	0.254	0.245	0.136	0.139	0.143	0.133	0.122	0.141	0.131	0.116	0.132	0.132	0.131	0.131
Al	1.928	1.891	1.840	1.791	1.805	1.801	1.786	1.870	1.801	1.794	1.810	1.809	1.817	1.823
Mn	1.681	1.616	1.148	1.184	1.148	1.177	1.187	1.131	1.139	1.177	1.167	1.085	1.143	1.168
Fe	1.065	1.094	1.287	1.291	1.288	1.265	1.291	1.211	1.297	1.260	1.251	1.306	1.270	1.259
Cr	0.000	0.000	0.001	0.001	0.003	0.002	0.001	0.000	0.001	0.000	0.000	0.000	0.000	0.000
Zn	0.004	0.000	0.000	0.003	0.008	0.001	0.000	0.000	0.004	0.003	0.009	0.005	0.005	0.011
Total	8.036	8.054	8.079	8.091	8.090	8.073	8.112	8.072	8.099	8.084	8.086	8.080	8.090	8.086
Spessartine	55.8	53.52	37.89	39.03	37.87	38.87	39.02	37.35	37.52	38.86	38.51	35.84	37.69	38.56
Pyrope	8.45	8.12	4.50	4.59	4.71	4.40	4.02	4.66	4.32	3.82	4.35	4.36	4.33	4.34
Almandine	31.15	30.87	34.68	33.63	33.84	34.58	31.42	32.82	33.10	33.41	33.08	35.30	33.15	33.44
Grossular	0.00	0.41	12.63	10.24	11.53	11.14	11.07	16.12	12.07	12.10	12.54	13.26	13.16	12.61
Andradite	3.49	6.39	9.34	11.71	10.91	10.70	12.66	7.91	11.55	11.39	10.68	10.62	10.61	10.10

Cont. Table 2

Sample Wt. %	AD-10-010 C4 P2	AD-10-010 C4 P4	AD-10-010 C5 P2	AD-10-010 C5 P3	AD-10-010 C5 P4	AD-10-010 C5 P5	AD-10-010 C9 P1	AD-10-010 C9 P2	AD-10-010 C9 P3	AD-10-010 C9 P4	AD-10-010 C9 P5	AD-10-010 C11 P1	AD-10-010 C11 P2	AD-10-010 C11 P3
SiO_2	36.341	36.723	36.515	36.556	36.845	36.745	36.821	37.135	36.443	36.775	36.510	36.561	36.582	36.352
P_2O_5	0.000	0.000	0.000	0.000	0.000	0.015	0.000	0.000	0.000	0.000	0.000	0.000	0.000	0.000
TiO_2	0.004	0.000	0.102	0.012	0.099	0.000	0.033	0.021	0.025	0.080	0.023	0.004	0.134	0.006
CaO	8.039	8.203	6.876	7.008	7.027	7.209	8.350	8.103	8.109	8.300	8.225	7.802	7.679	7.663
MgO	1.058	1.027	1.201	1.152	1.277	1.169	1.115	1.073	1.064	1.026	1.060	1.122	1.145	1.091
Al_2O_3	18.721	18.856	18.466	18.643	18.669	18.515	18.744	19.042	18.922	19.149	18.729	18.817	18.925	18.683
MnO	16.554	16.256	17.599	17.670	16.850	17.080	16.619	16.355	16.406	16.350	16.254	17.152	16.319	16.682
FeO	18.769	19.700	18.592	19.159	19.200	18.844	18.333	19.060	18.921	17.736	18.738	18.329	18.650	18.948
Cr_2O_3	0.000	0.023	0.000	0.000	0.012	0.000	0.019	0.021	0.017	0.000	0.025	0.000	0.025	0.083
ZnO	0.119	0.087	0.186	0.119	0.000	0.040	0.020	0.020	0.000	0.067	0.000	0.094	0.052	0.000
Total	99.605	100.875	99.537	100.319	99.979	99.617	100.054	100.83	99.907	99.483	99.564	99.881	99.511	99.508
Apfu based on 12 oxygen atoms														
Si	2.991	2.989	3.010	2.996	3.015	3.021	3.008	3.009	2.987	3.009	3.000	2.998	3.002	2.995
P	0.000	0.000	0.000	0.000	0.000	0.001	0.000	0.000	0.000	0.000	0.000	0.000	0.000	0.000
Ti	0.000	0.000	0.006	0.001	0.006	0.000	0.002	0.001	0.002	0.005	0.001	0.000	0.008	0.000
Ca	0.709	0.715	0.607	0.616	0.616	0.635	0.731	0.704	0.712	0.728	0.724	0.686	0.675	0.676
Mg	0.130	0.125	0.148	0.141	0.156	0.143	0.136	0.130	0.130	0.125	0.130	0.137	0.140	0.134
Al	1.816	1.809	1.794	1.801	1.801	1.794	1.805	1.819	1.828	1.847	1.814	1.819	1.830	1.814
Mn	1.154	1.121	1.229	1.227	1.168	1.189	1.150	1.123	1.139	1.133	1.131	1.191	1.134	1.164
Fe	1.292	1.341	1.282	1.313	1.314	1.296	1.253	1.292	1.297	1.214	1.288	1.257	1.280	1.306
Cr	0.000	0.002	0.000	0.000	0.001	0.000	0.001	0.001	0.001	0.000	0.002	0.000	0.002	0.005
Zn	0.007	0.005	0.011	0.007	0.000	0.002	0.001	0.001	0.000	0.004	0.000	0.006	0.003	0.000
Total	8.100	8.106	8.087	8.102	8.078	8.081	8.087	8.079	8.097	8.063	8.091	8.093	8.074	8.095
Spessartine	38.03	36.89	40.57	40.41	38.56	39.26	37.93	37.06	37.52	37.49	37.29	39.28	37.47	38.35
Pyrope	4.28	4.10	4.87	4.64	5.14	4.73	4.48	4.28	4.28	4.14	4.28	4.52	4.63	4.41
Almandine	32.91	33.85	34.10	33.41	35.71	34.77	32.77	34.82	33.18	34.01	33.50	32.46	35.04	33.63
Grossular	12.41	12.06	8.40	8.61	9.09	9.65	12.93	12.91	12.92	15.33	12.95	11.96	12.33	11.24
Andradite	10.94	11.42	11.34	11.63	10.91	11.31	11.02	10.19	10.41	8.50	10.77	10.63	9.49	10.75

Cont. Table 2

Sample Wt. %	AD-10-010 C11 P4	AD-10-010 C11 P5	AD-10-010 C11 P6	AD-10-010 C12 P1	AD-10-010 C12 P2	AD-10-010 C12 P3	AD-10-010 C13 P3	AD-10-010 C14 P2	AD-10-010 C14 P3	AD-10-010 C15 P1	AD-10-010 C15 P2	AD-10-010 C15 P4	AD-10-012 C1 P1	AD-10-012 C1 P2
SiO_2	36.723	36.912	36.891	36.331	36.675	36.511	36.603	36.679	36.741	36.581	36.324	36.432	36.487	36.449
P_2O_5	0.000	0.000	0.000	0.000	0.000	0.000	0.000	0.000	0.000	0.000	0.000	0.000	0.000	0.000
TiO_2	0.066	0.035	0.010	0.039	0.000	0.000	0.000	0.000	0.006	0.000	0.000	0.033	0.010	0.021
CaO	7.855	7.901	7.767	7.977	8.380	8.719	7.215	7.372	7.544	7.418	7.261	7.446	7.264	7.444
MgO	1.122	1.073	1.133	0.980	0.986	1.016	1.200	1.158	1.099	1.116	1.099	1.143	1.112	1.147
Al_2O_3	18.668	18.703	18.787	18.618	18.577	18.610	19.078	18.709	18.582	18.555	18.641	18.691	19.062	18.477
MnO	16.022	16.554	16.811	17.243	17.258	15.965	17.205	17.119	17.749	17.345	17.369	16.779	17.059	16.899
FeO	18.553	18.570	18.698	19.389	18.023	18.762	18.734	18.839	18.666	18.833	18.734	19.599	19.800	19.232
Cr_2O_3	0.050	0.006	0.054	0.000	0.015	0.037	0.027	0.025	0.031	0.029	0.000	0.008	0.000	0.021
ZnO	0.055	0.067	0.097	0.000	0.136	0.054	0.064	0.005	0.074	0.055	0.045	0.017	0.087	0.007
Total	99.114	99.821	100.25	100.577	100.05	99.674	100.126	99.906	100.492	99.932	99.473	100.15	100.88	99.697
Apfu based on 12 oxygen atoms														
Si	3.022	3.021	3.011	2.977	3.005	2.999	2.993	3.008	3.003	3.005	2.997	2.989	2.974	3.002
P	0.000	0.000	0.000	0.000	0.000	0.000	0.000	0.000	0.000	0.000	0.000	0.000	0.000	0.000
Ti	0.004	0.002	0.001	0.002	0.000	0.000	0.000	0.000	0.000	0.000	0.000	0.002	0.001	0.001
Ca	0.693	0.693	0.679	0.700	0.736	0.768	0.632	0.648	0.661	0.653	0.642	0.655	0.635	0.657
Mg	0.138	0.131	0.138	0.120	0.120	0.124	0.146	0.142	0.134	0.137	0.135	0.140	0.135	0.141
Al	1.811	1.804	1.807	1.798	1.794	1.802	1.839	1.808	1.790	1.796	1.813	1.807	1.832	1.794
Mn	1.117	1.148	1.162	1.197	1.198	1.111	1.192	1.189	1.229	1.207	1.214	1.166	1.178	1.179
Fe	1.277	1.271	1.276	1.329	1.235	1.289	1.281	1.292	1.276	1.294	1.293	1.345	1.350	1.325
Cr	0.003	0.000	0.004	0.000	0.001	0.002	0.002	0.002	0.002	0.002	0.000	0.001	0.000	0.001
Zn	0.003	0.004	0.006	0.000	0.008	0.003	0.004	0.000	0.005	0.003	0.003	0.001	0.005	0.001
Total	8.067	8.075	8.083	8.122	8.097	8.099	8.087	8.088	8.100	8.096	8.096	8.105	8.109	8.100
Spessartine	36.93	37.92	38.37	39.29	39.49	36.59	39.31	39.20	40.48	39.76	39.99	38.37	38.76	38.81
Pyrope	4.55	4.33	4.55	3.93	3.97	4.10	4.83	4.67	4.41	4.50	4.45	4.60	4.45	4.64
Almandine	35.61	34.76	34.08	31.60	31.36	32.83	33.74	33.94	32.29	33.23	33.15	33.92	33.81	33.80
Grossular	12.62	12.16	11.59	10.32	12.50	13.71	11.18	10.37	9.67	9.80	10.11	9.85	10.19	9.58
Andradite	9.81	10.61	10.63	12.55	11.71	11.45	9.58	10.91	11.98	11.62	11.04	11.56	10.65	11.92

Cont. Table 2

Sample Wt. %	AD-10-012 C1 P3	AD-10-012 C1 P4	AD-10-012 C2 P1	AD-10-012 C2 P2	AD-10-012 C3 P1	AD-10-012 C3 P2	AD-10-012 C3 P3	AD-10-012 C3 P4	AD-10-012 C4 P1	AD-10-012 C4 P2	AD-10-012 C4 P3	AD-10-012 C5 P1	AD-10-012 C5 P2	AD-10-012 C5 P4
SiO_2	36.557	36.093	36.948	37.013	37.087	37.140	36.910	36.513	37.074	36.900	36.974	36.554	36.872	36.666
P_2O_5	0.000	0.000	0.000	0.000	0.000	0.000	0.000	0.000	0.000	0.000	0.000	0.000	0.000	0.000
TiO_2	0.025	0.000	0.137	0.074	0.045	0.000	0.000	0.021	0.060	0.000	0.048	0.023	0.000	0.058
CaO	7.240	7.281	9.175	7.443	7.927	9.045	8.044	8.255	7.907	7.892	7.762	7.284	7.481	7.300
MgO	1.167	1.288	1.126	1.179	1.317	1.327	1.265	1.347	1.284	1.302	1.395	1.259	1.170	1.269
Al_2O_3	18.734	18.673	20.161	19.133	19.110	19.422	19.327	19.110	19.243	19.981	19.106	18.998	18.943	19.074
MnO	16.913	16.974	17.837	16.619	14.837	14.197	14.345	14.540	14.764	14.735	14.864	16.179	16.173	17.386
FeO	19.455	19.353	15.323	19.237	19.943	19.595	20.120	20.304	20.027	19.926	20.204	19.341	20.096	19.072
Cr_2O_3	0.000	0.042	0.000	0.000	0.046	0.054	0.025	0.000	0.050	0.000	0.031	0.006	0.000	0.010
ZnO	0.000	0.042	0.114	0.092	0.000	0.040	0.000	0.045	0.060	0.172	0.055	0.092	0.119	0.062
Total	100.091	99.746	100.82	100.790	100.31	100.82	100.036	100.14	100.469	100.91	100.44	99.736	100.85	100.90
Apfu based on 12 oxygen atoms														
Si	2.997	2.975	2.970	3.003	3.011	2.995	3.003	2.980	3.006	2.976	3.003	2.997	2.998	2.981
P	0.000	0.000	0.000	0.000	0.000	0.000	0.000	0.000	0.000	0.000	0.000	0.000	0.000	0.000
Ti	0.002	0.000	0.008	0.005	0.003	0.000	0.000	0.001	0.004	0.000	0.003	0.001	0.000	0.004
Ca	0.636	0.643	0.790	0.647	0.690	0.782	0.701	0.722	0.687	0.682	0.675	0.640	0.652	0.636
Mg	0.143	0.158	0.135	0.143	0.159	0.160	0.153	0.164	0.155	0.157	0.169	0.154	0.142	0.154
Al	1.810	1.814	1.910	1.829	1.829	1.846	1.853	1.838	1.839	1.899	1.829	1.836	1.815	1.828
Mn	1.175	1.185	1.215	1.142	1.021	0.970	0.989	1.005	1.014	1.007	1.023	1.124	1.114	1.197
Fe	1.334	1.334	1.030	1.305	1.354	1.322	1.369	1.386	1.358	1.344	1.372	1.326	1.367	1.297
Cr	0.000	0.003	0.000	0.000	0.003	0.004	0.002	0.000	0.003	0.000	0.002	0.000	0.000	0.001
Zn	0.000	0.003	0.007	0.006	0.000	0.002	0.000	0.003	0.004	0.010	0.003	0.006	0.007	0.004
Total	8.096	8.116	8.066	8.078	8.070	8.080	8.070	8.099	8.070	8.075	8.079	8.084	8.095	8.101
Spessartine	38.69	38.96	40.19	37.72	33.72	32.02	32.67	33.11	33.52	33.28	33.76	37.09	36.73	39.43
Pyrope	4.70	5.20	4.47	4.71	5.27	5.27	5.07	5.40	5.13	5.18	5.58	5.08	4.68	5.07
Almandine	34.44	32.5	27.76	35.53	37.83	35.8	38.32	35.92	38.14	37.40	37.61	35.69	35.96	32.86
Grossular	9.70	9.48	19.83	11.45	13.11	16.67	14.64	13.63	13.47	15.96	12.37	11.45	10.70	10.21
Andradite	11.18	11.52	5.91	9.70	9.40	8.97	8.45	10.09	8.90	6.59	9.69	9.59	10.79	10.53

Cont. Table 2

Sample Wt. %	AD-10-012 C6 P2	AD-10-012 C6 P4	AD-10-012 C7 P1	AD-10-012 C7 P3	AD-10-012 C7 P4	AD-10-012 C7 P6	AD-10-012 C8 P2	AD-10-012 C8 P4	AD-10-012 C9 P2	AD-10-012 C10 P2	AD-10-012 C10 P3	AD-10-013 C2 P2	AD-10-013 C2 P3	AD-10-013 C3 P3
SiO_2	37.244	36.976	36.581	36.854	36.910	36.553	36.845	36.238	36.783	36.979	36.792	36.452	36.594	36.953
P_2O_5	0.000	0.000	0.000	0.000	0.000	0.000	0.000	0.000	0.000	0.000	0.000	0.000	0.000	0.000
TiO_2	0.019	0.000	0.000	0.000	0.000	0.000	0.074	0.000	0.000	0.000	0.000	0.023	0.000	0.008
CaO	8.112	7.775	8.108	8.320	8.201	8.118	7.215	7.403	7.215	7.452	7.153	7.401	7.246	7.497
MgO	1.357	1.348	1.201	1.319	1.290	1.263	1.218	1.207	1.251	1.168	1.204	1.168	1.157	1.114
Al_2O_3	19.244	19.129	19.189	19.362	19.367	18.874	19.108	19.090	18.899	18.673	19.038	18.814	18.930	18.679
MnO	14.296	14.820	14.657	14.153	14.706	15.409	16.650	16.467	17.151	17.614	16.896	17.399	17.471	17.491
FeO	19.818	20.587	20.180	20.025	19.651	20.232	19.525	19.918	19.211	19.029	19.090	18.325	18.739	19.078
Cr_2O_3	0.017	0.015	0.008	0.000	0.010	0.000	0.006	0.000	0.000	0.000	0.044	0.000	0.000	0.000
ZnO	0.147	0.075	0.099	0.142	0.050	0.114	0.000	0.079	0.134	0.000	0.079	0.181	0.141	0.129
Total	100.254	100.725	100.02	100.175	100.19	100.56	100.641	100.40	100.644	100.92	100.30	99.763	100.28	100.95
Apfu based on 12 oxygen atoms														
Si	3.018	2.999	2.987	2.995	2.999	2.982	2.996	2.966	2.997	3.008	3.002	2.995	2.993	3.006
P	0.000	0.000	0.000	0.000	0.000	0.000	0.000	0.000	0.000	0.000	0.000	0.000	0.000	0.000
Ti	0.001	0.000	0.000	0.000	0.000	0.000	0.005	0.000	0.000	0.000	0.000	0.001	0.000	0.001
Ca	0.705	0.676	0.710	0.724	0.714	0.710	0.629	0.649	0.630	0.650	0.625	0.652	0.635	0.654
Mg	0.164	0.163	0.146	0.160	0.156	0.154	0.148	0.147	0.152	0.142	0.146	0.143	0.141	0.135
Al	1.838	1.829	1.847	1.855	1.855	1.815	1.831	1.842	1.815	1.790	1.831	1.822	1.825	1.791
Mn	0.981	1.018	1.014	0.974	1.012	1.065	1.147	1.142	1.184	1.214	1.168	1.211	1.210	1.205
Fe	1.343	1.396	1.378	1.361	1.335	1.380	1.328	1.363	1.309	1.294	1.303	1.259	1.282	1.298
Cr	0.001	0.001	0.001	0.000	0.001	0.000	0.000	0.000	0.000	0.000	0.003	0.000	0.000	0.000
Zn	0.009	0.005	0.006	0.009	0.003	0.007	0.000	0.005	0.008	0.000	0.005	0.011	0.009	0.008
Total	8.061	8.086	8.089	8.078	8.074	8.111	8.083	8.114	8.095	8.097	8.082	8.093	8.095	8.098
Spessartine	32.5	33.59	33.45	32.2	33.44	35.03	37.83	37.54	39.03	39.97	38.55	39.95	39.92	39.73
Pyrope	5.43	5.38	4.82	5.28	5.16	5.05	4.87	4.84	5.01	4.66	4.83	4.72	4.65	4.45
Almandine	38.74	37.69	36.88	37.56	36.89	34.68	35.55	33.8	34.02	33.04	35.08	32.69	33.2	33.39
Grossular	14.60	12.28	14.09	15.36	15.03	11.96	10.63	10.96	9.96	9.35	10.85	11.01	10.56	9.63
Andradite	8.61	9.97	9.29	8.58	8.53	11.38	9.86	10.39	10.81	12.04	9.65	10.41	10.38	11.89

Cont. Table 2

Sample Wt. %	AD-10-013 C3 P4	AD-10-013 C3 P5	AD-10-013 C4 P2	AD-10-013 C4 P3	AD-10-013 C4 P4	AD-10-013 C7 P1	AD-10-013 C7 P2	AD-10-013 C7 P3	AD-10-013 C7 P4	AD-10-013 C9 P3	AD-10-013 C9 P4	AD-10-013 C9 P5	AD-10-013 C10 P1	AD-10-013 C10 P2
SiO_2	36.788	37.070	36.764	36.680	36.547	36.757	36.798	36.813	36.568	36.537	37.114	36.659	36.792	36.410
P_2O_5	0.000	0.000	0.000	0.000	0.000	0.000	0.000	0.000	0.000	0.000	0.000	0.000	0.000	0.000
TiO_2	0.000	0.014	0.000	0.047	0.000	0.020	0.051	0.000	0.000	0.037	0.000	0.000	0.016	0.000
CaO	6.989	7.144	6.843	6.717	6.897	7.290	7.169	7.407	7.200	7.373	7.401	7.374	7.115	7.278
MgO	1.164	1.209	1.192	1.197	1.191	1.197	1.198	1.206	1.222	1.128	1.197	1.127	1.096	1.111
Al_2O_3	18.718	18.798	18.890	19.014	18.875	18.517	18.904	18.789	18.686	18.802	18.530	18.783	18.577	18.886
MnO	17.720	17.221	17.880	17.762	18.138	17.730	17.861	17.228	17.399	17.345	17.336	18.105	17.497	17.693
FeO	19.165	18.522	19.187	18.588	18.410	18.586	18.274	18.522	18.369	18.742	19.037	18.677	18.819	18.964
Cr_2O_3	0.017	0.037	0.000	0.000	0.000	0.000	0.000	0.035	0.000	0.004	0.025	0.021	0.000	0.004
ZnO	0.143	0.000	0.101	0.156	0.052	0.104	0.089	0.000	0.067	0.074	0.205	0.119	0.000	0.035
Total	100.704	100.015	100.86	100.161	100.11	100.20	100.344	100.00	99.511	100.04	100.85	100.87	99.912	100.38
Apfu based on 12 oxygen atoms														
Si	3.002	3.027	2.995	3.000	2.995	3.010	3.003	3.011	3.009	2.995	3.020	2.989	3.018	2.982
P	0.000	0.000	0.000	0.000	0.000	0.000	0.000	0.000	0.000	0.000	0.000	0.000	0.000	0.000
Ti	0.000	0.001	0.000	0.003	0.000	0.001	0.003	0.000	0.000	0.002	0.000	0.000	0.001	0.000
Ca	0.611	0.625	0.597	0.589	0.606	0.640	0.627	0.649	0.635	0.648	0.645	0.644	0.626	0.639
Mg	0.142	0.147	0.145	0.146	0.146	0.146	0.146	0.147	0.150	0.138	0.145	0.137	0.134	0.136
Al	1.800	1.809	1.814	1.833	1.823	1.788	1.819	1.812	1.812	1.817	1.777	1.805	1.796	1.823
Mn	1.225	1.191	1.234	1.230	1.259	1.230	1.235	1.194	1.213	1.204	1.195	1.250	1.216	1.227
Fe	1.308	1.265	1.307	1.271	1.262	1.273	1.247	1.267	1.264	1.285	1.295	1.274	1.291	1.299
Cr	0.001	0.002	0.000	0.000	0.000	0.000	0.000	0.002	0.000	0.000	0.002	0.001	0.000	0.000
Zn	0.009	0.000	0.006	0.009	0.003	0.006	0.005	0.000	0.004	0.005	0.012	0.007	0.000	0.002
Total	8.097	8.067	8.098	8.081	8.093	8.095	8.085	8.082	8.086	8.094	8.091	8.108	8.083	8.107
Spessartine	40.38	39.37	40.66	40.65	41.5	40.55	40.75	39.38	40.01	39.70	39.44	41.16	40.12	40.38
Pyrope	4.67	4.64	4.77	4.82	4.80	4.82	4.81	4.85	4.95	4.54	4.79	4.51	4.42	4.46
Almandine	33.78	35.16	33.59	34.29	32.47	32.83	32.97	33.7	33.38	33.22	34.15	31.52	34.45	32.25
Grossular	8.65	10.53	8.69	9.72	9.46	9.08	10.17	10.75	10.26	10.47	9.11	9.54	9.3	10.02
Andradite	11.44	9.93	10.99	9.58	10.50	11.95	10.36	10.56	10.68	10.75	12.10	11.60	11.29	10.98

Cont. Table 2

Sample Wt. %	AD-10-013 C10 P3	AD-10-013 C10 P4	AD-10-013 C11 P1	AD-10-013 C11 P4	AD-10-013 C12 P1	AD-10-013 C12 P4	AD-10-015 C1 P1	AD-10-015 C1 P2	AD-10-015 C1 P4	AD-10-015 C2 P2	AD-10-015 C2 P3	AD-10-015 C3 P1	AD-10-015 C3 P2	AD-10-015 C4 P3
SiO_2	37.268	36.865	36.496	36.635	36.591	36.493	37.180	37.406	37.301	36.962	36.868	37.269	37.077	37.084
P_2O_5	0.000	0.000	0.000	0.000	0.000	0.000	0.000	0.000	0.000	0.000	0.000	0.000	0.000	0.000
TiO_2	0.000	0.066	0.000	0.006	0.000	0.012	0.000	0.016	0.020	0.000	0.000	0.000	0.014	0.026
CaO	7.272	7.500	7.260	7.174	7.161	6.912	3.471	3.587	3.209	3.441	3.016	3.621	2.713	3.279
MgO	1.159	1.161	1.236	1.197	1.117	1.223	2.009	1.972	1.937	1.873	1.991	1.959	2.089	1.919
Al_2O_3	18.712	18.859	18.492	18.855	18.550	18.816	20.096	20.339	20.012	20.123	19.892	19.757	20.256	20.087
MnO	17.197	17.624	17.469	17.584	17.940	18.157	15.698	16.122	16.300	15.918	16.318	15.812	16.070	16.273
FeO	18.454	18.772	18.624	18.355	18.607	19.201	22.314	21.105	21.931	21.460	22.582	22.429	21.941	21.726
Cr_2O_3	0.037	0.002	0.050	0.023	0.035	0.000	0.000	0.008	0.000	0.031	0.000	0.000	0.070	0.023
ZnO	0.146	0.094	0.099	0.074	0.000	0.000	0.050	0.077	0.104	0.089	0.037	0.060	0.092	0.069
Total	100.245	100.943	99.726	99.903	100.00	100.81	100.818	100.63	100.814	99.897	100.70	100.91	100.32	100.49
Apfu based on 12 oxygen atoms														
Si	3.036	2.996	3.004	3.003	3.005	2.980	3.003	3.014	3.013	3.007	2.993	3.012	3.004	3.004
P	0.000	0.000	0.000	0.000	0.000	0.000	0.000	0.000	0.000	0.000	0.000	0.000	0.000	0.000
Ti	0.000	0.004	0.000	0.000	0.000	0.001	0.000	0.001	0.001	0.000	0.000	0.000	0.001	0.002
Ca	0.635	0.653	0.640	0.630	0.630	0.605	0.300	0.310	0.278	0.300	0.262	0.314	0.236	0.285
Mg	0.141	0.141	0.152	0.146	0.137	0.149	0.242	0.237	0.233	0.227	0.241	0.236	0.252	0.232
Al	1.797	1.807	1.794	1.822	1.796	1.811	1.913	1.931	1.905	1.930	1.903	1.882	1.934	1.918
Mn	1.187	1.213	1.218	1.221	1.248	1.256	1.074	1.100	1.115	1.097	1.122	1.083	1.103	1.117
Fe	1.257	1.276	1.282	1.258	1.278	1.311	1.507	1.422	1.482	1.460	1.533	1.516	1.487	1.472
Cr	0.002	0.000	0.003	0.002	0.002	0.000	0.000	0.001	0.000	0.002	0.000	0.000	0.005	0.002
Zn	0.009	0.006	0.006	0.005	0.000	0.000	0.003	0.005	0.006	0.005	0.002	0.004	0.006	0.004
Total	8.064	8.096	8.098	8.086	8.096	8.113	8.041	8.020	8.033	8.028	8.056	8.047	8.026	8.034
Spessartine	39.29	39.99	40.13	40.28	41.11	41.28	35.62	36.6	37.05	36.46	37.15	35.89	36.66	37.08
Pyrope	2.59	4.64	5.00	4.83	4.50	4.89	8.02	6.81	7.37	7.55	7.98	7.83	8.39	7.70
Almandine	35.56	32.74	32.76	33.2	32.62	31.93	46.00	45.48	46.07	45.97	45.28	45.76	47.02	45.59
Grossular	11.79	10.1	9.25	10.47	8.96	8.12	4.95	7.48	4.45	6.15	2.74	3.94	4.20	4.82
Andradite	9.11	11.22	11.68	10.22	11.68	11.72	5.02	2.70	4.66	3.72	5.94	6.46	3.37	4.48

Cont. Table 2

Sample Wt. %	AD-10-015 C6 P1	AD-10-015 C7 P1	AD-10-015 C7 P3	AD-10-015 C7 P4	AD-10-015 C8 P2	AD-10-015 C8 P3	AD-10-015 C9 P2	AD-10-015 C9 P3	AD-10-015 C9 P4	AD-10-015 C9 T1 L40	AD-10-015 C9 T1 L59	AD-10-015 C9 T1 L90	AD-10-019 C1 P3	AD-10-019 C1 P4
SiO_2	37.278	37.298	37.297	37.361	37.067	36.952	37.174	37.539	37.319	36.843	36.607	36.955	36.539	36.217
P_2O_5	0.000	0.000	0.000	0.000	0.000	0.000	0.000	0.000	0.000	0.000	0.000	0.000	0.000	0.000
TiO_2	0.000	0.029	0.000	0.000	0.047	0.000	0.073	0.035	0.016	0.000	0.000	0.022	0.089	0.171
CaO	3.590	3.565	3.526	2.787	3.455	3.402	3.733	3.677	3.641	2.774	2.195	2.952	2.234	2.257
MgO	1.898	1.953	1.991	2.091	1.988	2.051	1.958	2.034	2.047	2.003	2.040	1.609	0.438	0.429
Al_2O_3	19.816	19.838	20.111	20.284	20.372	19.705	19.869	19.771	20.105	20.423	20.521	20.151	20.376	20.150
MnO	15.841	15.489	16.473	16.095	16.501	16.576	15.787	16.300	15.948	16.032	16.471	14.102	30.306	30.093
FeO	22.375	22.608	21.512	22.109	21.288	22.234	21.559	21.408	21.898	23.125	23.006	24.257	10.402	10.179
Cr_2O_3	0.000	0.042	0.000	0.019	0.008	0.029	0.000	0.000	0.000	0.047	0.000	0.023	0.000	0.042
ZnO	0.097	0.000	0.050	0.069	0.000	0.037	0.109	0.050	0.000	0.062	0.000	0.005	0.000	0.000
Total	100.895	100.822	100.96	100.815	100.73	100.99	100.262	100.81	100.974	101.31	100.84	100.08	100.39	99.538
Apfu based on 12 oxygen atoms														
Si	3.013	3.014	3.006	3.011	2.992	2.993	3.014	3.027	3.006	2.972	2.967	3.009	2.990	2.989
P	0.000	0.000	0.000	0.000	0.000	0.000	0.000	0.000	0.000	0.000	0.000	0.000	0.000	0.000
Ti	0.000	0.002	0.000	0.000	0.003	0.000	0.005	0.002	0.001	0.000	0.000	0.001	0.006	0.011
Ca	0.311	0.309	0.305	0.241	0.299	0.295	0.324	0.318	0.314	0.240	0.191	0.258	0.196	0.200
Mg	0.229	0.235	0.239	0.251	0.239	0.248	0.237	0.245	0.246	0.241	0.246	0.195	0.053	0.053
Al	1.888	1.889	1.911	1.927	1.938	1.881	1.899	1.879	1.909	1.942	1.960	1.934	1.965	1.960
Mn	1.085	1.060	1.125	1.099	1.128	1.137	1.084	1.113	1.088	1.095	1.131	0.973	2.101	2.103
Fe	1.513	1.528	1.450	1.490	1.437	1.506	1.462	1.444	1.475	1.560	1.559	1.652	0.712	0.702
Cr	0.000	0.003	0.000	0.001	0.001	0.002	0.000	0.000	0.000	0.003	0.000	0.002	0.000	0.003
Zn	0.006	0.000	0.003	0.004	0.000	0.002	0.007	0.003	0.000	0.004	0.000	0.000	0.000	0.000
Total	8.043	8.039	8.039	8.025	8.036	8.065	8.032	8.031	8.039	8.056	8.053	8.022	8.022	8.020
Spessartine	35.98	35.16	37.32	36.53	37.43	37.61	36.03	36.98	36.09	36.27	37.44	32.33	69.82	69.94
Pyrope	7.59	7.80	7.94	7.87	7.94	8.19	7.20	5.89	8.15	7.98	8.16	6.43	1.78	1.75
Almandine	46.08	46.79	44.4	47.23	44.09	43.43	45.49	44.9	45.08	46.23	46.32	52.64	21.46	21.40
Grossular	4.25	4.19	5.10	4.47	5.92	2.59	5.92	5.86	5.22	3.60	2.78	5.02	4.01	3.71
Andradite	6.07	5.78	5.01	3.48	3.83	7.08	4.41	4.49	5.16	4.20	3.54	3.33	2.23	2.26

Cont. Table 2

Sample Wt. %	AD-10-019 C5 P1	AD-10-019 C5 P2	AD-10-019 C5 P3	AD-10-019 C5 P4	AD-10-019 C5 P5	AD-10-019 C7 P1	AD-10-019 C7 P2	AD-10-019 C7 P3	AD-10-019 C7 P4	AD-10-019 C8 P2	AD-10-019 C8 P4	AD-10-019 C8 P5	AD-10-019 C9 P2	AD-10-019 C9 P4
SiO_2	36.293	36.607	36.203	36.344	36.137	36.650	36.158	35.919	36.205	36.388	36.116	35.970	35.888	36.169
P_2O_5	0.000	0.000	0.000	0.000	0.000	0.000	0.000	0.000	0.000	0.000	0.000	0.000	0.000	0.000
TiO_2	0.054	0.052	0.016	0.117	0.133	0.032	0.115	0.070	0.052	0.070	0.060	0.137	0.165	0.014
CaO	2.466	2.451	2.393	2.433	2.423	2.334	2.444	2.524	2.427	2.462	2.360	2.469	2.540	2.437
MgO	0.296	0.328	0.306	0.282	0.275	0.305	0.310	0.370	0.338	0.350	0.353	0.361	0.342	0.354
Al_2O_3	20.136	19.924	19.956	20.008	19.998	20.014	19.724	19.753	19.935	19.592	19.635	20.341	19.781	20.004
MnO	30.781	30.806	31.469	30.858	31.221	32.021	31.036	30.616	30.555	31.687	30.759	30.434	31.497	31.124
FeO	9.326	9.021	9.694	9.281	8.678	8.894	9.659	9.938	9.772	10.210	10.265	9.465	9.676	9.744
Cr_2O_3	0.059	0.044	0.017	0.013	0.013	0.000	0.000	0.000	0.010	0.067	0.065	0.000	0.000	0.067
ZnO	0.084	0.002	0.000	0.037	0.057	0.022	0.069	0.111	0.089	0.000	0.000	0.158	0.067	0.072
Total	99.495	99.235	100.0	99.373	98.935	100.27	99.515	99.301	99.383	100.83	99.613	99.335	99.956	99.985
Apfu based on 12 oxygen atoms														
Si	2.996	3.023	2.986	3.004	2.999	3.007	2.995	2.984	2.997	2.988	2.993	2.975	2.969	2.983
P	0.000	0.000	0.000	0.000	0.000	0.000	0.000	0.000	0.000	0.000	0.000	0.000	0.000	0.000
Ti	0.003	0.003	0.001	0.007	0.008	0.002	0.007	0.004	0.003	0.004	0.004	0.009	0.010	0.001
Ca	0.218	0.217	0.211	0.216	0.215	0.205	0.217	0.225	0.215	0.217	0.210	0.219	0.225	0.215
Mg	0.036	0.040	0.038	0.035	0.034	0.037	0.038	0.046	0.042	0.043	0.044	0.045	0.042	0.044
Al	1.959	1.939	1.940	1.949	1.956	1.935	1.926	1.934	1.945	1.896	1.918	1.983	1.929	1.945
Mn	2.153	2.155	2.198	2.160	2.195	2.225	2.178	2.154	2.142	2.204	2.159	2.132	2.207	2.174
Fe	0.644	0.623	0.669	0.641	0.602	0.610	0.669	0.690	0.677	0.701	0.711	0.655	0.670	0.672
Cr	0.004	0.003	0.001	0.001	0.001	0.000	0.000	0.000	0.001	0.004	0.004	0.000	0.000	0.004
Zn	0.005	0.000	0.000	0.002	0.004	0.001	0.004	0.007	0.005	0.000	0.000	0.010	0.004	0.004
Total	8.019	8.003	8.043	8.015	8.014	8.024	8.035	8.045	8.027	8.057	8.042	8.026	8.056	8.042
Spessartine	71.63	71.8	72.88	71.89	73.06	73.97	72.32	71.47	71.22	72.94	71.59	70.92	73.1	72.13
Pyrope	1.21	0.00	1.25	1.16	1.13	1.24	1.27	1.52	1.39	1.42	1.45	1.48	1.40	1.44
Almandine	19.72	20.36	17.88	19.78	18.64	17.97	18.92	18.70	19.98	17.51	19.38	19.57	16.72	18.27
Grossular	4.80	4.76	2.93	4.41	4.60	3.25	2.62	3.06	3.85	0.60	1.83	5.41	2.10	3.36
Andradite	2.10	0.44	3.97	2.04	1.95	3.44	4.22	4.18	3.12	6.14	4.72	1.44	4.85	3.52

Cont. Table 2

Sample Wt. %	AD-10-020 C1 P1	AD-10-020 C1 P2	AD-10-020 C1 P6	AD-10-020 C1 P7	AD-10-020 C1 P9	AD-10-020 C2 P1	AD-10-020 C2 P2	AD-10-020 C2 P3	AD-10-020 C3 P1	AD-10-020 C3 P2	AD-10-020 C3 P3	AD-10-020 C3 P4	AD-10-020 C6 P1	AD-10-020 C6 P2
SiO_2	36.456	36.396	36.724	36.722	36.683	36.793	36.332	36.567	36.538	36.406	36.761	36.185	36.455	36.655
P_2O_5	0.000	0.000	0.000	0.000	0.000	0.000	0.000	0.000	0.000	0.000	0.000	0.000	0.000	0.000
TiO_2	0.174	0.110	0.058	0.030	0.060	0.074	0.102	0.110	0.056	0.122	0.114	0.038	0.146	0.146
CaO	2.082	2.016	2.244	2.016	1.949	2.063	2.032	2.101	2.155	1.919	1.985	1.909	2.072	2.024
MgO	0.409	0.422	0.336	0.350	0.376	0.332	0.390	0.388	0.339	0.363	0.356	0.350	0.402	0.343
Al_2O_3	19.803	20.274	20.187	20.246	20.191	20.660	20.373	20.553	19.847	20.381	20.173	20.684	20.451	20.098
MnO	30.942	31.217	31.833	31.218	31.232	31.897	31.361	30.970	32.163	32.109	31.935	32.909	30.895	31.824
FeO	9.150	8.493	9.012	8.988	8.690	8.765	8.851	8.549	8.727	8.275	8.431	7.876	9.169	8.129
Cr_2O_3	0.000	0.000	0.000	0.049	0.000	0.006	0.053	0.032	0.000	0.066	0.038	0.000	0.000	0.002
ZnO	0.000	0.153	0.000	0.071	0.010	0.000	0.000	0.000	0.025	0.130	0.148	0.025	0.076	0.054
Total	99.016	99.081	100.39	99.690	99.191	100.59	99.494	99.270	99.850	99.771	99.941	99.976	99.666	99.275
Apfu based on 12 oxygen atoms														
Si	3.019	3.007	3.005	3.017	3.025	2.998	2.994	3.008	3.011	2.994	3.016	2.973	2.996	3.022
P	0.000	0.000	0.000	0.000	0.000	0.000	0.000	0.000	0.000	0.000	0.000	0.000	0.000	0.000
Ti	0.011	0.007	0.004	0.002	0.004	0.005	0.006	0.007	0.004	0.008	0.007	0.002	0.009	0.009
Ca	0.185	0.179	0.197	0.178	0.172	0.180	0.179	0.185	0.190	0.169	0.175	0.168	0.183	0.179
Mg	0.050	0.052	0.041	0.043	0.046	0.040	0.048	0.048	0.042	0.045	0.044	0.043	0.049	0.042
Al	1.933	1.974	1.947	1.961	1.962	1.984	1.979	1.993	1.928	1.976	1.951	2.003	1.981	1.953
Mn	2.171	2.185	2.207	2.173	2.181	2.201	2.189	2.158	2.245	2.237	2.219	2.291	2.151	2.223
Fe	0.634	0.587	0.617	0.618	0.599	0.597	0.610	0.588	0.601	0.569	0.578	0.541	0.630	0.561
Cr	0.000	0.000	0.000	0.003	0.000	0.000	0.003	0.002	0.000	0.004	0.003	0.000	0.000	0.000
Zn	0.000	0.009	0.000	0.004	0.001	0.000	0.000	0.000	0.002	0.008	0.009	0.002	0.005	0.003
Total	8.003	7.999	8.018	7.999	7.990	8.006	8.009	7.988	8.022	8.009	8.001	8.023	8.004	7.992
Spessartine	72.33	72.91	73.39	72.48	72.8	73.32	72.89	72.03	74.64	74.55	74.05	76.14	71.7	74.19
Pyrope	0.00	1.55	1.36	0.00	1.45	1.34	1.60	1.59	0.94	1.48	0.00	1.43	1.64	1.13
Almandine	20.44	19.59	18.70	20.60	20.00	19.33	19.45	19.63	17.76	18.33	19.3	15.77	20.57	18.71
Grossular	3.85	4.79	3.64	5.03	3.98	4.91	4.43	6.08	2.80	4.09	4.28	4.82	4.98	3.76
Andradite	0.47	0.00	2.60	0.00	0.00	0.83	1.05	0.00	3.18	0.89	0.00	0.65	0.37	0.00

Cont. Table 2

Sample Wt. %	AD-10-020 C6 P4	AD-10-020 C10 P1	AD-10-020 C10 P2	AD-10-020 C10 P3	AD-10-020 C10 P4	AD-10-020 T1 L3	AD-10-020 T1 L5	AD-10-020 T1 L6	AD-10-020 T1 L9	AD-10-020 T1 L10	AD-10-020 T1 L11	AD-10-020 T1 L13	AD-10-020 T1 L14	AD-10-020 T1 L15
SiO_2	36.355	36.595	36.617	36.453	36.630	36.138	36.539	36.713	35.800	36.843	35.272	36.509	36.244	36.441
P_2O_5	0.000	0.000	0.000	0.000	0.000	0.000	0.000	0.000	0.000	0.000	0.000	0.000	0.000	0.000
TiO_2	0.114	0.104	0.062	0.132	0.090	0.110	0.064	0.056	0.070	0.028	0.000	0.088	0.146	0.076
CaO	2.105	2.140	2.126	2.021	2.056	2.030	2.067	2.030	1.978	2.170	2.035	2.223	2.116	1.993
MgO	0.376	0.370	0.389	0.459	0.349	0.343	0.460	0.350	0.432	0.385	0.377	0.402	0.362	0.303
Al_2O_3	20.185	20.186	20.221	20.085	20.287	20.354	20.463	20.206	19.591	20.420	19.737	20.200	20.250	20.554
MnO	31.655	32.177	31.495	30.868	31.731	32.108	31.550	31.581	30.933	32.179	30.308	31.205	32.256	32.048
FeO	8.506	8.319	8.695	9.446	8.348	8.479	8.691	8.554	10.280	7.585	11.595	8.692	8.156	8.259
Cr_2O_3	0.000	0.002	0.004	0.000	0.000	0.000	0.019	0.028	0.025	0.000	0.023	0.000	0.000	0.000
ZnO	0.076	0.010	0.000	0.037	0.101	0.000	0.057	0.064	0.020	0.000	0.017	0.131	0.000	0.012
Total	99.372	99.903	99.609	99.501	99.592	99.562	99.910	99.582	99.129	99.610	99.364	99.450	99.530	99.686
Apfu based on 12 oxygen atoms														
Si	3.001	3.006	3.012	3.006	3.012	2.983	2.997	3.019	2.984	3.021	2.948	3.008	2.990	2.995
P	0.000	0.000	0.000	0.000	0.000	0.000	0.000	0.000	0.000	0.000	0.000	0.000	0.000	0.000
Ti	0.007	0.006	0.004	0.008	0.006	0.007	0.004	0.004	0.004	0.002	0.000	0.006	0.009	0.005
Ca	0.186	0.188	0.187	0.179	0.181	0.180	0.182	0.179	0.177	0.191	0.182	0.196	0.187	0.176
Mg	0.046	0.045	0.048	0.056	0.043	0.042	0.056	0.043	0.054	0.047	0.047	0.049	0.045	0.037
Al	1.964	1.954	1.961	1.952	1.967	1.980	1.978	1.959	1.925	1.974	1.944	1.962	1.969	1.991
Mn	2.213	2.239	2.194	2.156	2.210	2.245	2.192	2.200	2.184	2.235	2.145	2.178	2.254	2.231
Fe	0.587	0.571	0.598	0.651	0.574	0.585	0.596	0.588	0.717	0.520	0.810	0.599	0.563	0.568
Cr	0.000	0.000	0.000	0.000	0.000	0.000	0.001	0.002	0.002	0.000	0.002	0.000	0.000	0.000
Zn	0.005	0.001	0.000	0.002	0.006	0.000	0.003	0.004	0.001	0.000	0.001	0.008	0.000	0.001
Total	8.010	8.011	8.004	8.010	7.999	8.021	8.010	7.997	8.048	7.990	8.079	8.006	8.016	8.004
Spessartine	73.73	74.52	73.11	71.79	73.74	74.62	73.01	73.39	72.38	74.6	70.82	72.61	74.98	74.35
Pyrope	1.54	1.24	0.19	1.51	0.50	1.40	1.87	0.10	1.78	1.57	1.55	0.44	1.48	1.24
Almandine	18.53	17.76	19.41	20.48	19.16	17.39	19.02	19.63	19.03	17.36	18.92	19.5	17.09	18.53
Grossular	4.29	4.05	5.26	3.72	5.01	4.06	4.66	4.89	0.85	5.27	0.93	5.56	3.90	5.12
Andradite	1.24	1.57	0.58	1.41	0.00	1.57	1.13	0.00	4.71	0.000	5.01	0.44	1.87	0.49

Cont. Table 2

Sample Wt. %	AD-10-020 T1 L20	AD-10-020 T1 L36	AD-10-020 T1 L41	AD-10-020 T1 L43	AD-10-020 T1 L44	AD-10-020 T1 L48	AD-10-020 T1 L50	AD-10-020 T1 L53	AD-10-020 T1 L60	AD-10-020 T1 L72	AD-10-020 T1 L78	AD-10-020 T1 L82	AD-10-020 T1 L83	AD-10-020 T1 L84
SiO_2	36.742	36.580	36.594	36.586	36.516	36.421	36.625	36.658	36.659	36.359	36.833	36.497	36.302	36.506
P_2O_5	0.000	0.000	0.000	0.000	0.000	0.000	0.000	0.000	0.000	0.000	0.000	0.000	0.000	0.000
TiO_2	0.056	0.118	0.062	0.088	0.110	0.086	0.000	0.064	0.080	0.060	0.100	0.048	0.156	0.076
CaO	2.118	1.934	2.109	2.036	2.227	2.157	2.218	2.121	2.176	2.155	2.074	2.226	2.084	2.079
MgO	0.297	0.346	0.346	0.413	0.402	0.317	0.386	0.372	0.443	0.430	0.353	0.422	0.500	0.367
Al_2O_3	20.133	20.178	20.238	20.333	20.419	19.890	20.493	20.107	20.313	20.192	20.280	20.178	20.407	20.397
MnO	32.024	31.650	32.221	31.404	31.594	31.219	30.756	31.839	30.845	31.869	31.141	32.614	30.293	31.421
FeO	8.322	8.798	8.276	9.058	7.940	9.172	9.111	8.245	9.057	8.227	8.593	7.640	9.532	8.266
Cr_2O_3	0.000	0.000	0.000	0.000	0.023	0.000	0.023	0.025	0.000	0.034	0.000	0.000	0.000	0.008
ZnO	0.035	0.000	0.000	0.000	0.000	0.010	0.000	0.099	0.000	0.069	0.108	0.000	0.012	0.106
Total	99.727	99.604	99.846	99.918	99.231	99.272	99.612	99.530	99.573	99.395	99.482	99.625	99.286	99.226
Apfu based on 12 oxygen atoms														
Si	3.020	3.011	3.007	3.002	3.007	3.013	3.008	3.018	3.012	3.000	3.026	3.004	2.993	3.009
P	0.000	0.000	0.000	0.000	0.000	0.000	0.000	0.000	0.000	0.000	0.000	0.000	0.000	0.000
Ti	0.004	0.007	0.004	0.005	0.007	0.005	0.000	0.004	0.005	0.004	0.006	0.003	0.010	0.005
Ca	0.187	0.171	0.186	0.179	0.197	0.191	0.195	0.187	0.192	0.191	0.183	0.196	0.184	0.184
Mg	0.036	0.043	0.042	0.051	0.049	0.039	0.047	0.046	0.054	0.053	0.043	0.052	0.061	0.045
Al	1.951	1.958	1.960	1.967	1.982	1.940	1.984	1.951	1.967	1.964	1.964	1.958	1.983	1.982
Mn	2.230	2.207	2.243	2.183	2.204	2.188	2.139	2.220	2.147	2.228	2.167	2.274	2.116	2.194
Fe	0.572	0.606	0.569	0.622	0.547	0.635	0.626	0.568	0.622	0.568	0.590	0.526	0.657	0.570
Cr	0.000	0.000	0.000	0.000	0.002	0.000	0.002	0.002	0.000	0.002	0.000	0.000	0.000	0.001
Zn	0.002	0.000	0.000	0.000	0.000	0.001	0.000	0.006	0.000	0.004	0.007	0.000	0.001	0.007
Total	8.001	8.002	8.009	8.009	7.994	8.012	8.000	8.002	7.999	8.013	7.986	8.014	8.005	7.995
Spessartine	74.33	73.54	74.66	72.68	73.52	72.83	71.31	74.05	71.56	74.17	72.42	75.68	70.48	73.23
Pyrope	0.00	0.00	0.99	1.68	1.65	0.07	0.59	0.00	0.36	1.76	1.44	1.72	2.05	1.51
Almandine	18.92	19.71	17.86	19.67	18.24	19.82	20.86	18.85	20.66	17.73	19.73	16.07	21.34	19.02
Grossular	4.28	4.61	4.37	4.15	5.76	4.13	6.42	4.71	5.78	4.28	4.84	4.23	4.81	5.46
Andradite	0.05	0.35	1.43	1.31	0.00	1.70	0.00	0.00	0.00	1.73	0.00	2.03	0.78	0.00

Cont. Table 2

Sample Wt. %	AD-10-020 T1 L92	AD-10-020 T1 L93	AD-10-020 T1 L96	AD-10-020 T1 L97	AD-10-020 T1 L99	AD-10-020 T1 L107	AD-10-020 T1 L108	AD-10-021 C1 P2	AD-10-021 C1 P3	AD-10-021 C1 P4	AD-10-021 C3 P1	AD-10-021 C3 P2	AD-10-021 C3 P3	AD-10-021 C3 P4
SiO_2	36.900	36.550	36.522	36.450	36.762	36.573	36.135	36.493	36.399	36.431	36.762	36.849	36.438	36.649
P_2O_5	0.000	0.000	0.000	0.000	0.000	0.000	0.000	0.000	0.000	0.000	0.000	0.000	0.000	0.000
TiO_2	0.116	0.084	0.132	0.014	0.104	0.104	0.080	0.094	0.057	0.000	0.108	0.049	0.108	0.073
CaO	2.055	2.057	1.873	2.082	2.049	2.046	2.008	4.486	4.579	4.475	4.296	4.389	4.342	4.506
MgO	0.379	0.378	0.385	0.442	0.390	0.343	0.391	0.783	0.759	0.577	0.732	0.752	0.503	0.546
Al_2O_3	20.067	20.007	20.254	20.633	20.837	20.356	19.999	19.897	20.160	19.872	20.057	19.862	20.177	19.935
MnO	32.428	31.187	32.399	32.400	31.522	31.264	31.996	25.713	25.592	26.880	26.869	25.643	26.588	25.656
FeO	8.220	8.848	8.079	7.858	8.373	8.443	8.248	11.962	11.674	11.611	11.391	11.760	10.892	11.774
Cr_2O_3	0.000	0.000	0.019	0.000	0.000	0.000	0.000	0.019	0.013	0.046	0.057	0.036	0.015	0.000
ZnO	0.000	0.084	0.113	0.059	0.133	0.005	0.143	0.047	0.062	0.035	0.074	0.000	0.000	0.117
Total	100.165	99.195	99.776	99.938	100.17	99.134	99.000	99.494	99.295	99.927	100.35	99.340	99.063	99.256
Apfu based on 12 oxygen atoms														
Si	3.021	3.020	3.003	2.989	2.999	3.015	2.999	2.997	2.990	2.990	2.996	3.022	3.000	3.013
P	0.000	0.000	0.000	0.000	0.000	0.000	0.000	0.000	0.000	0.000	0.000	0.000	0.000	0.000
Ti	0.007	0.005	0.008	0.001	0.006	0.007	0.005	0.006	0.004	0.000	0.007	0.003	0.007	0.005
Ca	0.180	0.182	0.165	0.183	0.179	0.181	0.179	0.395	0.403	0.394	0.375	0.386	0.383	0.397
Mg	0.046	0.047	0.047	0.054	0.048	0.042	0.048	0.096	0.093	0.071	0.089	0.092	0.062	0.067
Al	1.937	1.948	1.963	1.994	2.004	1.978	1.956	1.926	1.952	1.922	1.927	1.920	1.958	1.932
Mn	2.249	2.183	2.257	2.250	2.178	2.184	2.249	1.789	1.781	1.869	1.855	1.782	1.854	1.787
Fe	0.563	0.611	0.556	0.539	0.571	0.582	0.573	0.822	0.802	0.797	0.776	0.807	0.750	0.810
Cr	0.000	0.000	0.001	0.000	0.000	0.000	0.000	0.001	0.001	0.003	0.004	0.002	0.001	0.000
Zn	0.000	0.005	0.007	0.004	0.008	0.000	0.009	0.003	0.004	0.002	0.005	0.000	0.000	0.007
Total	8.003	8.001	8.007	8.013	7.993	7.989	8.018	8.034	8.030	8.047	8.032	8.013	8.014	8.017
Spessartine	74.93	72.79	75.22	74.92	72.74	72.88	74.89	59.39	59.17	61.94	61.61	59.28	61.69	59.48
Pyrope	0.00	0.00	1.14	1.80	1.58	1.41	1.61	3.18	3.09	2.34	2.95	0.76	2.05	0.94
Almandine	18.19	20.3	17.81	16.73	19.08	19.43	17.55	24.03	23.82	21.79	22.72	25.4	23.51	25.39
Grossular	3.66	4.37	3.97	5.39	5.98	5.32	3.43	8.60	10.24	8.17	7.99	10.4	10.19	10.65
Andradite	0.49	0.00	0.65	0.65	0.00	0.00	2.23	4.16	2.93	4.72	3.96	2.02	2.10	2.12

Cont. Table 2

Sample Wt. %	AD-10-021 C5 P2	AD-10-021 C5 P3	AD-10-021 C5 P4	AD-10-021 C7 P3	AD-10-021 C7 P4	AD-10-021 C8 P1	AD-10-021 C8 P2	AD-10-021 C8 P3	AD-10-021 C8 P4
SiO_2	36.209	36.454	36.495	36.723	36.310	36.544	36.580	36.828	36.418
P_2O_5	0.000	0.000	0.000	0.000	0.000	0.000	0.000	0.000	0.000
TiO_2	0.053	0.061	0.045	0.018	0.000	0.028	0.026	0.000	0.012
CaO	4.178	4.108	4.172	4.204	4.346	4.241	4.313	4.380	4.277
MgO	0.525	0.536	0.590	0.769	0.645	0.596	0.795	0.689	0.764
Al_2O_3	19.869	19.894	19.899	20.221	20.146	19.784	20.056	19.885	19.997
MnO	27.148	26.283	26.550	26.635	26.418	26.248	25.834	26.123	26.337
FeO	11.130	11.795	11.831	11.922	11.876	12.341	11.643	11.611	11.775
Cr_2O_3	0.000	0.050	0.006	0.000	0.019	0.044	0.061	0.021	0.000
ZnO	0.010	0.121	0.000	0.134	0.000	0.000	0.000	0.000	0.000
Total	99.122	99.302	99.588	100.626	99.760	99.826	99.308	99.537	99.580
Apfu based on 12 oxygen atoms									
Si	2.993	3.003	3.000	2.988	2.981	3.001	3.003	3.019	2.992
P	0.000	0.000	0.000	0.000	0.000	0.000	0.000	0.000	0.000
Ti	0.003	0.004	0.003	0.001	0.000	0.002	0.002	0.000	0.001
Ca	0.370	0.363	0.368	0.367	0.382	0.373	0.380	0.385	0.376
Mg	0.065	0.066	0.072	0.093	0.079	0.073	0.097	0.084	0.094
Al	1.936	1.932	1.928	1.939	1.949	1.915	1.941	1.921	1.936
Mn	1.901	1.834	1.849	1.835	1.837	1.826	1.797	1.814	1.833
Fe	0.769	0.813	0.813	0.811	0.815	0.847	0.800	0.796	0.809
Cr	0.000	0.003	0.000	0.000	0.001	0.003	0.004	0.001	0.000
Zn	0.001	0.007	0.000	0.008	0.000	0.000	0.000	0.000	0.000
Total	8.036	8.025	8.033	8.042	8.044	8.039	8.023	8.020	8.040
Spessartine	63.07	61.00	61.37	60.92	60.89	60.56	59.72	60.31	60.78
Pyrope	2.15	2.19	2.40	3.10	2.62	2.42	3.23	1.28	3.10
Almandine	21.93	24.74	23.72	23.02	22.63	24.24	24.32	24.48	22.88
Grossular	8.16	8.28	7.90	8.25	8.99	7.35	9.24	9.74	8.40
Andradite	3.95	3.40	4.14	3.86	3.62	4.79	3.09	2.98	4.05

Cont. Table 2

Sample	GA1-C1	GA1-C1	GA1-C1	GA1-C1	GA1-C1	GA1-C1	GA1-C1	GA1-C2	GA1-C2	GA1-C2	GA1-C2	GA1-C2	GA1-C2
Wt. %	T1 L1	T1 L2	T1 L4	T1 L5	T1 L6	T1 L8	T1 L9	T1 L1	T1 L2	T1 L3	T1 L4	T1 L5	T1 L7
MgO	2.395	2.426	2.329	2.304	2.254	2.420	2.466	2.376	2.385	2.276	2.325	2.358	2.336
F	0.000	0.000	0.000	0.000	0.000	0.000	0.000	0.000	0.000	0.000	0.000	0.000	0.000
FeO	28.057	28.126	28.056	28.286	28.114	28.389	28.177	28.035	28.536	28.098	27.700	27.811	28.252
TiO_2	0.000	0.067	0.078	0.039	0.072	0.011	0.017	0.000	0.000	0.000	0.000	0.000	0.056
K_2O	0.000	0.004	0.000	0.010	0.000	0.015	0.000	0.000	0.000	0.000	0.000	0.000	0.000
Al_2O_3	21.696	21.600	21.436	21.437	21.388	21.741	21.491	21.584	21.399	21.285	21.403	21.218	21.488
ZnO	0.013	0.040	0.058	0.000	0.027	0.016	0.040	0.032	0.066	0.000	0.041	0.069	0.034
MnO	8.913	9.250	9.075	8.801	8.787	9.132	9.083	8.866	9.318	9.144	8.828	9.224	8.898
CaO	2.237	2.399	2.562	2.586	2.638	2.423	2.377	2.525	2.500	2.620	2.549	2.570	2.502
SiO_2	36.667	36.473	36.927	36.993	36.430	36.481	36.204	36.525	35.892	36.785	36.406	36.236	36.394
Cr_2O_3	0.000	0.011	0.000	0.015	0.000	0.049	0.040	0.000	0.011	0.032	0.000	0.094	0.094
P_2O_5	0.024	0.005	0.009	0.000	0.014	0.014	0.001	0.013	0.002	0.000	0.006	0.007	0.000
Total	100.002	100.401	100.530	100.471	99.724	100.691	99.896	99.956	100.109	100.240	99.258	99.587	100.054
Apfu based on 24 oxygen atoms													
Mg	0.576	0.583	0.558	0.552	0.545	0.580	0.596	0.572	0.578	0.548	0.564	0.572	0.563
F	0.000	0.000	0.000	0.000	0.000	0.000	0.000	0.000	0.000	0.000	0.000	0.000	0.000
Fe	3.786	3.793	3.772	3.803	3.813	3.819	3.822	3.790	3.879	3.793	3.768	3.784	3.823
Ti	0.000	0.008	0.009	0.005	0.009	0.001	0.002	0.000	0.000	0.000	0.000	0.000	0.007
K	0.000	0.001	0.000	0.002	0.000	0.003	0.000	0.000	0.000	0.000	0.000	0.000	0.000
Al	4.127	4.105	4.062	4.062	4.089	4.122	4.108	4.113	4.099	4.050	4.104	4.069	4.098
Zn	0.002	0.005	0.007	0.000	0.003	0.002	0.005	0.004	0.008	0.000	0.005	0.008	0.004
Mn	1.218	1.263	1.236	1.199	1.207	1.244	1.248	1.214	1.283	1.250	1.216	1.271	1.220
Ca	0.387	0.415	0.441	0.446	0.459	0.418	0.413	0.437	0.435	0.453	0.444	0.448	0.434
Si	5.917	5.881	5.936	5.947	5.909	5.868	5.871	5.904	5.833	5.938	5.922	5.896	5.889
Cr	0.000	0.001	0.000	0.002	0.000	0.006	0.005	0.000	0.001	0.004	0.000	0.012	0.012
P	0.003	0.001	0.001	0.000	0.002	0.002	0.000	0.002	0.000	0.000	0.001	0.001	0.000
Total	16.015	16.057	16.022	16.017	16.035	16.065	16.070	16.037	16.116	16.036	16.025	16.062	16.049
Spessartine	20.29	20.99	20.58	19.96	20.08	20.66	20.71	20.19	21.23	20.79	20.25	21.12	20.27
Pyrope	9.60	9.69	9.29	9.19	9.07	9.64	9.90	9.52	9.57	9.11	9.39	9.50	9.36
Almandine	62.22	60.29	61.79	62.54	61.67	60.24	60.03	61.23	58.56	61.31	61.56	59.88	61.14
Grossular	6.44	6.65	7.11	7.25	7.41	6.75	6.68	7.28	7.17	7.43	7.40	7.14	6.74
Andradite	0.00	0.00	0.00	0.00	0.00	0.00	0.00	0.00	0.00	0.00	0.00	0.00	0.00

Sample Wt. %	GA1-C2 T1 L8	GA1-C2 T1 L9	GA1-C2 T1 L10	GA1-C3 T1 L2	GA1-C3 T1 L3	GA1-C3 T1 L4	GA1-C3 T1 L5	GA1-C3 T1 L6	GA1-C3 T1 L8	GA1-C3 T1 L10	GA1-C4 T1 L1	GA1-C4 T1 L2	GA1-C4 T1 L3
MgO	2.282	2.238	2.335	2.580	2.457	2.253	2.375	2.406	2.460	2.355	2.360	2.375	2.378
F	0.000	0.000	0.000	0.000	0.000	0.000	0.000	0.000	0.000	0.000	0.000	0.000	0.000
FeO	27.975	28.011	27.873	27.872	27.489	28.184	27.621	27.883	28.537	27.256	28.083	27.849	28.225
TiO_2	0.000	0.045	0.145	0.084	0.033	0.022	0.033	0.000	0.028	0.034	0.034	0.000	0.000
K_2O	0.000	0.006	0.001	0.000	0.004	0.008	0.000	0.010	0.009	0.002	0.000	0.003	0.000
Al_2O_3	21.376	21.209	21.664	21.478	21.291	21.087	21.103	21.438	21.206	21.585	21.762	21.380	21.265
ZnO	0.000	0.000	0.000	0.040	0.000	0.042	0.056	0.045	0.102	0.076	0.074	0.000	0.088
MnO	9.415	8.847	8.733	8.936	9.115	9.312	9.363	9.258	9.139	9.083	8.712	9.391	9.263
CaO	2.483	2.517	2.501	2.424	2.464	2.636	2.521	2.382	2.277	2.470	2.502	2.407	2.504
SiO_2	36.106	36.379	36.504	36.557	36.263	36.074	36.115	36.207	35.897	36.675	37.266	36.515	36.661
Cr_2O_3	0.000	0.060	0.000	0.000	0.011	0.000	0.000	0.000	0.040	0.006	0.006	0.000	0.000
P_2O_5	0.014	0.000	0.000	0.000	0.004	0.009	0.000	0.030	0.000	0.000	0.011	0.013	0.009
Total	99.651	99.312	99.756	99.971	99.131	99.627	99.187	99.659	99.695	99.542	100.810	99.933	100.393
Apfu based on 24 oxygen atoms													
Mg	0.554	0.544	0.563	0.621	0.597	0.548	0.578	0.583	0.598	0.568	0.562	0.573	0.572
F	0.000	0.000	0.000	0.000	0.000	0.000	0.000	0.000	0.000	0.000	0.000	0.000	0.000
Fe	3.808	3.816	3.770	3.766	3.747	3.844	3.774	3.789	3.892	3.690	3.753	3.771	3.810
Ti	0.000	0.006	0.018	0.010	0.004	0.003	0.004	0.000	0.003	0.004	0.004	0.000	0.000
K	0.000	0.001	0.000	0.000	0.001	0.002	0.000	0.002	0.002	0.000	0.000	0.001	0.000
Al	4.101	4.072	4.130	4.090	4.090	4.054	4.064	4.105	4.076	4.118	4.098	4.080	4.046
Zn	0.000	0.000	0.000	0.005	0.000	0.005	0.007	0.005	0.012	0.009	0.009	0.000	0.011
Mn	1.298	1.221	1.196	1.223	1.258	1.286	1.296	1.274	1.262	1.245	1.179	1.288	1.267
Ca	0.433	0.439	0.433	0.420	0.430	0.461	0.441	0.415	0.398	0.428	0.428	0.418	0.433
Si	5.876	5.925	5.904	5.906	5.910	5.883	5.900	5.883	5.854	5.936	5.954	5.912	5.918
Cr	0.000	0.008	0.000	0.000	0.001	0.000	0.000	0.000	0.005	0.001	0.001	0.000	0.000
P	0.002	0.000	0.000	0.000	0.001	0.001	0.000	0.004	0.000	0.000	0.002	0.002	0.001
Total	16.071	16.030	16.014	16.040	16.040	16.087	16.064	16.060	16.103	16.000	15.990	16.045	16.058
Spessartine	21.54	20.31	19.92	20.33	20.92	21.33	21.52	21.17	20.92	20.77	19.68	21.41	21.05
Pyrope	9.19	9.04	9.37	10.33	9.93	9.09	9.61	9.68	9.91	9.48	9.38	9.53	9.51
Almandine	59.61	62.02	62.09	60.74	60.34	59.56	59.60	60.01	59.66	61.53	62.62	60.40	60.60
Grossular	7.19	6.98	6.78	6.72	7.02	7.22	7.23	6.89	6.38	7.02	7.03	6.94	7.20
Andradite	0.00	0.00	0.00	0.00	0.00	0.35	0.00	0.00	0.00	0.00	0.00	0.00	0.00

Cont. Table 2

Sample Wt. %	GA1-C4 T1 L4	GA1-C4 T1 L6	GA1-C4 T1 L9	GA1-C4 T1 L10	GA3 C1 T1 L1	GA3 C1 T1 L3	GA3 C1 T1 L4	GA3 C1 T1 L6	GA3 C1 T1 L7	GA3 C1 T1 L8	GA3 C1 T1 L9	GA3 C1 T1 L10	GA3 C1 T1 L11
MgO	2.232	2.314	2.473	2.353	1.262	1.627	1.582	1.527	1.598	1.622	1.662	1.653	1.602
F	0.000	0.000	0.000	0.000	0.000	0.000	0.000	0.000	0.000	0.000	0.000	0.000	0.000
FeO	27.485	28.614	28.283	28.182	25.368	24.969	25.481	25.444	25.608	24.842	24.949	25.582	25.740
TiO_2	0.045	0.017	0.045	0.017	0.586	0.000	0.006	0.090	0.034	0.056	0.017	0.006	0.011
K_2O	0.003	0.000	0.000	0.002	0.000	0.002	0.000	0.006	0.005	0.002	0.005	0.002	0.001
Al_2O_3	21.005	21.148	21.252	21.377	21.127	21.769	21.658	21.335	21.325	21.303	21.452	21.397	21.706
ZnO	0.056	0.000	0.007	0.062	0.000	0.062	0.064	0.007	0.023	0.022	0.000	0.000	0.019
MnO	8.950	8.815	8.779	9.213	8.217	8.175	8.041	7.980	8.201	8.416	8.012	8.216	8.048
CaO	2.411	2.455	2.456	2.348	7.078	6.773	6.751	6.736	6.794	6.782	6.769	6.690	6.840
SiO_2	37.930	36.985	35.981	36.242	36.261	37.294	36.936	37.144	37.111	36.318	36.259	36.150	36.838
Cr_2O_3	0.000	0.030	0.000	0.006	0.004	0.013	0.000	0.000	0.017	0.000	0.000	0.000	0.026
P_2O_5	0.007	0.016	0.002	0.001	0.004	0.002	0.018	0.000	0.001	0.008	0.008	0.007	0.000
Total	100.124	100.394	99.278	99.803	99.907	100.686	100.537	100.269	100.717	99.371	99.133	99.703	100.831
Apfu based on 24 oxygen atoms													
Mg	0.534	0.556	0.602	0.570	0.304	0.386	0.378	0.365	0.381	0.392	0.402	0.399	0.382
F	0.000	0.000	0.000	0.000	0.000	0.000	0.000	0.000	0.000	0.000	0.000	0.000	0.000
Fe	3.688	3.856	3.861	3.828	3.431	3.327	3.410	3.412	3.426	3.369	3.386	3.466	3.440
Ti	0.005	0.002	0.006	0.002	0.071	0.000	0.001	0.011	0.004	0.007	0.002	0.001	0.001
K	0.001	0.000	0.000	0.000	0.000	0.000	0.000	0.001	0.001	0.000	0.001	0.000	0.000
Al	3.972	4.017	4.089	4.093	4.027	4.088	4.085	4.032	4.021	4.072	4.104	4.086	4.089
Zn	0.007	0.000	0.001	0.008	0.000	0.007	0.008	0.001	0.003	0.003	0.000	0.000	0.002
Mn	1.216	1.203	1.214	1.268	1.126	1.103	1.090	1.084	1.111	1.156	1.102	1.128	1.090
Ca	0.414	0.424	0.430	0.409	1.226	1.156	1.158	1.157	1.164	1.178	1.177	1.161	1.171
Si	6.085	5.960	5.874	5.887	5.864	5.942	5.911	5.956	5.936	5.889	5.885	5.857	5.887
Cr	0.000	0.004	0.000	0.001	0.001	0.002	0.000	0.000	0.002	0.000	0.000	0.000	0.003
P	0.001	0.002	0.000	0.000	0.001	0.000	0.003	0.000	0.000	0.001	0.001	0.001	0.000
Total	15.923	16.024	16.076	16.065	16.051	16.013	16.042	16.018	16.049	16.067	16.060	16.099	16.066
Spessartine	20.38	20.03	20.14	21.05	18.70	18.38	18.13	18.04	18.47	19.19	18.29	18.68	18.09
Pyrope	8.94	9.25	9.98	9.46	5.06	6.44	6.28	6.08	6.33	6.51	6.68	6.61	6.34
Almandine	61.79	62.90	60.29	60.50	54.48	54.92	54.67	55.95	54.58	52.62	53.25	52.51	53.89
Grossular	6.94	6.90	6.99	6.72	18.26	19.22	19.24	19.00	18.84	19.39	19.50	19.22	19.33
Andradite	0.00	0.01	0.00	0.00	0.00	0.00	0.00	0.00	0.00	0.00	0.00	0.00	0.00

Cont. Table 2

Sample	GA3 C1	GA3 C1	GA3 C2	GA3 C2	GA3 C2	GA3 C2	GA3 C2	GA3 C2	GA3 C2	GA3 C2	GA3 C2	GA3 C2	GA3 C3
Wt. %	T1 L12	T1 L13	T1 L2	T1 L3	T1 L4	T1 L6	T1 L7	T1 L8	T1 L9	T1 L12	T1 L13	T1 L14	T1 L3
MgO	1.716	1.730	1.523	1.642	1.589	1.650	1.625	1.670	1.742	1.653	1.606	1.612	1.570
F	0.000	0.000	0.000	0.000	0.000	0.000	0.000	0.000	0.000	0.000	0.000	0.000	0.000
FeO	24.904	25.774	25.333	25.241	25.322	25.316	25.419	25.188	24.886	25.379	25.455	25.514	25.328
TiO_2	0.000	0.006	0.084	0.067	0.101	0.084	0.101	0.034	0.023	0.023	0.090	0.023	0.028
K_2O	0.002	0.004	0.000	0.005	0.000	0.001	0.004	0.003	0.012	0.000	0.005	0.010	0.000
Al_2O_3	21.637	21.619	21.854	21.497	21.461	21.615	21.745	21.687	21.840	21.532	21.469	21.634	21.154
ZnO	0.066	0.048	0.132	0.066	0.018	0.000	0.006	0.000	0.016	0.000	0.000	0.035	0.071
MnO	8.156	8.079	8.108	8.038	7.635	8.183	8.242	7.918	7.739	7.969	8.126	8.099	7.888
CaO	6.591	6.472	6.669	6.737	7.054	6.929	6.737	6.723	6.789	7.070	6.761	6.624	6.808
SiO_2	36.788	37.130	37.273	36.890	37.080	37.063	36.779	37.132	37.518	36.909	36.428	37.431	36.611
Cr_2O_3	0.000	0.028	0.000	0.000	0.019	0.000	0.004	0.000	0.000	0.028	0.000	0.000	0.060
P_2O_5	0.004	0.000	0.012	0.000	0.005	0.000	0.028	0.021	0.000	0.000	0.000	0.016	0.007
Total	99.864	100.890	100.988	100.183	100.284	100.841	100.690	100.376	100.565	100.563	99.940	100.998	99.525
Apfu based on 24 oxygen atoms													
Mg	0.411	0.411	0.361	0.393	0.379	0.392	0.387	0.398	0.413	0.394	0.386	0.382	0.379
F	0.000	0.000	0.000	0.000	0.000	0.000	0.000	0.000	0.000	0.000	0.000	0.000	0.000
Fe	3.349	3.438	3.370	3.388	3.391	3.377	3.399	3.367	3.309	3.397	3.435	3.394	3.428
Ti	0.000	0.001	0.010	0.008	0.012	0.010	0.012	0.004	0.003	0.003	0.011	0.003	0.003
K	0.000	0.001	0.000	0.001	0.000	0.000	0.001	0.001	0.003	0.000	0.001	0.002	0.000
Al	4.101	4.064	4.097	4.067	4.051	4.064	4.098	4.085	4.093	4.062	4.083	4.056	4.035
Zn	0.008	0.006	0.016	0.008	0.002	0.000	0.001	0.000	0.002	0.000	0.000	0.004	0.009
Mn	1.111	1.092	1.092	1.093	1.036	1.106	1.116	1.072	1.042	1.080	1.110	1.091	1.081
Ca	1.136	1.106	1.137	1.159	1.210	1.184	1.154	1.151	1.157	1.212	1.169	1.129	1.181
Si	5.916	5.922	5.928	5.921	5.938	5.912	5.880	5.934	5.965	5.907	5.877	5.953	5.925
Cr	0.000	0.004	0.000	0.000	0.003	0.000	0.001	0.000	0.000	0.004	0.000	0.000	0.008
P	0.001	0.000	0.002	0.000	0.001	0.000	0.004	0.003	0.000	0.000	0.000	0.002	0.001
Total	16.033	16.044	16.011	16.038	16.022	16.046	16.053	16.015	15.987	16.058	16.072	16.015	16.049
Spessartine	18.49	18.15	18.21	18.18	17.24	18.37	18.55	17.85	17.39	17.94	18.43	18.18	17.98
Pyrope	6.85	6.84	6.02	6.54	6.31	6.52	6.44	6.63	6.89	6.55	6.41	6.37	6.30
Almandine	54.22	55.11	55.83	54.65	55.35	53.85	53.76	55.25	55.22	53.52	53.48	55.88	54.66
Grossular	18.90	18.29	18.70	19.07	19.78	19.43	18.86	19.07	19.23	19.97	19.12	18.74	19.35
Andradite	0.00	0.00	0.00	0.00	0.00	0.00	0.00	0.00	0.00	0.00	0.00	0.00	0.00

Cont. Table 2

Sample	GA3 C3	GA3 C3	GA3 C3	GA3 C3	GA3 C3	GA3 C7	GA3 C7	GA3 C7	GA3 C7	GA3 C7	GA3 C7	GA3 C7	GA3 C7
Wt. %	T1 L5	T1 L8	T1 L11	T1 L14	T1 L15	T1 L1	T1 L2	T1 L4	T1 L7	T1 L8	T1 L9	T1 L10	T1 L12
MgO	1.667	1.323	1.640	1.466	1.315	1.714	1.655	1.663	1.742	1.703	1.670	1.617	1.639
F	0.000	0.000	0.000	0.000	0.000	0.000	0.000	0.000	0.000	0.000	0.000	0.000	0.000
FeO	25.270	25.743	25.494	25.463	25.529	24.679	25.374	25.159	25.179	25.106	25.275	24.698	25.573
TiO_2	0.000	0.000	0.000	0.096	0.096	0.000	0.000	0.039	0.006	0.028	0.000	0.006	0.073
K_2O	0.004	0.000	0.009	0.000	0.002	0.000	0.013	0.000	0.000	0.000	0.001	0.000	0.000
Al_2O_3	21.823	21.558	21.774	21.446	21.747	21.883	21.658	21.769	21.392	21.631	21.719	21.410	21.612
ZnO	0.052	0.000	0.000	0.000	0.044	0.000	0.097	0.070	0.061	0.052	0.080	0.046	0.003
MnO	7.819	7.981	8.037	8.318	8.206	8.040	8.077	8.138	8.102	7.722	8.355	8.102	7.942
CaO	6.735	6.595	6.664	6.873	6.833	6.806	6.907	6.597	6.711	6.874	6.727	6.756	6.777
SiO_2	37.509	36.604	36.739	36.592	36.918	37.509	36.931	36.828	36.709	36.883	37.043	36.925	36.898
Cr_2O_3	0.011	0.000	0.000	0.026	0.000	0.011	0.000	0.013	0.056	0.000	0.000	0.000	0.000
P_2O_5	0.009	0.012	0.014	0.002	0.016	0.016	0.017	0.018	0.002	0.011	0.000	0.007	0.000
Total	100.899	99.816	100.371	100.282	100.706	100.658	100.729	100.294	99.960	100.010	100.870	99.567	100.517
Apfu based on 24 oxygen atoms													
Mg	0.395	0.318	0.392	0.352	0.314	0.406	0.394	0.397	0.418	0.407	0.397	0.388	0.391
F	0.000	0.000	0.000	0.000	0.000	0.000	0.000	0.000	0.000	0.000	0.000	0.000	0.000
Fe	3.356	3.475	3.418	3.426	3.414	3.279	3.391	3.371	3.390	3.369	3.372	3.329	3.423
Ti	0.000	0.000	0.000	0.012	0.012	0.000	0.000	0.005	0.001	0.003	0.000	0.001	0.009
K	0.001	0.000	0.002	0.000	0.000	0.000	0.003	0.000	0.000	0.000	0.000	0.000	0.000
Al	4.085	4.102	4.114	4.067	4.099	4.098	4.079	4.111	4.060	4.092	4.084	4.067	4.078
Zn	0.006	0.000	0.000	0.000	0.005	0.000	0.012	0.008	0.007	0.006	0.010	0.005	0.000
Mn	1.052	1.091	1.091	1.134	1.112	1.082	1.093	1.104	1.105	1.050	1.129	1.106	1.077
Ca	1.146	1.141	1.145	1.185	1.171	1.159	1.183	1.133	1.158	1.182	1.150	1.167	1.162
Si	5.957	5.909	5.889	5.887	5.904	5.960	5.901	5.901	5.910	5.919	5.909	5.951	5.906
Cr	0.001	0.000	0.000	0.003	0.000	0.001	0.000	0.002	0.007	0.000	0.000	0.000	0.000
P	0.001	0.002	0.002	0.000	0.002	0.002	0.002	0.002	0.000	0.002	0.000	0.001	0.000
Total	15.999	16.038	16.052	16.066	16.032	15.988	16.057	16.034	16.056	16.030	16.050	16.014	16.046
Spessartine	17.54	18.15	18.13	18.82	18.50	18.05	18.17	18.38	18.36	17.47	18.77	18.42	6.47
Pyrope	6.58	5.29	6.51	5.84	5.22	6.77	6.55	6.61	6.95	6.78	6.60	17.89	6.50
Almandine	55.97	55.85	54.20	53.60	55.24	54.71	53.72	54.44	53.68	54.65	53.75	18.72	6.71
Grossular	19.08	18.97	19.02	19.30	19.20	19.29	19.66	18.69	19.04	19.59	19.11	18.27	6.35
Andradite	0.00	0.00	0.00	0.00	0.00	0.00	0.00	0.00	0.00	0.00	0.00	0.00	0.00

Cont. Table 2

Sample Wt. %	GA3 C7 T1 L13	GA3 C7 T1 L15	GA4 C2 T1 L2	GA4 C2 T1 L9	GA4 C2 T1 L10	GA4 C2 T1 L14	GA4 C2 T1 L15	GA4 C6 T1 L1	GA4 C6 T1 L2	GA4 C6 T1 L3	GA4 C6 T1 L8	GA4 C6 T1 L10	GA4 C6 T1 L14
MgO	1.691	1.601	2.339	2.494	2.429	2.479	2.341	2.182	2.564	2.732	2.517	2.543	2.564
F	0.000	0.000	0.000	0.000	0.000	0.000	0.000	0.000	0.000	0.000	0.000	0.000	0.000
FeO	25.045	25.066	29.207	28.991	28.695	29.227	29.283	28.449	29.102	29.647	29.549	29.234	28.972
TiO_2	0.051	0.039	0.061	0.000	0.006	0.045	0.006	0.017	0.028	0.028	0.000	0.117	0.000
K_2O	0.005	0.015	0.001	0.000	0.005	0.000	0.000	0.000	0.009	0.000	0.004	0.004	0.005
Al_2O_3	21.488	21.589	21.611	22.000	21.798	21.789	21.814	21.550	21.720	21.787	21.406	21.502	21.848
ZnO	0.019	0.049	0.088	0.012	0.121	0.000	0.000	0.075	0.000	0.080	0.039	0.037	0.046
MnO	8.309	8.109	7.329	7.477	7.446	7.441	7.135	7.505	7.678	7.131	7.387	7.310	7.262
CaO	6.896	6.818	2.996	3.069	3.073	2.790	2.993	3.124	2.572	2.298	2.734	2.887	2.868
SiO_2	36.971	37.222	36.456	36.899	36.482	36.785	37.133	36.865	36.831	37.259	36.204	36.588	36.599
Cr_2O_3	0.000	0.006	0.004	0.023	0.000	0.000	0.000	0.017	0.032	0.000	0.000	0.000	0.009
P_2O_5	0.002	0.011	0.028	0.000	0.000	0.017	0.016	0.000	0.009	0.016	0.005	0.000	0.012
Total	100.477	100.525	100.120	100.965	100.055	100.573	100.721	99.784	100.545	100.978	99.845	100.222	100.185
Apfu based on 24 oxygen atoms													
Mg	0.404	0.381	0.563	0.594	0.584	0.593	0.558	0.525	0.613	0.649	0.609	0.611	0.615
F	0.000	0.000	0.000	0.000	0.000	0.000	0.000	0.000	0.000	0.000	0.000	0.000	0.000
Fe	3.353	3.348	3.943	3.871	3.870	3.921	3.916	3.841	3.905	3.953	4.009	3.940	3.898
Ti	0.006	0.005	0.007	0.000	0.001	0.005	0.001	0.002	0.003	0.003	0.000	0.014	0.000
K	0.001	0.003	0.000	0.000	0.001	0.000	0.000	0.000	0.002	0.000	0.001	0.001	0.001
Al	4.055	4.064	4.112	4.140	4.144	4.120	4.111	4.100	4.107	4.094	4.093	4.084	4.143
Zn	0.002	0.006	0.010	0.002	0.014	0.000	0.000	0.009	0.000	0.010	0.005	0.004	0.005
Mn	1.127	1.097	1.002	1.011	1.017	1.011	0.966	1.026	1.043	0.963	1.015	0.998	0.990
Ca	1.183	1.167	0.518	0.525	0.531	0.479	0.513	0.540	0.442	0.393	0.475	0.499	0.494
Si	5.918	5.945	5.885	5.891	5.883	5.900	5.937	5.951	5.909	5.940	5.873	5.897	5.888
Cr	0.000	0.001	0.001	0.003	0.000	0.000	0.000	0.002	0.004	0.000	0.000	0.000	0.001
P	0.000	0.001	0.004	0.000	0.000	0.002	0.002	0.000	0.001	0.002	0.001	0.000	0.002
Total	16.049	16.018	16.046	16.037	16.045	16.031	16.004	15.996	16.031	16.007	16.080	16.048	16.038
Spessartine	54.81	19.42	16.67	16.82	16.92	16.82	16.10	17.12	17.36	16.05	16.84	16.59	16.46
Pyrope	54.59	19.10	9.36	9.87	9.71	9.86	9.30	8.76	10.20	10.83	10.10	10.16	10.23
Almandine	53.38	19.51	63.37	62.56	62.42	63.60	65.01	64.06	63.45	65.67	62.62	63.22	63.04
Grossular	55.05	19.30	8.42	8.66	8.82	7.84	8.53	8.91	7.17	6.46	7.88	7.93	8.20
Andradite	0.00	0.00	0.00	0.00	0.00	0.00	0.00	0.00	0.00	0.00	0.00	0.00	0.00

Cont. Table 2

Sample	GA4 C7	GA4 C7	GA4 C7	GA4 C7	GA4 C7	GA4 C7	GA4 C7	GA4 C7	GA4 C7	GA4 C7	GA4 C7	GA4 C7	GA4 C7
Wt. %	T1 L1	T1 L2	T1 L3	T1 L5	T1 L6	T1 L7	T1 L8	T1 L9	T1 L10	T1 L11	T1 L12	T1 L14	T1 L15
MgO	1.962	2.029	2.458	2.688	2.696	2.649	2.746	2.766	2.779	2.800	2.553	2.279	2.060
F	0.000	0.000	0.000	0.000	0.000	0.000	0.000	0.000	0.000	0.000	0.000	0.000	0.000
FeO	29.602	29.105	29.999	29.110	28.961	29.046	29.135	29.333	29.714	29.233	28.791	29.253	29.132
TiO_2	0.061	0.100	0.117	0.039	0.045	0.000	0.050	0.017	0.017	0.000	0.050	0.056	0.022
K_2O	0.003	0.000	0.000	0.004	0.008	0.002	0.000	0.000	0.007	0.005	0.000	0.000	0.014
Al_2O_3	21.655	20.834	21.793	21.647	21.698	21.789	21.730	21.734	21.778	21.593	21.587	21.555	21.248
ZnO	0.000	0.000	0.048	0.003	0.107	0.091	0.007	0.056	0.073	0.000	0.060	0.000	0.053
MnO	7.191	7.322	7.532	7.519	7.210	7.423	7.359	7.106	7.083	7.337	7.447	7.470	7.666
CaO	3.105	2.604	2.134	2.322	2.556	2.690	2.643	2.511	2.361	2.368	2.518	2.494	2.910
SiO_2	36.831	37.337	36.587	36.114	36.381	36.716	36.785	36.840	36.953	37.113	37.049	36.946	36.155
Cr_2O_3	0.000	0.000	0.000	0.000	0.000	0.015	0.000	0.030	0.000	0.000	0.000	0.000	0.021
P_2O_5	0.007	0.016	0.050	0.028	0.024	0.031	0.031	0.044	0.042	0.015	0.012	0.019	0.022
Total	100.417	99.347	100.718	99.474	99.686	100.452	100.486	100.437	100.807	100.464	100.067	100.072	99.303
Apfu based on 24 oxygen atoms													
Mg	0.471	0.490	0.588	0.651	0.650	0.634	0.657	0.661	0.662	0.669	0.612	0.547	0.501
F	0.000	0.000	0.000	0.000	0.000	0.000	0.000	0.000	0.000	0.000	0.000	0.000	0.000
Fe	3.984	3.946	4.029	3.952	3.917	3.899	3.907	3.934	3.973	3.917	3.871	3.941	3.976
Ti	0.007	0.012	0.014	0.005	0.005	0.000	0.006	0.002	0.002	0.000	0.006	0.007	0.003
K	0.001	0.000	0.000	0.001	0.002	0.000	0.000	0.000	0.001	0.001	0.000	0.000	0.003
Al	4.107	3.981	4.125	4.142	4.136	4.122	4.107	4.108	4.104	4.077	4.090	4.093	4.087
Zn	0.000	0.000	0.006	0.000	0.013	0.011	0.001	0.007	0.009	0.000	0.007	0.000	0.006
Mn	0.980	1.005	1.025	1.034	0.988	1.009	1.000	0.965	0.959	0.996	1.014	1.019	1.060
Ca	0.535	0.452	0.367	0.404	0.443	0.463	0.454	0.431	0.404	0.407	0.434	0.431	0.509
Si	5.926	6.052	5.876	5.863	5.883	5.894	5.899	5.908	5.908	5.946	5.956	5.952	5.900
Cr	0.000	0.000	0.000	0.000	0.000	0.002	0.000	0.004	0.000	0.000	0.000	0.000	0.003
P	0.001	0.002	0.007	0.004	0.003	0.004	0.004	0.006	0.006	0.002	0.002	0.003	0.003
Total	16.012	15.942	16.038	16.056	16.039	16.038	16.035	16.026	16.030	16.013	15.991	15.992	16.050
Spessartine	16.32	16.82	17.05	17.18	16.44	16.80	16.63	16.07	15.97	16.58	16.92	17.00	17.62
Pyrope	7.84	8.20	9.79	10.81	10.82	10.55	10.92	11.01	11.03	11.14	10.21	9.13	8.33
Almandine	65.76	66.02	65.06	62.79	63.39	63.04	63.13	64.15	64.68	64.54	64.58	65.73	63.74
Grossular	8.73	7.57	5.76	6.59	7.23	7.65	7.40	7.04	6.68	6.77	7.09	7.01	8.33
Andradite	0.00	0.00	0.00	0.00	0.00	0.00	0.00	0.00	0.00	0.00	0.00	0.00	0.00

Cont. Table 2

Sample Wt. %	GA4 C8 T1 L1	GA4 C8 T1 L5	GA4 C8 T1 L9	GA4 C8 T1 L10	GA4 C8 T1 L11	GA4 C8 T1 L12	GA4 C8 T1 L13	GA4 C8 T1 L14	GA6-C2 T1 L1	GA6-C2 T1 L2	GA6-C2 T1 L3	GA6-C2 T1 L4	GA6-C2 T1 L6
MgO	2.152	2.668	2.511	0.265	2.474	2.469	2.474	2.341	1.518	1.589	1.690	1.844	1.880
F	0.000	0.000	0.000	0.076	0.000	0.000	0.000	0.000	0.000	0.000	0.000	0.000	0.000
FeO	29.028	28.934	29.157	4.229	28.477	29.232	28.817	28.456	24.298	24.625	24.194	24.208	24.093
TiO_2	0.000	0.022	0.028	0.000	0.006	0.033	0.056	0.000	0.074	0.091	0.085	0.102	0.062
K_2O	0.022	0.004	0.000	0.005	0.004	0.006	0.004	0.000	0.004	0.000	0.000	0.002	0.013
Al_2O_3	21.603	21.632	21.571	2.573	21.850	21.547	21.753	21.953	21.166	21.069	21.362	21.382	21.436
ZnO	0.007	0.026	0.055	0.000	0.059	0.050	0.037	0.000	0.013	0.079	0.094	0.038	0.052
MnO	7.659	7.703	7.121	1.009	7.276	7.312	7.252	7.589	8.111	7.642	7.771	8.112	7.780
CaO	2.876	2.600	2.817	0.384	2.874	2.860	2.939	2.922	7.614	7.809	7.909	7.847	7.754
SiO_2	37.285	37.262	37.189	91.244	37.135	36.236	36.847	37.233	36.488	36.365	37.455	37.241	37.226
Cr_2O_3	0.000	0.023	0.023	0.000	0.000	0.000	0.000	0.000	0.004	0.017	0.024	0.000	0.024
P_2O_5	0.000	0.015	0.012	0.032	0.037	0.044	0.025	0.014	0.004	0.000	0.003	0.014	0.023
Total	100.632	100.889	100.484	99.785	100.192	99.789	100.204	100.508	99.294	99.286	100.587	100.790	100.343
Apfu based on 24 oxygen atoms													
Mg	0.514	0.635	0.600	0.049	0.591	0.596	0.593	0.558	0.367	0.384	0.401	0.438	0.447
F	0.000	0.000	0.000	0.030	0.000	0.000	0.000	0.000	0.000	0.000	0.000	0.000	0.000
Fe	3.889	3.862	3.906	0.441	3.816	3.961	3.872	3.804	3.292	3.340	3.222	3.223	3.215
Ti	0.000	0.003	0.003	0.000	0.001	0.004	0.007	0.000	0.009	0.011	0.010	0.012	0.008
K	0.005	0.001	0.000	0.001	0.001	0.001	0.001	0.000	0.001	0.000	0.000	0.000	0.003
Al	4.079	4.070	4.073	0.379	4.127	4.115	4.119	4.136	4.042	4.027	4.009	4.012	4.031
Zn	0.001	0.003	0.007	0.000	0.007	0.006	0.004	0.000	0.002	0.009	0.011	0.004	0.006
Mn	1.039	1.041	0.966	0.107	0.988	1.003	0.987	1.027	1.113	1.050	1.048	1.094	1.052
Ca	0.494	0.445	0.484	0.051	0.494	0.497	0.506	0.500	1.322	1.357	1.349	1.338	1.326
Si	5.972	5.947	5.957	11.387	5.950	5.871	5.919	5.951	5.911	5.897	5.964	5.928	5.940
Cr	0.000	0.003	0.003	0.000	0.000	0.000	0.000	0.000	0.001	0.002	0.003	0.000	0.003
P	0.000	0.002	0.002	0.003	0.005	0.006	0.003	0.002	0.001	0.000	0.000	0.002	0.003
Total	15.991	16.011	15.999	12.449	15.979	16.060	16.010	15.978	16.059	16.077	16.019	16.051	16.032
Spessartine	17.33	0.00	16.11	2.29	17.02	16.68	16.44	17.15	18.49	17.42	17.46	18.18	17.50
Pyrope	8.57	0.00	10.00	1.06	10.19	9.91	9.87	9.31	6.09	6.38	6.68	7.27	7.44
Almandine	64.87	0.00	65.14	8.84	65.77	62.80	64.01	63.49	51.80	51.74	52.91	51.04	51.98
Grossular	8.23	0.00	7.91	0	0	8.15	8.26	8.35	21.58	21.52	22.15	21.32	21.80
Andradite	0.00	0.00	0.00	0.00	0.00	0.00	0.00	0.00	0.14	0.67	0.00	0.62	0.00

Cont. Table 2

Sample Wt. %	GA6-C2 T1 L7	GA6-C2 T1 L8	GA6-C2 T1 L10	GA6-C3 T1 L1	GA6-C3 T1 L4	GA6-C3 T1 L5	GA6-C3 T1 L7	GA6-C3 T1 L8	GA6-C3 T1 L9	GA6-C4 T1 L3	GA6-C4 T1 L4	GA6-C4 T1 L5	GA6-C4 T1 L9
MgO	1.807	1.692	1.580	1.753	1.685	1.774	1.703	1.794	2.383	1.506	1.592	1.643	1.828
F	0.000	0.000	0.000	0.000	0.000	0.000	0.000	0.000	0.000	0.000	0.000	0.000	0.000
FeO	24.015	24.385	24.340	24.581	24.486	24.693	24.681	24.557	27.050	24.775	24.095	24.484	24.550
TiO_2	0.102	0.085	0.068	0.000	0.040	0.051	0.000	0.040	0.204	0.051	0.023	0.017	0.073
K_2O	0.002	0.000	0.000	0.002	0.002	0.008	0.000	0.009	0.009	0.003	0.010	0.005	0.003
Al_2O_3	21.287	21.069	21.450	21.668	21.566	21.609	21.288	21.143	21.759	21.552	21.642	21.639	21.870
ZnO	0.052	0.000	0.000	0.010	0.000	0.018	0.033	0.000	0.123	0.000	0.110	0.037	0.073
MnO	7.959	7.331	7.501	7.969	8.031	7.861	7.786	8.211	5.995	7.468	8.057	7.842	8.036
CaO	7.969	7.835	8.212	7.323	7.660	7.675	7.677	7.399	6.448	7.892	7.909	7.654	7.231
SiO_2	37.010	36.749	37.400	37.507	37.094	36.891	36.850	36.130	35.704	37.141	37.154	37.035	37.025
Cr_2O_3	0.028	0.026	0.000	0.015	0.057	0.017	0.000	0.009	0.024	0.000	0.000	0.000	0.009
P_2O_5	0.007	0.010	0.008	0.022	0.001	0.006	0.006	0.023	0.007	0.006	0.002	0.010	0.003
Total	100.238	99.182	100.559	100.850	100.622	100.603	100.024	99.315	99.706	100.394	100.594	100.366	100.701
Apfu based on 24 oxygen atoms													
Mg	0.431	0.408	0.375	0.415	0.401	0.422	0.408	0.434	0.574	0.359	0.378	0.391	0.434
F	0.000	0.000	0.000	0.000	0.000	0.000	0.000	0.000	0.000	0.000	0.000	0.000	0.000
Fe	3.214	3.297	3.242	3.264	3.267	3.298	3.316	3.334	3.657	3.310	3.213	3.272	3.270
Ti	0.012	0.010	0.008	0.000	0.005	0.006	0.000	0.005	0.025	0.006	0.003	0.002	0.009
K	0.000	0.000	0.000	0.000	0.000	0.002	0.000	0.002	0.002	0.001	0.002	0.001	0.001
Al	4.016	4.015	4.026	4.055	4.055	4.067	4.032	4.045	4.145	4.059	4.067	4.076	4.105
Zn	0.006	0.000	0.000	0.001	0.000	0.002	0.004	0.000	0.015	0.000	0.013	0.004	0.009
Mn	1.079	1.004	1.012	1.072	1.085	1.063	1.060	1.129	0.821	1.011	1.088	1.062	1.084
Ca	1.367	1.357	1.401	1.246	1.309	1.313	1.322	1.287	1.117	1.351	1.351	1.311	1.234
Si	5.923	5.941	5.956	5.955	5.917	5.891	5.921	5.865	5.771	5.934	5.924	5.919	5.896
Cr	0.004	0.003	0.000	0.002	0.007	0.002	0.000	0.001	0.003	0.000	0.000	0.000	0.001
P	0.001	0.001	0.001	0.003	0.000	0.001	0.001	0.003	0.001	0.001	0.000	0.001	0.000
Total	16.054	16.037	16.021	16.013	16.047	16.068	16.063	16.104	16.130	16.030	16.040	16.040	16.042
Spessartine	17.93	16.69	16.84	17.85	18.03	17.65	17.60	18.70	13.58	16.81	18.11	17.66	18.03
Pyrope	7.17	6.78	6.24	6.91	6.66	7.01	6.77	7.19	9.50	5.97	6.30	6.51	7.22
Almandine	50.84	52.93	52.87	53.69	51.97	51.44	52.01	50.02	54.36	53.57	51.74	52.51	52.45
Grossular	21.83	21.94	23.12	20.71	21.46	21.59	21.53	20.30	17.79	22.32	22.42	21.75	20.28
Andradite	0.49	0.29	0.00	0.00	0.00	0.00	0.00	0.86	0.00	0.00	0.00	0.00	0.00

Cont. Table 2

Sample	GA6-C4 T1 L10	GA6-C6 T1 L1	GA6-C6 T1 L2	GA6-C6 T1 L5	GA6-C6 T1 L6	GA6-C6 T1 L7	GA6-C6 T1 L9
MgO	1.432	1.609	1.827	1.922	1.900	1.868	1.809
F	0.000	0.000	0.000	0.000	0.000	0.000	0.000
FeO	24.065	26.082	24.262	23.937	24.465	24.711	24.493
TiO_2	0.045	0.000	0.090	0.034	0.124	0.079	0.108
K_2O	0.002	0.008	0.003	0.006	0.004	0.000	0.000
Al_2O_3	21.423	21.550	21.566	21.598	21.375	21.621	21.492
ZnO	0.067	0.028	0.159	0.075	0.010	0.065	0.000
MnO	8.001	7.200	7.622	8.004	7.800	7.422	7.721
CaO	8.152	6.272	7.591	7.527	7.420	7.468	7.634
SiO_2	36.816	36.695	36.481	36.710	36.556	37.214	36.653
Cr_2O_3	0.000	0.006	0.000	0.011	0.000	0.004	0.000
P_2O_5	0.022	0.000	0.009	0.005	0.018	0.039	0.012
Total	100.025	99.450	99.610	99.829	99.672	100.491	99.922
Apfu based on 24 oxygen atoms							
Mg	0.343	0.387	0.439	0.460	0.456	0.444	0.433
F	0.000	0.000	0.000	0.000	0.000	0.000	0.000
Fe	3.232	3.524	3.269	3.214	3.296	3.292	3.291
Ti	0.006	0.000	0.011	0.004	0.015	0.010	0.013
K	0.001	0.002	0.001	0.001	0.001	0.000	0.000
Al	4.055	4.104	4.095	4.088	4.059	4.060	4.070
Zn	0.008	0.003	0.019	0.009	0.001	0.008	0.000
Mn	1.088	0.985	1.040	1.089	1.064	1.002	1.051
Ca	1.403	1.086	1.310	1.295	1.281	1.275	1.314
Si	5.912	5.928	5.877	5.895	5.889	5.929	5.888
Cr	0.000	0.001	0.000	0.001	0.000	0.001	0.000
P	0.003	0.000	0.001	0.001	0.002	0.005	0.002
Total	16.050	16.020	16.063	16.056	16.064	16.024	16.061
Spessartine	18.10	16.41	17.29	18.09	17.67	16.68	17.45
Pyrope	5.70	6.45	7.29	7.65	7.58	7.39	7.19
Almandine	51.28	57.78	51.52	50.77	51.52	53.60	51.53
Grossular	23.19	18.06	21.51	21.38	20.89	20.98	21.49
Andradite	0.00	0.00	0.00	0.00	0.00	0.00	0.00

Table 3. Major element composition of magnetite, hematite, and gahnite from the studied rocks.

Magnetite and hematite																
Sample wt.%	**AD-10-00**3-C1-P1	3-C1-P2	3-C1-P3	3-C1-P4	3-C2-P1	3-C2-P2	3-C2-P3	3-C2-P4	3-C5-P2	3-C5-P3	3-C5-P4	3-C5-P5	3-C8-P1	3-C8-P2	3-C8-P3	3-C8-P4
SiO_2	0.22	0.15	0.06	0.31	0.05	0.23	0.22	0.12	0.08	0.18	0.08	0.05	0.06	0.11	0.09	0.05
TiO_2	0.08	0.04	0.11	0.00	0.69	0.15	0.11	0.02	0.14	0.12	0.17	0.14	0.15	0.03	0.09	0.16
Al_2O_3	0.21	0.26	0.26	0.20	0.30	0.35	0.39	0.31	0.26	0.43	0.23	0.27	0.26	0.35	0.30	0.28
MgO	0.00	0.05	0.03	0.01	0.00	0.05	0.04	0.03	0.00	0.04	0.00	0.00	0.00	0.01	0.01	0.00
MnO	0.28	0.12	0.07	0.25	0.18	0.17	0.19	0.14	0.26	1.77	0.13	0.14	0.08	0.11	0.22	0.25
FeO	91.01	90.76	91.24	87.79	91.03	90.55	91.40	91.31	90.52	89.60	91.29	92.14	92.12	91.15	91.37	90.78
Cr_2O_3	0.02	0.00	0.01	0.00	0.05	0.05	0.00	0.04	0.06	0.04	0.01	0.06	0.01	0.02	0.01	0.00
CoO	0.18	0.21	0.14	0.15	0.16	0.16	0.20	0.17	0.16	0.17	0.22	0.13	0.15	0.22	0.21	0.18
Total	92.00	91.59	91.92	88.70	92.47	91.70	92.55	92.14	91.47	92.35	92.12	92.93	92.82	91.99	92.29	91.70
Apfu based on 12 oxygen atoms																
Si	0.02	0.02	0.01	0.03	0.01	0.03	0.02	0.01	0.01	0.02	0.01	0.01	0.01	0.01	0.01	0.01
Ti	0.01	0.00	0.01	0.00	0.06	0.01	0.01	0.00	0.01	0.01	0.01	0.01	0.01	0.00	0.01	0.01
Al	0.03	0.03	0.03	0.02	0.04	0.05	0.05	0.04	0.03	0.06	0.03	0.04	0.03	0.05	0.04	0.04
Mg	0.00	0.01	0.00	0.00	0.00	0.01	0.01	0.00	0.00	0.01	0.00	0.00	0.00	0.00	0.00	0.00
Mn	0.03	0.01	0.01	0.02	0.02	0.02	0.02	0.01	0.02	0.17	0.01	0.01	0.01	0.01	0.02	0.02
Fe	8.50	8.38	8.51	7.52	8.58	8.37	8.64	8.56	8.34	8.43	8.56	8.83	8.81	8.51	8.60	8.41
Cr	0.00	0.00	0.00	0.00	0.00	0.00	0.00	0.00	0.00	0.00	0.00	0.01	0.00	0.00	0.00	0.00
Co	0.02	0.02	0.01	0.01	0.01	0.01	0.02	0.02	0.01	0.02	0.02	0.01	0.01	0.02	0.02	0.02
Total	8.60	8.48	8.58	7.61	8.73	8.49	8.77	8.66	8.43	8.71	8.64	8.92	8.88	8.60	8.70	8.51

Cont.Table 3

Magnetite and hematite

Sample Wt. %	3-C14-P1	3-C14-P2	3-C14-P3	3-C14-P4	3-C14-P5	8-T1-L14	8-T1-L15	8-T1-L17	8-T1-L25	13-C3-P1	13-C3-P2	13-C3-P3	13-C3-P4	13-C4-P1	13-C4-P2	13-C4-P3
SiO_2	0.29	0.21	0.07	0.11	0.05	0.17	0.23	0.24	0.22	0.10	0.06	0.09	0.05	0.02	0.08	0.09
TiO_2	0.28	0.07	0.04	0.16	0.14	0.02	0.01	0.07	0.09	0.17	0.10	0.18	0.15	0.17	0.19	0.09
Al_2O_3	0.48	0.35	0.26	0.32	0.24	0.21	0.19	0.12	0.28	0.17	0.23	0.16	0.11	0.13	0.32	0.31
MgO	0.06	0.01	0.00	0.01	0.00	0.03	0.03	0.00	0.01	0.00	0.01	0.00	0.00	0.00	0.00	0.00
MnO	0.09	0.29	0.02	0.06	0.17	0.09	0.08	0.03	0.06	0.21	0.08	0.05	0.03	0.08	0.06	0.07
FeO	89.30	90.48	90.74	90.02	93.00	87.82	91.21	91.14	91.22	91.02	92.21	92.78	93.10	92.40	91.44	92.37
Cr_2O_3	0.03	0.00	0.01	0.02	0.06	0.01	0.01	0.00	0.00	0.05	0.03	0.00	0.05	0.03	0.00	0.07
CoO	0.20	0.14	0.14	0.20	0.24	0.21	0.21	0.23	0.20	0.24	0.18	0.22	0.19	0.14	0.17	0.17
Total	90.72	91.55	91.28	90.88	93.90	88.55	91.96	91.83	92.07	91.95	92.90	93.47	93.70	92.98	92.26	93.17
Apfu based on 12 oxygen atoms																
Si	0.03	0.02	0.01	0.01	0.01	0.02	0.03	0.03	0.03	0.01	0.01	0.01	0.01	0.00	0.01	0.01
Ti	0.02	0.01	0.00	0.01	0.01	0.00	0.00	0.01	0.01	0.01	0.01	0.02	0.01	0.02	0.02	0.01
Al	0.06	0.05	0.03	0.04	0.03	0.03	0.03	0.02	0.04	0.02	0.03	0.02	0.02	0.02	0.04	0.04
Mg	0.01	0.00	0.00	0.00	0.00	0.00	0.00	0.00	0.00	0.00	0.00	0.00	0.00	0.00	0.00	0.00
Mn	0.01	0.03	0.00	0.01	0.02	0.01	0.01	0.00	0.01	0.02	0.01	0.01	0.00	0.01	0.01	0.01
Fe	8.02	8.34	8.32	8.15	9.17	7.50	8.51	8.47	8.53	8.49	8.84	9.04	9.13	8.88	8.60	8.91
Cr	0.00	0.00	0.00	0.00	0.01	0.00	0.00	0.00	0.00	0.00	0.00	0.00	0.00	0.00	0.00	0.01
Co	0.02	0.01	0.01	0.02	0.02	0.02	0.02	0.02	0.02	0.02	0.02	0.02	0.02	0.01	0.02	0.02
Total	8.17	8.45	8.38	8.24	9.26	7.58	8.59	8.54	8.62	8.59	8.91	9.11	9.19	8.94	8.69	9.00

Cont. Table 3

Magnetite and hematite																
Sample	13-C4-	13-C7-	13-C7-	13-	13-	13-	13-	13-	13-	13-	13-	13-	13-	18-	18-	18-
Wt. %	P4	P1	P2	C7-	C7-	C9-	C9-	C9-	C9-	C10-	C10-	C10-	C10-	C1-	C1-	C1-
				P3	P4	P1	P2	P3	P4	P-1	P-2	P-3	P-4	P1	P2	P3
SiO_2	0.17	0.15	0.10	0.19	0.09	0.07	0.11	0.08	0.07	0.18	0.18	0.15	0.07	0.01	0.01	0.02
TiO_2	0.17	0.16	0.12	0.14	0.08	0.16	0.16	0.20	0.20	0.10	0.16	0.16	0.13	0.10	0.15	0.13
Al_2O_3	0.46	0.32	0.16	0.17	0.13	0.10	0.18	0.18	0.13	0.26	0.21	0.14	0.09	0.03	0.04	0.07
MgO	0.00	0.00	0.05	0.00	0.00	0.00	0.00	0.01	0.00	0.04	0.03	0.01	0.02	0.00	0.02	0.00
MnO	0.06	0.31	0.08	0.18	0.35	0.11	0.15	0.03	0.11	0.15	0.07	0.05	0.00	0.33	0.49	0.71
FeO	89.80	91.81	91.74	90.17	89.61	91.63	92.08	90.99	92.68	90.13	91.48	91.49	90.77	95.59	94.67	95.18
Cr_2O_3	0.02	0.00	0.03	0.04	0.03	0.00	0.03	0.02	0.02	0.04	0.02	0.01	0.01	0.00	0.01	0.00
CoO	0.15	0.16	0.18	0.20	0.18	0.20	0.17	0.14	0.16	0.17	0.15	0.19	0.17	0.20	0.21	0.20
Total	90.83	92.91	92.45	91.09	90.46	92.27	92.89	91.64	93.38	91.06	92.30	92.19	91.25	96.26	95.60	96.31
Apfu based on 12 oxygen atoms																
Si	0.02	0.02	0.01	0.02	0.01	0.01	0.01	0.01	0.01	0.02	0.02	0.02	0.01	0.00	0.00	0.00
Ti	0.01	0.01	0.01	0.01	0.01	0.01	0.01	0.02	0.02	0.01	0.01	0.01	0.01	0.01	0.01	0.01
Al	0.06	0.04	0.02	0.02	0.02	0.01	0.02	0.02	0.02	0.03	0.03	0.02	0.01	0.00	0.01	0.01
Mg	0.00	0.00	0.01	0.00	0.00	0.00	0.00	0.00	0.00	0.01	0.00	0.00	0.00	0.00	0.00	0.00
Mn	0.01	0.03	0.01	0.02	0.03	0.01	0.01	0.00	0.01	0.01	0.01	0.00	0.00	0.04	0.05	0.08
Fe	8.11	8.78	8.68	8.22	8.05	8.64	8.82	8.42	9.00	8.20	8.61	8.59	8.32	10.13	9.83	10.10
Cr	0.00	0.00	0.00	0.00	0.00	0.00	0.00	0.00	0.00	0.00	0.00	0.00	0.00	0.00	0.00	0.00
Co	0.01	0.01	0.02	0.02	0.02	0.02	0.02	0.01	0.02	0.01	0.01	0.02	0.02	0.02	0.02	0.02
Total	8.22	8.90	8.76	8.31	8.13	8.70	8.90	8.49	9.07	8.30	8.70	8.67	8.37	10.20	9.93	10.22

Cont. Table 3

Magnetite and hematite

Sample Wt. %	18-C1-P4	18-C1-P5	18-C2-P1	18-C2-P2	18-C2-P3	18-C2-P4	18-C3-P1	18-C3-P2	18-C3-P3	18-C3-P4	18-C5-P1	18-C5-P2	18-C5-P3
SiO_2	0.02	0.01	0.03	0.01	0.03	0.04	0.02	0.02	0.01	0.03	0.02	0.05	0.01
TiO_2	0.12	0.10	0.13	0.09	0.10	0.16	0.13	0.18	0.12	0.12	0.07	0.14	0.11
Al_2O_3	0.07	0.05	0.07	0.08	0.12	0.07	0.06	0.05	0.07	0.05	0.10	0.09	0.14
MgO	0.00	0.01	0.03	0.02	0.02	0.01	0.02	0.02	0.00	0.00	0.00	0.03	0.02
MnO	0.53	0.29	0.68	0.76	0.77	0.61	0.46	0.61	0.58	0.50	0.75	0.72	0.69
FeO	95.11	95.77	95.32	95.64	95.85	95.50	95.51	95.39	96.48	94.08	94.71	95.52	95.37
Cr_2O_3	0.04	0.00	0.00	0.00	0.00	0.02	0.00	0.00	0.01	0.02	0.01	0.01	0.00
CoO	0.19	0.17	0.12	0.14	0.19	0.19	0.19	0.23	0.17	0.19	0.16	0.17	0.15
Total	96.07	96.40	96.38	96.73	97.08	96.59	96.38	96.51	97.44	94.99	95.81	96.73	96.47
Apfu based on 12 oxygen atoms													
Si	0.00	0.00	0.00	0.00	0.00	0.00	0.00	0.00	0.00	0.00	0.00	0.01	0.00
Ti	0.01	0.01	0.01	0.01	0.01	0.01	0.01	0.02	0.01	0.01	0.01	0.01	0.01
Al	0.01	0.01	0.01	0.01	0.02	0.01	0.01	0.01	0.01	0.01	0.01	0.01	0.02
Mg	0.00	0.00	0.01	0.00	0.00	0.00	0.00	0.00	0.00	0.00	0.00	0.01	0.00
Mn	0.06	0.03	0.07	0.08	0.09	0.07	0.05	0.07	0.06	0.05	0.08	0.08	0.07
Fe	10.02	10.19	10.13	10.28	10.41	10.22	10.16	10.18	10.61	9.59	9.90	10.26	10.16
Cr	0.00	0.00	0.00	0.00	0.00	0.00	0.00	0.00	0.00	0.00	0.00	0.00	0.00
Co	0.02	0.02	0.01	0.01	0.02	0.02	0.02	0.02	0.02	0.02	0.02	0.02	0.02
Total	10.12	10.26	10.25	10.41	10.55	10.33	10.25	10.30	10.72	9.68	10.02	10.39	10.29

Cont. Table 3

	Gahnite										
Sample Wt. %	GH3 AB C1 T1-L20	GH3 AB C1 T1-L2	GH3 AB C1 T1-L5	GH3 AB C1 T1-L6	GH3 AB C1 T1-L7	GH3 AB C1 T1-L8	GH3 AB C1 T1-L9	GH3 AB C1 T1-L12	GH3 AB C1 T1-L13	GH3 AB C1 T1-L14	GH3 AB C1 T1-L16
SiO_2	0.000	0.101	0.000	0.000	0.004	0.000	0.136	0.005	0.000	0.000	0.027
K_2O	0.013	0.010	0.008	0.000	0.000	0.012	0.028	0.023	0.011	0.021	0.013
CaO	0.019	0.019	0.005	0.000	0.000	0.000	0.019	0.000	0.000	0.000	0.000
TiO_2	0.000	0.000	0.000	0.016	0.000	0.000	0.000	0.008	0.000	0.000	0.000
MgO	1.605	1.545	1.528	1.478	1.541	1.554	1.488	1.553	1.484	1.541	1.497
Al_2O_3	57.152	56.717	56.909	56.991	56.580	57.308	55.863	56.989	56.925	57.326	57.250
MnO	0.371	0.402	0.307	0.323	0.380	0.396	0.282	0.361	0.348	0.374	0.345
FeO	8.555	8.454	8.509	8.437	8.497	8.487	8.366	8.536	8.637	8.495	8.337
Cr_2O_3	0.003	0.004	0.000	0.022	0.012	0.012	0.023	0.000	0.000	0.019	0.024
ZnO	33.235	33.304	32.844	33.315	32.896	33.202	33.061	33.219	33.058	33.105	33.302
Total	100.953	100.556	100.110	100.582	99.910	100.971	99.266	100.694	100.463	100.881	100.795
Apfu based on 3 oxygen atoms											
Si	0.000	0.003	0.000	0.000	0.000	0.000	0.004	0.000	0.000	0.000	0.001
K	0.001	0.000	0.000	0.000	0.000	0.000	0.001	0.001	0.000	0.001	0.001
Ca	0.001	0.001	0.000	0.000	0.000	0.000	0.001	0.000	0.000	0.000	0.000
Ti	0.000	0.000	0.000	0.000	0.000	0.000	0.000	0.000	0.000	0.000	0.000
Mg	0.071	0.068	0.068	0.065	0.069	0.068	0.067	0.069	0.066	0.068	0.066
Al	1.989	1.983	1.994	1.991	1.990	1.992	1.981	1.989	1.991	1.994	1.994
Mn	0.009	0.010	0.008	0.008	0.010	0.010	0.007	0.009	0.009	0.009	0.009
Fe	0.211	0.210	0.212	0.209	0.212	0.209	0.211	0.211	0.214	0.210	0.206
Cr	0.000	0.000	0.000	0.001	0.000	0.000	0.001	0.000	0.000	0.000	0.001
Zn	0.725	0.730	0.721	0.729	0.725	0.723	0.734	0.726	0.724	0.721	0.727
total	3.006	3.005	3.003	3.004	3.005	3.004	3.006	3.006	3.005	3.003	3.002

Cont. Table 3

Gahnite

Sample Wt. %	GH3 AB C1 T1-L19	GH3 AB C1 T1-L21	GH3 AB C2 T1-L1	GH3 AB C2 T1-L2	GH3 AB C2 T1-L3	GH3 AB C2 T1-L4	GH3 AB C2 T1-L7	GH3 AB C2 T1-L8	GH3 AB C2 T1-L9	GH3 AB C2 T1-L11	GH3 AB C2 T1-L12
SiO_2	0.000	0.013	0.000	0.000	0.000	0.008	0.023	0.000	0.007	0.012	0.032
K_2O	0.006	0.000	0.035	0.005	0.026	0.008	0.024	0.000	0.032	0.021	0.026
CaO	0.002	0.000	0.000	0.012	0.000	0.000	0.010	0.014	0.009	0.000	0.000
TiO_2	0.006	0.000	0.000	0.003	0.000	0.000	0.000	0.000	0.009	0.000	0.000
MgO	1.541	1.401	1.537	1.468	1.546	1.385	1.325	1.385	1.439	1.472	1.501
Al_2O_3	56.729	57.140	56.800	56.991	57.005	56.663	56.882	56.840	56.641	56.450	56.904
MnO	0.358	0.393	0.367	0.335	0.421	0.392	0.335	0.313	0.370	0.414	0.269
FeO	8.877	8.527	7.826	7.751	7.772	8.158	7.953	7.807	8.201	7.804	8.096
Cr_2O_3	0.005	0.000	0.000	0.000	0.000	0.032	0.000	0.008	0.018	0.021	0.012
ZnO	32.924	33.142	33.867	33.669	33.934	34.224	33.675	33.814	33.700	34.201	33.825
Total	100.448	100.616	100.432	100.234	100.704	100.870	100.227	100.181	100.426	100.395	100.665
Apfu based on 3 oxygen atoms											
Si	0.000	0.000	0.000	0.000	0.000	0.000	0.001	0.000	0.000	0.000	0.001
K	0.000	0.000	0.001	0.000	0.001	0.000	0.001	0.000	0.001	0.001	0.001
Ca	0.000	0.000	0.000	0.000	0.000	0.000	0.000	0.000	0.000	0.000	0.000
Ti	0.000	0.000	0.000	0.000	0.000	0.000	0.000	0.000	0.000	0.000	0.000
Mg	0.068	0.062	0.068	0.065	0.068	0.061	0.059	0.061	0.064	0.065	0.066
Al	1.986	1.994	1.990	1.996	1.991	1.983	1.995	1.995	1.987	1.983	1.989
Mn	0.009	0.010	0.009	0.008	0.011	0.010	0.009	0.008	0.009	0.011	0.007
Fe	0.221	0.211	0.195	0.193	0.193	0.203	0.198	0.194	0.204	0.195	0.201
Cr	0.000	0.000	0.000	0.000	0.000	0.001	0.000	0.000	0.000	0.001	0.000
Zn	0.722	0.725	0.743	0.739	0.742	0.750	0.740	0.744	0.741	0.753	0.741
total	3.007	3.002	3.006	3.002	3.005	3.008	3.002	3.003	3.007	3.008	3.005

Cont. Table 3

Gahnite

Sample Wt. %	GH3 AB C2 T1-L13	GH3 AB C3 T1-L3	GH3 AB C3 T1-L4	GH3 AB C3 T1-L5	GH3 AB C3 T1-L6	GH3 AB C3 T1-L7	GH3 AB C3 T1-L8	GH3 AB C3 T1-L10	GH3 AB C3 T1-L11	GH3 AB C4 T1-L1	GH3 AB C4 T1-L3
SiO_2	0.032	0.004	0.000	0.000	0.013	0.021	0.000	0.000	0.000	0.007	0.000
K_2O	0.021	0.002	0.014	0.041	0.018	0.011	0.021	0.005	0.013	0.020	0.029
CaO	0.026	0.000	0.000	0.000	0.000	0.000	0.018	0.011	0.020	0.000	0.000
TiO_2	0.000	0.018	0.000	0.000	0.000	0.000	0.000	0.003	0.000	0.000	0.000
MgO	1.508	1.405	1.472	1.386	1.378	1.487	1.318	1.443	1.336	1.423	1.325
Al_2O_3	56.908	56.943	57.000	56.675	56.693	56.907	56.894	56.726	56.267	56.647	56.883
MnO	0.374	0.348	0.339	0.370	0.313	0.288	0.326	0.379	0.291	0.354	0.307
FeO	7.677	7.821	7.697	7.934	7.836	8.061	8.145	7.602	7.851	8.327	8.257
Cr_2O_3	0.011	0.000	0.000	0.000	0.000	0.000	0.000	0.000	0.000	0.014	0.000
ZnO	33.822	34.213	33.696	34.331	33.962	34.197	34.036	34.160	33.671	33.632	33.778
Total	100.379	100.754	100.218	100.737	100.213	100.972	100.758	100.329	99.449	100.424	100.579
Apfu based on 3 oxygen atoms											
Si	0.001	0.000	0.000	0.000	0.000	0.001	0.000	0.000	0.000	0.000	0.000
K	0.001	0.000	0.001	0.002	0.001	0.000	0.001	0.000	0.001	0.001	0.001
Ca	0.001	0.000	0.000	0.000	0.000	0.000	0.001	0.000	0.001	0.000	0.000
Ti	0.000	0.000	0.000	0.000	0.000	0.000	0.000	0.000	0.000	0.000	0.000
Mg	0.067	0.062	0.065	0.061	0.061	0.066	0.058	0.064	0.060	0.063	0.059
Al	1.992	1.990	1.997	1.985	1.991	1.986	1.990	1.990	1.992	1.987	1.991
Mn	0.009	0.009	0.009	0.009	0.008	0.007	0.008	0.010	0.007	0.009	0.008
Fe	0.191	0.194	0.191	0.197	0.195	0.200	0.202	0.189	0.197	0.207	0.205
Cr	0.000	0.000	0.000	0.000	0.000	0.000	0.000	0.000	0.000	0.000	0.000
Zn	0.742	0.749	0.740	0.753	0.747	0.748	0.746	0.751	0.747	0.739	0.741
total	3.003	3.004	3.002	3.008	3.004	3.007	3.006	3.005	3.004	3.006	3.005

Table 4. Major and trace element composition of banded and massive IFs from the Broken Hill, Little Broken Hill, Wild Dog, and Pinnacles deposits, and garnet- and gahnite-quartz rocks from the Nine Mile deposit, Southern Curnamona Province, Australia.

Sample	AD-10-001	AD-10-002	AD-10-003	AD-10-004	AD-10-006	AD-10-007	AD-10-008	AD-10-009	AD-10-010	AD-10-011	AD-10-012	AD-10-013	AD-10-014	AD-10-015	AD-10-016
SiO_2 (wt. %)	20.92	29.00	22.50	32.16	7.45	36.76	6.41	58.70	33.58	28.72	30.10	19.97	32.13	24.47	29.08
Al_2O_3	5.09	5.73	4.95	5.09	0.38	0.28	0.53	1.08	6.20	6.89	6.19	5.69	8.32	6.30	6.62
Fe_2O_3	50.05	47.01	59.12	46.60	87.98	61.40	89.90	37.19	41.77	46.42	45.68	60.24	40.80	54.80	44.67
MgO	0.46	0.56	0.41	0.54	<0.01	<0.01	0.07	0.10	0.38	0.46	0.49	0.34	0.86	0.54	0.69
CaO	10.10	5.88	4.63	5.33	0.11	0.08	0.32	0.34	8.20	7.63	7.47	4.85	6.96	4.94	7.79
Na_2O	<0.01	0.02	<0.01	<0.01	<0.01	<0.01	0.13	<0.01	<0.01	<0.01	0.02	<0.01	<0.01	<0.01	<0.01
K_2O	<0.01	<0.01	<0.01	<0.01	<0.01	<0.01	0.06	0.04	0.05	0.04	0.11	0.04	0.34	0.09	0.03
TiO_2	0.16	0.20	0.17	0.17	<0.01	<0.01	0.02	0.10	0.19	0.23	0.24	0.20	0.27	0.24	0.24
P_2O_5	7.11	4.52	3.55	3.91	0.18	0.15	0.17	0.20	4.66	4.24	4.64	2.70	3.83	3.32	5.28
MnO	5.32	6.01	4.99	5.29	0.05	0.05	0.04	0.02	4.53	5.04	3.68	4.10	4.18	4.73	4.79
Cr_2O_3	0.01	0.01	0.01	0.01	<0.002	<0.002	<0.002	<0.002	0.01	0.01	0.01	0.01	0.01	0.01	0.01
LOI	0.60	0.60	-0.60	0.70	3.80	1.20	2.30	2.20	0.30	0.20	1.20	1.70	2.10	0.40	0.60
Sum	99.82	99.55	99.70	99.82	99.93	99.92	99.92	99.97	99.86	99.87	99.80	99.78	99.76	99.80	99.82
C_{total}	0.02	0.05	0.02	0.02	0.11	0.03	0.18	0.07	<0.02	0.04	0.05	0.04	0.04	<0.02	0.03
S_{total}	<0.02	<0.02	<0.02	<0.02	0.17	0.08	0.10	0.04	<0.02	<0.02	<0.02	<0.02	<0.02	<0.02	<0.02
Ba (ppm)	31.00	109.00	9.00	103.00	16.00	12.00	13.00	66.00	28.00	28.00	115.00	87.00	96.00	94.00	99.00
Be	<1	<1	<1	<1	<1	<1	2.00	<1	<1	<1	<1	<1	<1	<1	<1
Co	29.20	31.80	27.10	18.60	8.40	9.60	183.60	21.30	11.90	21.10	27.00	13.40	55.70	23.90	15.20
Cs	<0.1	<0.1	0.30	<0.1	<0.1	<0.1	<0.1	2.10	0.40	0.10	0.80	0.10	2.20	0.20	<0.1
Ga	17.50	17.00	17.30	16.90	13.50	12.80	14.50	13.20	14.00	37.70	26.60	18.40	56.30	20.00	20.70
Hf	1.60	1.60	1.50	1.40	<0.1	<0.1	0.30	1.00	1.50	1.70	1.10	1.70	1.90	1.90	2.40
Nb	5.10	5.80	6.40	4.90	0.20	<0.1	<0.1	2.50	4.60	2.30	4.40	4.70	3.40	4.90	3.50
Rb	0.40	<0.1	0.90	<0.1	0.20	<0.1	0.20	5.60	7.30	3.80	12.50	3.10	30.90	7.20	3.20
Sn	11.00	7.00	5.00	7.00	24.00	35.00	22.00	29.00	5.00	3.00	3.00	4.00	3.00	13.00	7.00
Sr	247.30	98.70	53.30	328.20	6.50	5.70	13.40	32.50	220.50	31.90	350.80	168.70	34.20	58.70	85.10
Ta	0.60	0.40	0.40	0.30	<0.1	<0.1	<0.1	0.20	0.30	0.30	0.40	0.40	0.40	0.40	0.40
Th	7.00	6.00	5.10	4.20	0.40	0.20	0.40	2.60	6.90	7.70	6.30	6.30	7.50	5.70	9.00
U	45.60	49.90	23.60	17.00	1.70	0.80	4.10	5.10	21.20	12.80	31.00	12.90	18.20	18.10	25.10
V	448.00	380.00	308.00	322.00	155.00	307.00	128.00	72.00	380.00	433.00	414.00	546.00	514.00	398.00	329.00
W	0.70	0.60	1.70	<0.5	6.70	3.70	5.20	8.00	44.70	1.80	1.50	118.40	1.90	<0.5	0.90
Zr	46.00	51.10	53.70	45.90	1.60	1.40	5.20	26.90	48.30	54.10	42.00	49.30	72.20	65.50	72.10
Mo	0.40	8.50	19.30	26.70	1.90	2.80	8.40	2.60	0.70	0.80	1.40	0.80	3.40	1.50	0.70
Cu	94.20	572.20	137.20	150.30	22.50	45.40	72.40	28.90	82.90	56.30	131.70	148.50	279.30	100.50	135.40
Pb	102.90	2492.30	1543.40	94.40	5.30	4.40	2.10	5.60	40.30	24.40	23.20	74.30	77.00	100.50	68.50

Cont. Table 4

Sample	AD-10-001	AD-10-002	AD-10-003	AD-10-004	AD-10-006	AD-10-007	AD-10-008	AD-10-009	AD-10-010	AD-10-011	AD-10-012	AD-10-013	AD-10-014	AD-10-015	AD-10-016
Zn	37.00	63.00	110.00	68.00	20.00	21.00	28.00	23.00	39.00	92.00	142.00	35.00	392.00	112.00	73.00
Ni	55.40	113.10	105.20	103.30	7.30	2.30	39.50	7.70	23.20	43.10	44.60	29.50	103.40	114.70	68.90
As	89.30	20.30	23.20	29.20	1.60	1.70	3.20	2.90	9.20	9.20	7.70	5.60	8.20	7.80	11.80
Cd	0.60	1.10	0.70	0.80	<0.1	<0.1	<0.1	0.20	0.90	1.30	1.20	0.30	0.70	1.40	1.30
Sb	<0.1	0.10	<0.1	<0.1	<0.1	<0.1	<0.1	<0.1	<0.1	<0.1	<0.1	<0.1	0.20	<0.1	<0.1
Bi	0.50	2.40	2.40	0.20	4.90	0.80	5.60	1.10	0.80	0.30	0.20	0.50	0.60	0.70	0.30
Ag	0.20	0.60	1.60	0.10	0.90	0.10	0.40	0.30	0.20	0.30	0.20	0.10	0.70	0.20	0.10
Au (ppb)	24.40	13.80	11.90	18.70	3.90	8.30	20.60	8.30	7.00	3.20	5.00	1.20	5.60	0.70	2.00
Hg	<0.01	<0.01	<0.01	<0.01	<0.01	<0.01	<0.01	<0.01	<0.01	0.01	<0.01	<0.01	0.03	<0.01	<0.01
Tl	<0.1	<0.1	<0.1	<0.1	<0.1	<0.1	<0.1	<0.1	<0.1	<0.1	<0.1	<0.1	0.20	<0.1	<0.1
Se	<0.5	<0.5	<0.5	<0.5	<0.5	<0.5	<0.5	0.90	<0.5	<0.5	<0.5	<0.5	1.50	<0.5	<0.5
Ni	87.00	129.00	118.00	115.00	24.00	<20	40.00	<20	40.00	56.00	65.00	56.00	116.00	142.00	92.00
Sc	3.00	4.00	3.00	4.00	2.00	4.00	5.00	4.00	5.00	5.00	5.00	4.00	5.00	4.00	5.00
Y	11.90	12.20	10.60	12.80	1.20	1.80	1.00	10.20	12.40	16.50	14.50	15.20	21.20	16.40	16.90
La	21.10	21.60	18.80	13.50	9.10	54.60	3.00	11.70	20.80	26.30	29.10	23.00	37.40	18.10	27.70
Ce	40.30	38.20	31.10	24.70	18.60	114.30	6.00	20.90	36.00	35.70	41.20	34.60	45.30	32.20	52.40
Pr	4.95	4.34	3.78	2.96	2.15	13.58	0.80	2.39	3.98	5.82	5.62	4.42	8.35	4.07	6.74
Nd	16.80	16.00	16.20	11.70	7.10	48.90	4.10	8.40	15.50	24.10	21.40	16.50	30.70	15.00	21.50
Sm	3.38	2.82	2.33	2.38	1.32	8.93	0.80	1.88	2.74	4.57	3.62	2.66	5.93	2.66	4.52
Eu	1.34	1.28	1.16	1.19	0.25	1.34	0.13	0.51	0.91	1.11	1.22	0.71	1.46	1.01	1.54
Gd	2.72	2.17	2.20	2.21	0.78	4.94	0.63	1.94	2.31	4.03	2.97	2.55	5.20	2.66	3.46
Tb	0.37	0.34	0.30	0.31	0.08	0.35	0.07	0.33	0.34	0.55	0.42	0.39	0.69	0.38	0.50
Dy	2.16	1.99	1.77	1.94	0.37	0.82	0.34	2.13	1.75	2.72	2.69	2.29	3.41	2.26	2.33
Ho	0.38	0.43	0.35	0.36	0.03	0.03	0.03	0.39	0.39	0.53	0.47	0.51	0.61	0.42	0.55
Er	1.12	1.13	1.03	1.18	0.11	0.05	0.11	0.96	1.34	1.59	1.25	1.36	1.78	1.23	1.53
Tm	0.14	0.16	0.14	0.16	<0.01	<0.01	<0.01	0.13	0.17	0.22	0.22	0.20	0.25	0.16	0.18
Yb	0.90	1.10	0.96	1.07	0.15	0.11	0.10	0.84	1.22	1.40	1.44	1.46	1.71	1.26	1.61
Lu	0.15	0.16	0.15	0.14	0.01	<0.01	0.02	0.13	0.15	0.21	0.18	0.18	0.23	0.16	0.22
∑REE	107.71	103.92	90.87	76.60	41.26	249.77	17.14	62.83	100.00	125.35	126.30	106.03	164.22	97.97	141.68
Ce/Ce*	0.91	0.91	0.85	0.90	0.97	0.97	0.89	0.91	0.91	0.67	0.74	0.79	0.59	0.87	0.88
Eu/Eu*	2.22	2.47	2.65	2.65	1.21	1.02	0.96	1.30	1.79	1.32	1.85	1.36	1.35	1.96	1.90
Pr/Pr*	1.12	1.03	0.99	1.02	1.10	1.07	0.92	1.06	0.99	1.14	1.11	1.09	1.28	1.09	1.18
Pr*/Yb*	1.78	1.27	1.27	0.89	4.63	39.85	2.58	0.92	1.05	1.34	1.26	0.98	1.58	1.04	1.35
Y/Ho	31.32	28.37	30.29	35.56	40.00	60.00	33.33	26.15	31.79	31.13	30.85	29.80	34.75	39.05	30.73

Cont. Table 4

Sample	AD-10-017	AD-10-018	AD-10-019	AD-10-20	AD-10-21	GA 2	GA 3	GA 4	GA 5	GA 6	GH2	GH4	GH5	GH6	GH7
SiO_2 (wt. %)	68.27	64.65	59.60	49.36	49.71	50.04	51.53	73.44	48.36	49.27	30.54	87.55	63.16	43.98	46.85
Al_2O_3	0.27	0.24	4.92	8.95	0.91	15.28	14.56	6.63	14.79	15.13	38.53	6.11	20.77	32.12	30.12
Fe_2O_3	23.92	32.33	14.21	25.23	19.54	19.93	20.22	11.78	24.20	20.66	6.29	2.58	5.04	8.75	8.08
MgO	1.06	0.13	0.09	0.19	1.05	1.15	1.37	1.30	2.67	1.90	1.07	0.17	0.44	0.83	0.52
CaO	1.28	0.39	0.66	1.71	1.62	1.94	5.11	0.96	2.96	6.07	1.30	0.09	0.05	0.05	0.04
Na_2O	<0.01	<0.01	0.03	<0.01	0.04	<0.01	0.14	0.05	0.04	0.28	0.02	0.01	<0.01	<0.01	0.02
K_2O	<0.01	<0.01	0.50	0.02	0.25	<0.01	0.14	0.54	1.17	0.12	0.09	0.09	0.08	0.07	0.10
TiO_2	0.12	0.05	0.08	0.09	0.02	1.38	1.82	2.36	2.58	2.16	0.14	0.04	0.01	0.08	0.02
P_2O_5	0.90	0.24	0.24	0.56	0.18	0.11	0.33	0.19	0.24	0.23	1.04	0.03	0.04	0.04	0.01
MnO	1.68	0.35	15.93	13.82	16.67	10.48	5.00	1.84	3.66	5.05	0.29	0.08	0.10	0.14	0.14
Cr_2O_3	<0.002	<0.002	<0.002	<0.002	<0.002	0.01	<0.002	<0.002	<0.002	<0.002	0.01	<0.002	<0.002	0.00	<0.002
LOI	0.50	0.30	3.00	0.00	9.60	-0.90	-0.70	0.10	-1.00	-1.10	0.00	0.50	-0.10	-0.40	-0.30
Sum	98.03	98.70	99.22	99.93	99.58	99.45	99.57	99.18	99.67	99.75	79.31	97.24	89.58	85.67	85.58
C_{total}	0.06	0.02	0.04	<0.02	0.03	0.03	0.03	0.04	0.08	0.02	0.05	0.07	0.05	0.02	0.07
S_{total}	1.24	0.77	<0.02	0.03	<0.02	<0.02	<0.02	0.05	0.02	0.03	<0.02	<0.02	<0.02	<0.02	<0.02
Ba (ppm)	235.00	199.00	1901.00	131.00	4.00	6.00	47.00	135.00	266.00	48.00	26.00	20.00	31.00	10.00	31.00
Be	<1	<1	2.00	<1	5.00	<1	3.00	<1	<1	3.00	9.00	<1	3.00	<1	<1
Co	35.60	19.10	21.80	7.20	11.40	10.00	21.50	16.60	30.50	38.30	87.30	14.70	58.50	75.10	47.10
Cs	0.10	<0.1	<0.1	<0.1	<0.1	0.30	5.70	7.50	23.00	1.10	0.80	0.40	0.40	0.20	0.80
Ga	14.60	14.30	22.60	33.20	21.60	23.00	18.50	11.00	20.90	25.20	51.10	10.90	33.90	45.90	45.30
Hf	<0.1	<0.1	0.30	0.30	<0.1	2.30	5.80	4.50	4.30	3.40	2.20	0.20	<0.1	1.20	0.30
Nb	1.20	0.20	0.20	0.60	<0.1	7.90	8.70	8.70	15.50	7.40	6.70	0.60	0.30	2.20	0.40
Rb	0.60	0.50	0.90	<0.1	0.70	0.60	21.90	55.10	119.40	8.10	6.90	4.30	4.50	5.60	7.00
Sn	4.00	3.00	<1	<1	<1	11.00	29.00	1.00	3.00	6.00	3.00	<1	<1	<1	<1
Sr	25.50	8.80	538.90	19.90	988.80	14.10	71.70	20.20	11.70	65.00	31.70	6.50	3.80	25.20	4.00
Ta	<0.1	0.20	0.10	<0.1	<0.1	0.50	0.70	0.60	1.30	0.60	0.80	<0.1	<0.1	0.80	<0.1
Th	0.30	<0.2	0.50	0.50	<0.2	0.50	3.20	<0.2	0.50	1.50	24.10	<0.2	0.40	5.50	2.00
U	1.90	1.30	4.30	1.80	15.00	1.30	1.20	0.30	0.60	0.70	16.30	0.40	0.60	1.90	0.40
V	135.00	174.00	103.00	156.00	87.00	387.00	193.00	389.00	541.00	440.00	103.00	21.00	62.00	88.00	47.00
W	0.80	76.10	<0.5	0.50	<0.5	1.80	5.60	1.40	1.70	0.90	6.60	0.70	<0.5	1.10	0.90
Zr	1.40	0.80	30.90	8.90	4.60	90.80	198.90	139.50	146.70	116.20	67.70	3.60	2.50	42.80	4.00
Mo	7.10	15.70	23.00	1.80	78.60	0.60	0.30	1.00	0.50	0.70	0.50	1.10	0.60	0.70	1.00
Cu	279.90	112.80	1352.80	44.10	19.20	155.60	180.70	143.90	29.10	15.60	28.90	16.40	15.50	14.90	47.50
Pb	342.30	318.30	828.60	24.90	278.50	1409.30	527.00	220.00	114.40	156.60	3787.30	30.10	139.80	14.90	60.70

Cont. Table 4

Sample	AD-10-017	AD-10-018	AD-10-019	AD-10-20	AD-10-021	GA 2	GA 3	GA 4	GA 5	GA 6	GH2	GH4	GH5	GH6	GH7
Zn	>10000	9854.00	1815.00	346.00	1873.00	530.00	757.00	727.00	753.00	390.00	855.00	129.00	308.00	335.00	419.00
Ni	4.00	3.60	16.40	14.60	45.70	4.10	3.60	20.10	13.60	15.70	4.70	3.60	3.60	1.60	4.40
As	5.40	2.90	21.10	3.20	13.50	136.90	81.30	36.30	16.80	162.60	164.40	24.00	15.20	8.80	6.70
Cd	48.60	23.10	35.10	0.60	13.10	4.10	3.80	3.00	2.00	11.50	3.10	0.70	0.20	0.20	0.30
Sb	0.20	0.30	1.00	<0.1	0.20	<0.1	<0.1	<0.1	<0.1	0.10	0.10	<0.1	<0.1	<0.1	<0.1
Bi	2.20	0.60	9.00	<0.1	<0.1	1.90	0.20	1.60	0.20	0.10	0.50	<0.1	<0.1	<0.1	1.50
Ag	1.90	2.70	3.30	0.20	0.30	5.00	0.40	1.40	0.20	0.70	0.80	0.10	<0.1	<0.1	0.80
Au (ppb)	2.50	3.20	23.10	<0.5	6.30	3.40	<0.5	1.60	<0.5	8.00	<0.5	<0.5	<0.5	<0.5	1.70
Hg	0.14	0.20	0.04	<0.01	0.04	<0.01	<0.01	<0.01	<0.01	<0.01	<0.01	<0.01	<0.01	<0.01	<0.01
Tl	<0.1	<0.1	0.30	0.10	<0.1	<0.1	0.10	0.50	1.00	<0.1	<0.1	<0.1	<0.1	<0.1	<0.1
Se	<0.5	<0.5	<0.5	<0.5	<0.5	<0.5	<0.5	1.00	<0.5	<0.5	<0.5	<0.5	<0.5	<0.5	<0.5
Ni	<20	<20	22.00	<20	55.00	<20	<20	23.00	<20	21.00	20.00	<20	<20	21.00	<20
Sc	<1	<1	6.00	2.00	<1	30.00	31.00	25.00	54.00	36.00	2.00	<1	<1	<1	<1
Y	2.00	0.50	18.30	12.00	4.90	35.40	56.40	20.00	67.10	37.30	56.60	0.50	1.20	6.80	1.80
La	12.80	1.60	16.90	8.30	1.50	2.00	10.50	2.60	6.20	4.60	159.40	1.60	3.00	16.20	5.80
Ce	29.10	3.40	22.30	19.10	2.60	4.70	24.80	6.60	15.00	12.50	329.40	2.80	6.60	31.20	11.80
Pr	3.48	0.49	4.21	2.42	0.32	0.84	3.95	1.05	2.23	2.14	43.50	0.38	0.86	3.51	1.40
Nd	13.70	2.20	17.30	8.90	1.10	4.10	19.60	6.50	11.70	11.60	190.00	1.60	3.90	12.10	4.60
Sm	2.39	0.46	3.28	1.73	0.39	2.46	6.91	1.79	4.56	4.34	39.96	0.32	0.78	2.11	0.78
Eu	1.06	0.16	1.35	1.01	0.14	0.54	1.84	0.45	1.51	1.73	5.17	0.04	0.12	0.20	0.09
Gd	1.18	0.24	3.02	1.61	0.46	4.48	10.63	3.00	10.22	6.87	31.73	0.21	0.69	1.75	0.57
Tb	0.11	0.01	0.45	0.26	0.07	0.88	1.75	0.56	2.00	1.12	3.63	0.03	0.08	0.25	0.08
Dy	0.39	0.13	2.51	1.49	0.58	6.05	10.79	3.29	12.71	6.66	16.13	0.19	0.39	1.35	0.44
Ho	0.04	<0.02	0.49	0.31	0.11	1.26	2.20	0.77	2.41	1.33	2.08	0.02	0.03	0.23	0.06
Er	0.11	0.03	1.45	0.79	0.41	3.91	6.20	2.46	6.63	4.09	4.91	0.07	0.04	0.61	0.19
Tm	<0.01	<0.01	0.19	0.09	0.05	0.57	0.95	0.34	0.88	0.57	0.56	<0.01	0.01	0.08	0.01
Yb	0.09	<0.05	1.21	0.73	0.26	3.64	6.03	2.46	5.71	3.65	3.36	0.09	0.19	0.50	0.17
Lu	<0.01	<0.01	0.19	0.09	0.03	0.55	0.88	0.34	0.84	0.54	0.41	<0.01	<0.01	0.08	0.03
∑REE	66.47	9.31	93.15	58.83	12.92	71.38	163.43	52.21	149.70	99.04	886.84	7.87	17.90	76.97	27.82
Ce/Ce*	1.00	0.88	0.61	0.98	0.87	0.80	0.86	0.89	0.91	0.87	0.91	0.83	0.94	0.95	0.96
Eu/Eu*	2.96	2.51	2.15	2.95	1.70	0.75	1.09	0.92	1.00	1.61	0.76	0.73	0.88	0.52	0.66
Pr/Pr*	1.02	1.03	1.21	1.09	1.11	1.06	1.01	0.87	0.95	0.97	1.01	1.04	0.98	1.06	1.12
Pr*/Yb*	12.48	3.16	1.12	1.07	0.40	0.07	0.21	0.14	0.13	0.19	4.18	1.36	1.46	2.27	2.66
Y/Ho	50.00	25.00	37.35	38.71	44.55	28.10	25.64	25.97	27.84	28.05	27.21	25.00	40.00	29.57	30.00

Note: Major elements are in wt. % and trace elements are in ppm, except for Au that is in ppb. < means below detection limits. Cerium, and europium anomalies are defined as follows: $Ce/Ce^* = Ce_{SN}/(0.5Pr_{SN} + 0.5La_{SN})$, $Eu/Eu^* = Eu_{SN}/(0.66Sm_{SN} + 0.33Tb_{SN})$, $Pr/Pr^* = Pr_{SN}/(0.5Ce_{SN} + 0.5Nd_{SN})$.